Wind-Induced Pounding of Tall Buildings

by

Tristen Brown

A thesis

submitted to the Faculty of Graduate Studies

in partial fulfilment of the requirements for the

Degree of Master of Science

in

Civil Engineering

Supervisors:

Dr. Ahmed Elshaer

Assistant Professor – Department of Civil Engineering

Dr. Anas Issa

Assistant Professor - Department of Civil Engineering

Lakehead University

Thunder Bay, Ontario

August 2022

Author's Declaration Page

I hereby declare that I am the sole author of this thesis. This is a true copy of the thesis, including any required final revisions, as accepted by my examiners. Chapter 2 of this thesis has been published as a state-of-the-art review in the **Journal of Building Engineering**. Chapter 3 and Chapter 4 of this thesis has been submitted and under review for a Journal Publication. I understand that this thesis may be made electronically available to the public.

Abstract

Pounding of adjacent structures under lateral loads (e.g., earthquake and wind) due to proximity has been a major cause of building damage in the past. The effects of pounding can be mitigated by providing a suitable gap distance between structures, adequate shock absorbers or by designing for the additional pounding loads. However, if not properly considered, these abnormal supplementary loads can damage the structures, notably when the attentive structure experiences a dynamic vibration in an out-of-phase order. Multiple pounding incidents have been reported to occur under lateral loads, which resulted in local and global damages. With the new generation of tall buildings, which are becoming taller and more flexible, these structures are becoming more susceptible to wind-induced pounding due to the large sway developed during high wind problematic affairs. The study first investigates wind-induced pounding forces of two equal height structures with similar dynamic properties. This will first rely on using Large Eddy Simulation (LES) modelling for the wind load evaluations. Then, the wind loads will be extracted from the LES models and applied to a Finite Element Method (FEM) analysis software to determine the examined structures' deflections, minimum separation gap distance, and pounding forces. To correlate a reasonable mathematical formula, training data values must be prepared. This will include varying values of the structure's heights, applied wind velocities, flexure of the structure, and the separation distance between the examined buildings. Lastly, a Genetic Algorithm (GA) is then utilized with varying parameters of the tall structures to correlate the minimum separation gap distance and maximum pounding force that can be performed. To achieve a more accurate mapping for the trained database, the more complex the mathematical formula will be developed.

Acknowledgements

ᑕᐁᓯ (Tansi: Hello)

I would like to take this opportunity to acknowledge the traditional territories of Robinson-Superior Treaty territory and the land on which we gather is the traditional territory of the Anishnaabeg and the Métis. I would also like to acknowledge my homeland, Treaty 6 territory, on which we gather is a traditional meeting ground and home for many Indigenous Peoples, including Cree, Saulteauz, Niitsitapi (Blackfoot), Métis, and Nakota Sioux Peoples.

I first would like to give my deepest gratitude to my graduate supervisor, Dr. Ahmed Elshaer, for all the help and commitment he has offered during the time of pleasurable research I have completed thus far. I am very grateful for the chance at meeting him during my undergraduate studies at Lakehead University. He was the main reason I have continued with my educational career into graduate studies. All his support, knowledge, and expertise are in top performance when working under his supervision in the field of engineering. Dr. Elshaer has helped me when needed and knows how to ethically push me to my highest performance during my amazing time during my graduate experience.

I would also give great acknowledgment to my other supervisor, Dr. Anas Issa. He has chose to be my other supervisor in a short notice while starting my Masters. He has given top notch advice and superb educational support and knowledge in aiding many of my arising questions and answers I were uncertain of. Dr. Issa has help complete difficult steps in my research progress in such a timely matter which has helped improve my success in an exponential rate.

I would like to give a huge recognition to my family. My father, Bryan, my mother, Matricia, step-mother, Lori-Ann, and sister, Mackenzie, for their support, encouragement, and many prayers and wishes. I would also like to give recognition to my grandparents who have helped with accommodation during my first two years of schooling.

ᑭᓇᓈᐢᑯᒥᑎᐣ (Kinanâskomitin: Thank you)

Table of Contents

List of Tables

9

List of Equations

List of Figures

11

12

14

List of Symbols

$d_{g,min}$	Separation Gap Distance
Δ	Displacement
S	Double-difference combination rule
X_A	Maximum displacement for first building,
X_B	Maximum displacement for second building
ρ	Cross-correlation coefficient
H_{max}	Maximum total height
u_x	Velocity component in the distance of x
t	Time (seconds)
H	Height of structure (m)
C_P	Pressure Coefficient
v	Velocity (m/s)
k	Stiffness
d_g	Separation gap distance (mm)
δ	Relative displacement (mm)
F_I	Pounding impact force (kN)
k_T	Structure stiffness
V	Shear force
Δu	Lateral displacement of the structure (mm)
F_n	Natural Frequency (Hz)
m	Mass (kg)
F	Force
$F_I(t)$	Pounding impact force relative to time

$\delta (t)$ Relative displacement at a specified time

$u_i (t)$ Displacement of the element node relative to time

Abbreviations

AEM   Applied Element Method

AISC   American Institute of Steel Construction

ASCE   American Society of Civil Engineers

CAARC   Commonwealth Advisory Aeronautical Research Council

CD   Computational Domain

CFD   Computational Fluid Dynamics

CFL   Courant Friedrichs-Lewy

EC   Eurocode

FEM   Finite Element Method

GA   Genetic Algorithm

HPC   High-performance computer

IBC   International Building Code

LES   Large Eddy Simulation

MDOF   Multi-Degree-of-Freedom

NBCC   National Building Code of Canada

NEHRP   National Earthquake Hazards Reduction Program

RC   Reinforce Concrete

RMS   Root Mean Squared

SDOF   Single-Degree-of-Freedom

UBC   Uniform Building Code

1   Chapter 1 – Introduction

1.1   Background

Pounding of structures occurs when two or more structures are within proximity subjected to extensive lateral loading leading to a collision of structures. These lateral loads can occur from ground vibration produced during earthquakes or from airflow generated during extreme wind events. Tall structures in proximity are more susceptible to pounding phenomena, where many pounding incidents have been reported over the past three decades. Building damage can transpire when structures experience pounding phenomena depending on how severe the structural collision event occurs. The structural damages from pounding can cause local or global failures and possibly lead to a total collapse. Pounding can be mitigated by providing a suitable gap distance between structures or by designing for the additional pounding loads between the colliding structures. Providing an adequate gap distance between structures is ultimately the best solution to prevent a pounding phenomenon; however, owners and architects often object to this solution due to architectural and space-related considerations. This solution also is not applicable to structures that are already pre-existing without sufficient lateral spacing. Therefore, mitigation measures towards this issue have been developed as an alternative to an adequate separation distance. These non-typical additional pounding loads, if not properly taken into account, can produce damages within the structures, especially when the pounding structures are vibrating out-of-phase.

1.2   Research Problem Gap

Buildings are constructed within dense metropolitan locations, ultimately in proximity to surrounding structures due to limited available land space and the increase in population. With the design of new, tall, and slender buildings, the term pounding has become an important objective when a structure is built within proximity. Pounding can be considered as a major risk to tall structures; for instance, (Rosenblueth and Meli, 1986) explored a historical earthquake event resulting in many structural pounding occurrences. A pounding occurrence can also be produced when the structures involved are subjected to extreme wind events (Brown and Elshaer, 2022; Huang et al., 2012). In comparison to an earthquake, the same structure under wind loading can develop a more considerable lateral deflection and inter-storey drift magnitudes within an exact geological location (e.g., eight times larger in lateral deflection and 2.5 times more prominent in inter-storey drifts) (Aly and Abburu, 2015). As many studies have conducted structural pounding experimental and numerical analysis from earthquake-induced phenomena, wind-induced structural pounding can transpire when one's structure exceeds the separation distance between its other adjacent structure due to lateral deflection produced by wind similarly to earthquake-induced structural pounding. The study gap to this date is identifying possible mitigation measures towards avoiding a wind-induced pounding of tall structures. One approach can be determining a required minimum separation distance for possible structures located in proximity during hazardous wind events. Alternatively, when a required separation distance cannot be achieved, it is challenging to quantify the developed pounding forces produced when a wind-induced structural pounding event arises.

1.3   Research Objectives

The analytical research study detailed in this thesis has been produced to correlate mathematical formulas from an optimization process through Genetic Algorithm (GA) for determining a minimal required separation gap distance to mitigate pounding of structures from wind events. In addition, a different mathematical formula will be produced for determining the maximum pounding force of the examined two structures when a minimum separation gap distance cannot be achieved. Accordingly, this study aims to examine two structures in proximity with varying wind intensity, heights, flexibility of the structures and alteration of the separation gap distance after estimating the required minimum Separation Gap Distance ($d_{g,min}$) to mitigate the arising risk of damages and failures due to wind-induced structural pounding. To achieve this, a summary of the specific research objectives for this study are as follows:

1. Validate and conduct an initial set of Computational Fluid Dynamic (CFD) simulations while altering the applied mean wind velocities to determine the wind forces acting on two adjacent tall structures.

2. Validate a set of Finite Element Method (FEM) models to determine the developed deflections for the two adjacent structures when subjected to the extracted time-history wind forces.

3. Determine the dynamic responses of each structure throughout the applied wind forces to establish the lateral deflection of each structure, which then can correlate an estimated $d_{g,min}$ to mitigate wind-induced structural pounding.

4. Determine the maximum developed pounding forces for various structural configurations when the gap distance between adjacent structures is less than $d_{g,min}$.

5. Formulate the most accurate mathematical formula for estimating the required $d_{g,min}$ based on the structural natural frequency, building heights, and the applied wind using Genetic Algorithm (GA).

6. Develop a mathematical formula that can correlate the maximum pounding forces to the adjacent structures height, flexibility and the wind load encountered when a collision occurs if the determined $d_{g,min}$ cannot be provided.

1.4   Thesis Outline

This thesis is outlined and organized into five chapters, which contain the following content:

- Chapter 1 (this chapter) provides a general introduction of pounding from wind-induced events, in addition with the scope and objectives of this thesis

- Chapter 2 summarizes a literature review that outlines existing research from the most recent state-of-the-art review towards pounding. This section reviews large city-scale earthquake pounding occurrences, out-of-phase vibrations leading to pounding, and pounding within the same structure through expansion joints, in addition to experimental and numerical modelling towards pounding. It also discusses lateral deflections within tall structures resulting from wind events and how this sway can trigger a structural pounding phenomenon.

- Chapter 3 presents the numerical analysis in achieving a formulated mathematical equation for determining the estimated minimum separation gap distance for mitigating wind-induced pounding of two tall structures in proximity.

- Chapter 4 describes the potential pounding forces from wind-induced events for proximate tall structures from numerical analysis, following a potential pounding force formulation from optimization through GA.

- Chapter 5 concludes this thesis by summarizing the key research findings, conclusions drawn, and provided recommendations for future research needs.

2 Chapter 2 – Literature Review

2.1 Background

At dense metropolitan locations, buildings are placed in proximity due to the increase in populations and to maximize the building use within the restricted availability of land space. Traditionally, high-rise structures are used for commercial office occupancy, but residential usage has recently gained popularity (Ali and Moon, 2006). The pounding of structures is becoming a new important commodity with the design of new structures when built within proximity. The term "pounding" is defined by past scholars (Anagnostopoulos and Spiliopoulos, 1992a; Efraimiadou et al., 2013; Kasai and Maison, 1997; Maison and Kasai, 1990, 1992) when two adjacent neighbouring structures are in close proximity causing a collision when subjected to lateral loading. "Pounding of structures" has also been defined by past scholars labelled as "interaction between adjacent structures" (Favvata et al., 2012; Favvata and Karayannis, 2013, 2009; Karayannis and Favvata, 2005a, 2005b; Karayannis and Naoum, 2018a, 2017a, 2017b). In addition, (Jankowski, 2009) also mentions the pounding phenomenon occurs when different dynamic characteristics of a structure (i.e., mass or stiffness) collide due to their out-of-phase vibration from earthquake excitation. (Abdullah et al., 2001a) defined structural pounding as similar to (Jankowski, 2009) but added that the out-of-phase vibrations can also occur during high wind proceedings. The pounding phenomenon from past field evidence has ranged from light to heavy structural damages to the extent of initiating global structural failures (Rosenblueth and Meli, 1986). Although the majority of pounding cases have occurred during earthquakes causing induced ground motion and transferring to the structures, it can also be generated when structures are subjected to very strong lateral loads, such as extensive wind loads (Huang et al., 2012). Many past scholars have extensively studied these pounding events, more particularly from past

26

earthquake occurrences (Anagnostopoulos, 1995, 1988; Jankowski, 2012, 2009; Kasai and Maison, 1997; Kaushik et al., 2006; Maison and Kasai, 1992; Rosenblueth and Meli, 1986).

Tall and slender structures are ultimately sensitive towards lateral loading (Huang et al., 2012; Lam et al., 2009), where wind forces applied are towards the building's exposed surfaces. Alternatively, seismic forces applied are inertial, resulting from inertial resistance of the structure and distortion of the ground (Rahman et al., 2012). The lateral loads applied can develop a high value of lateral forces, producing intensive sway movement or causing strong vibrations throughout the structure (Stafford Smith and Coull, 1991). Meeting the lateral deflection requirements or controlling the extensive vibrations can be, in some cases, more challenging than meeting the strength and capacity requirements within the building (Elshaer and Bitsuamlak, 2018). Lateral deflection and structural sway in tall buildings can affect the non-structural elements (i.e., cladding and partition); the main structural elements; and possible adjacent structures (Chenna and Ramancharla, 2018; Rahman et al., 2012; Wolfgang, 1977). For the adequate designs in new tall structures in proximity, extreme measures for large deflection and structural sway need to be properly addressed in the design.

Tall buildings may experience large significant lateral deflections during wind and seismic events (Chan et al., 2000; Coull and Wahab, 1993; Halis Gunel and Emre Ilgin, 2007; Huang et al., 2012) without sustainable building measures such as shear walls (Beck, 1962; Coull and Choudhury, 1967; Rosmon, 1964), braced frames or rigid frames (Stafford Smith et al., 1984, 1982; Stafford Smith and Crowe, 1986). Without proper measures can make the structure more susceptible to pounding, despite having an insufficient separation gap between structures. Intensive studies have been carried out to mitigate these safety precautions to avoid such pounding hazard phenomena. An objective in the past was to develop procedures for evaluating adequate separation distances

between structures in order to prevent contact during extensive lateral motion events (Jankowski, 2005; Jankowski and Mahmoud, 2015; Penzien, 1997). Modern codes (i.e., the International Building Code (IBC) 2018, National Building Code of Canada (NBCC) 2015, National Earthquake Hazards Reduction Program code (NEHRP) 2012, Codes for Seismic Design of Buildings (GB50011-2010) 2010, American Society of Civil Engineers (ASCE7-05) 2006, Eurocode 8 (EC8) 1994, and the Uniform Building Code (UBC 97) 1997) have included required separation distances between building for earthquakes occurrences as countless locations around the world may have experienced such significant circumstances (Miari et al., 2019). However, these requirements are not correlated to the dynamic properties of the adjacent buildings or the lateral loads from such natural hazards (Chau and Wei, 2001). More accordingly, numerous buildings and structures were designed and built before such requirements in their codes and provisions, leading to pre-existing structural pounding failures (Rezavandi and Moghadam, 2007). Design codes (e.g., NBCC 2015) do not fully address nor provide sufficient safety guidelines on the effects of tall structures undergoing strong winds within flexible foundations. Namely, tall structures should provide reliable analysis and a correct basis for selecting load factors in these building provisions (Halabian et al., 2003). While most building codes identify these necessities towards standards and hazards for deflection, limited cases for building codes are identified for the required minimum separation distance for structures at proximity during wind evaluations. Mitigation can be implemented for structural pounding if minimal or no required spacing between structures is considered during wind evaluations for the design of these building codes. Despite past scholars regarding earthquake-induced pounding, colliding of structures (such as buildings or bridges) can be motivated by building deflections generated from their out-of-phase vibrations, depending on their dynamic structural properties. Namely, out-of-phase vibrations arise from intensive lateral

loading (e.g., wind events), making the occurrence of wind affairs problematic for these specific pounding phenomena. This chapter presents the current state of the art for structural pounding at proximity.

This chapter is divided into five sections, where the first section (this section) provides an overview of the pounding phenomenon. Section 2.2 explains the effects and principles of certain pounding phenomena (*Causes of pounding*). It defines key terms such as pounding, proximity, load cases of pounding, in addition to the types of pounding failures. Afterward, the paper reviews the historical incidents and past issues from previous studies that have reported the occurrence of structural pounding (Section 2.3: *Historical pounding incidents*). The following two sections (Sections 2.4 and 2.5) investigate past research studies that used experimental and numerical modelling for pounding structures (*Experimental modelling towards pounding and Numerical modelling towards pounding*). The review paper summarizes the important vital evidence related to pounding phenomena in conclusion.

2.2 Causes of Pounding

Structural pounding occurs when two or more structures at proximity are subjected to lateral loading developing an out-of-phase vibration due to the difference in their dynamic properties, causing a collision between the structures (Jankowski, 2009). These lateral loads can occur from ground vibration produced during earthquakes or from airflow generated during extreme wind events. Tall structures at proximity are more susceptible to pounding phenomena, and many pounding incidents have been reported over the past three decades (Chenna and Ramancharla, 2018; Mariam Ehab et al., 2014; Papadrakakis and Mouzakism, 1995; Sołtysik and Jankowski, 2016). The pounding risk is typically triggered by the lateral deflection of tall buildings subjected to lateral loads, such as earthquakes, tsunamis, hurricanes, tornados, cyclones and extreme wind gusts. While most scholars have intensively examined pounding from earthquake excitation due

to its unpredicted occurrences, very few studies have investigated the other hazardous events generating lateral motion leading to structural pounding.

Building damage can transpire when structures experience pounding phenomena depending on how severe the structural collision event occurs. The structural damages from pounding can cause local or global failures and possibly lead to a total collapse of structures (Jankowski, 2009; Petronijević et al., 2014; Wolfgang, 1977). Many cases of structural damage due to pounding were reported from previous studies (Kasai et al., 1996; Penzien, 1997), which are further discussed in the following section. Local failures from pounding can arise when the point of impact from the two buildings have different heights, storey levels and phases, especially when the shorter structure is less flexible than the taller structure (Anagnostopoulos and Karamaneas, 2008). In addition, local pounding can be experienced through thermal expansion or construction joints (Petronijević et al., 2014). Local damages from pounding can occur when adjacent structures do not provide sufficient separation distances (Kasai and Maison, 1997; Maison and Kasai, 1992) or from the structures not having satisfactory lateral resistance (Chan, 2001; Stafford Smith et al., 1984). Accordingly, pounding risk can be minimized when the adjacent buildings have similar dynamic properties with equal heights (Chenna and Ramancharla, 2018). Failures from pounding may result in irregular responses of structures due to the differences in building heights. Local damages may arise to the columns as the roof of one building collides with the columns of the other. Global damage may occur from the collapse of damaged floors, or global failures can occur due to the entire structure's total collapse (Rosenblueth and Meli, 1986). Pounding mitigation should be considered either by providing safe separation distances between structures (Jankowski, 2008a; Lin, 1997) or by designing for the additional lateral loads resulting from pounding (Chan, 2001; Godínez-Domínguez and Tena-Colunga, 2010; Pantelides and Ma, 1998), which can be tested

through the use of either experimental or numerical modelling, which is further explained in Sections 2.4 and 2.5, respectively.

The main reason for structural interactions between the adjacent buildings under the effects of an earthquake (or wind excitations) is due to the difference in their dynamic properties, as mentioned in previous studies (Malhotra et al., 2020). Their structural properties will mostly always differ, leading to out-of-phase vibrations causing structural pounding due to the high urbanization in regions worldwide (Mahmoud et al., 2013). In order to eliminate or minimize the pounding forces between the structural interactions, effective utilization of adequate gap distances between the two adjacent structures must be present. Evidentially, coupling the adjacent structures with suitable control mechanisms can be an effective solution to minimize the overall responses of the structural systems under the effects of earthquake and wind excitations (Bhaskararao and Jangid, 2006; Patel and Jangid, 2010; Wang et al., 2015). Alternatively, the possibility of using dissipative links and semi-active devices to reduce the response of adjacent buildings under the wind excitation has also been previously studied (Klein and Stukel, 1972). Under the wind excitation, the two adjacent buildings were modelled by a couple of uniform shear beams coupled by a single flexible and damped link and acquired the optimal stiffness and damping in the link in the case of primary structures, which was presented in their study (Aldemir and Aydin, 2005; Gurley et al., 1994). Moreover, dampers (e.g. friction dampers) can be adopted for braced frames, buildings with shear walls and low-rise buildings to mitigate the large deformations caused by earthquake ground motions and winds (Chung et al., 2009; Colajanni and Papia, 1995; Pall and Marsh, 1981). Passive single and multiple mass dampers can also be installed in civil structures to mitigate wind or earthquake-induced vibrations (Aldemir et al., 2001; Chen and Wu, 2001; Park and Reed, 2001). Although the passive devices are simple and yet completely applicable in civil structures, they

have limitations in achieving desired performance measures primarily due to the highly uncertain nature of the wind and seismic disturbances (Aldemir and Güney, 2005). As seen from the presented literature, a mathematical correlation can be created between the dynamic structural properties and the expected structural response (i.e., deflection and acceleration). This correlation can be further related to the predicted pounding impact between structures, thus developing proper guidelines between the structural properties of the adjacent building and (1) the required gap distance, or (2) the required resiliency of the tall building to withstand the potential pounding forces.

Providing an adequate gap distance between structures is ultimately the best solution to prevent a pounding phenomenon; however, owners and architects often object to this solution due to architectural and space-related considerations. This solution also is not applicable to structures that are already pre-existing without sufficient lateral spacing. Therefore, mitigation measures towards this issue have been developed as an alternative to an adequate separation distance. Firstly, collision shear walls and bracing systems for pounding interactions have been previously presented in many studies and were proven to be sufficient in minimizing the interaction of earthquake-induced structural pounding (Jamal and Vidyadhara, 2013; NK and Nair, 2016). In this case, the maximum out-of-phase displacement of the pounding structures, the top displacement, and the number of impacts will be decreased (A. Hameed, M. Saleem, A.U. Qazi, 2012). Buildings with shear walls can also absorb a higher energy impact than moment-resistant concrete frame structures, decreasing the high impact load (Barros and Khatami, 2012). Secondly, the use of impact-absorbing materials such as rubber shock absorbers (Lin and Weng, 2001; Polycarpou et al., 2013; Takabatake et al., 2014), polystyrene (Rezavandi and Moghadam, 2007, 2004) or polymers (Sołtysik et al., 2020, 2017) on isolated buildings (Komodromos, 2008; Polycarpou and

Komodromos, 2011) may be used on the response of the colliding structures, which have been explored in past studies on fixed-based structures. Shock absorbers were concluded to reduce the peak acceleration and impact forces of the pounding structures; however, this increased the number of pounding phenomena because of the softness of its behaviour. Another common mitigation measure is making the adjacent buildings vibrate in-phase by connecting the adjacent structures with links. Numerous study results have proven that this mitigation measure significantly decreases the displacement of the flexible adjacent structure and has insignificant effects on the response of the stiff adjacent building (Jankowski and Mahmoud, 2016; A. Richardson et al., 2013; Andy Richardson et al., 2013). The use of dampers is the following type of mitigation measure that has been investigated. The influence of viscous dampers on the pounding mitigation and its arrangement was examined by (Patel and Jangid, 2010) and (Tubaldi et al., 2012). It was established that the use of the viscous dampers at the isolation level of the isolated buildings could regulate the large structural displacement, which can mitigate the interaction between the adjacent structures, leading to a significant reduction in the damaging forces. Other dampers can include fluid viscous dampers (Kazemi et al., 2018; Pratesi et al., 2014, 2013; Sorace and Terenzi, 2013), magnetorheological dampers (Abdeddaim et al., 2017; M Abdeddaim et al., 2016; M. Abdeddaim et al., 2016), tuned mass dampers (Wang et al., 2017; Xue et al., 2016b, 2017; Zhang et al., 2015), passive shared tuned mass dampers (Abdullah et al., 2001b), and semi-active shared tuned mass dampers (Kim, 2016). The last mitigation measure includes the use of the roll-in-cage isolators from (Ismail et al., 2014). This measure can control the significant response (displacement) from installing the isolated system at the isolation level. This method was proven to be effective in controlling both rotational and translational pounding through the use of passive and active

controls by the performance of numerical analysis on these types of isolation systems (Ismail, 2015a, 2015b, 2015c; Ismail et al., 2015, 2014).

2.3 Historical Pounding Incidents

This section reviews the historical incidents that have reported the occurrences of structural pounding and its damages. The interaction of structures has been countlessly reported in many cases, such as large city-scale earthquake occurrences, out-of-phase vibrations leading to the pounding of adjacent structures, even to the extent of internal pounding such as expansion joints. With the past historical events that have occurred, if adjacent buildings at proximity encounter such lateral loads in the future, extensive measures of those loads may experience specific pounding effects, leading to the possibilities of structural damage (Anagnostopoulos, 1988; Jankowski, 2012, 2009; Kaushik et al., 2006).

2.3.1 City-scale assessment of pounding-induced damages during earthquakes

The pounding of structures has occurred in many seismic scenarios and has been intensively studied in the past decades. Within many events of large-scale earthquake phenomena, occurrences of structural pounding within a big city-scale have led to several cases of structural damage or failures (Abdel Raheem, 2013; Anagnostopoulos, 1995; Chouw and Hao, 2012; Cole et al., 2012; Mariam Ehab et al., 2014; Kasai and Maison, 1997; Maison and Kasai, 1992; Rosenblueth and Meli, 1986; Stone et al., 1987). In the event of structural pounding, magnification of property loss and substantial amounts of expenses for repair and maintenance can be generated. Large-scale earthquake events within dense metropolitan cities such as the Mexico City earthquake in 1985 have led to significant structural failures from pounding cases. An investigating team was assigned to investigate this earthquake (National Bureau of Standards Building Science, 1987). Their report addressed the origin and characteristics of the observed ground motion, the ability of buildings designed in accordance with present and proposed seismic design provisions to resist this type of

ground motion and observed data on structural and foundation failures. The original earthquake reached a Richter scale magnitude of 8.1, following an aftershock of 7.5 after a day and a half, which was at a focal depth of approximately 18 km. The intense motion duration was approximately 60 seconds and a peak acceleration of 168 cm/s^2. With this force of ground motion, a high percentage of structures failed that were within the danger zone, ranging with heights of 6 to 17 stories tall. While lower and taller structures performed relatively well in respect to these structural failures, this is due to these middle-range structures having fundamental periods close to that of the ground motion. Concerning the pounding of structures, 40% of the severely damaged 330 structures were involved in pounding, and 15% of those structures led to a total collapse due to pounding phenomena (Figure 2.1 and Figure 2.2) (Anagnostopoulos, 1995; Rosenblueth and Meli, 1986; Stone et al., 1987).
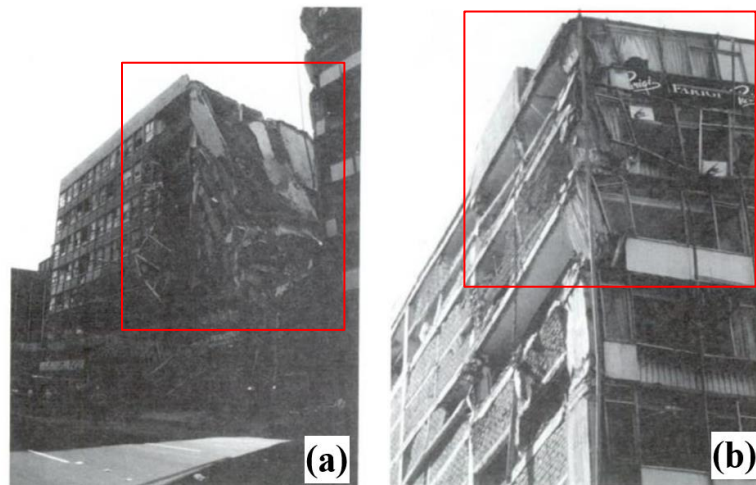
Figure 2.1. Typical pounding damage in similar height buildings: (a) seven-storey office building on Ave 20th de Novembre, which collapsed due to pounding; and (b) neighbouring nine-storey building showing impact damage to columns, adapted from the (National Bureau of Standards Building Science, 1987)
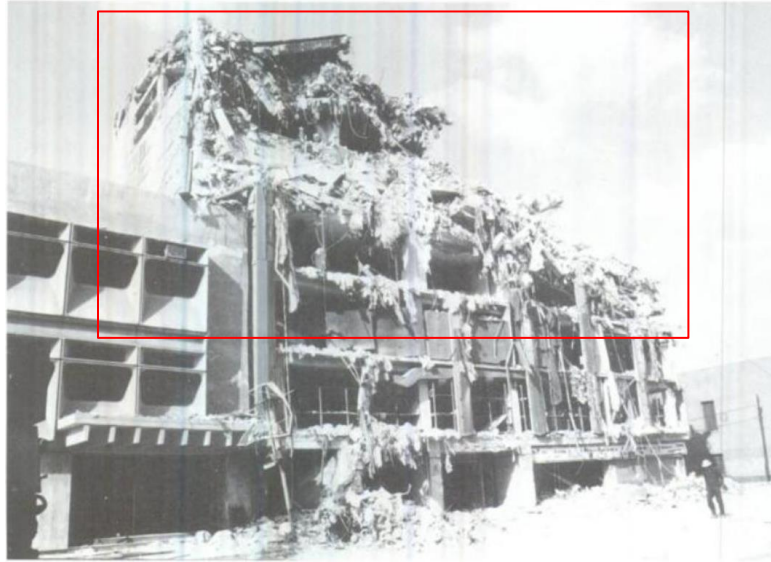
Figure 2.2. Pounding damage between buildings of dissimilar heights and stiffness with separation between the structures approximately 10 cm, adapted from the (National Bureau of Standards Building Science, 1987)

The Canadian perspective towards the pounding of buildings during earthquake events was illustrated by (Filiatrault et al., 1994) in their review paper. This study provides information to structural engineers on how to consider and mitigate the pounding phenomenon between adjacent buildings more accurately during earthquake events. It reviews the problems of seismic pounding, more specifically observations of damages from pounding during earthquakes, and the potential pounding effects for structures in large Canadian cities. Studies such as analytical and numerical research were also conducted in their paper, and methods were proposed to mitigate these pounding phenomena. (Filiatrault et al., 1994) also investigated the seismic behaviours of three closely spaced steel frame structures, considering the Canadian codes for design. The first part details the pounding potential for Canadian cities such as the Notre-Dame Pavilion in Quebec and the Shipshaw Bridge located 10 km northeast of Jonquiere, Quebec that crosses the Saguenay River. The Notre-Dame Pavilion was an incident of a seven-storey unreinforced masonry wall that was severely cracked when it pounded against an adjacent two-storey building during the 1988

Saguenay earthquake (Tinawi et al., 1990). At the same time, the Shipshaw Bridge incident underwent a longitudinal motion and pounded against both abutments during the same 1988 Saguenay earthquake. Local buckling of the horizontal bracing members underneath the deck and massive cracking of the concrete cover at the abutments was generated because of the repeated pounding from the earthquake excitation, which led to complete failure of one of the four anchorage plates connecting the deck to one abutment. The Shipshaw Bridge event is further detailed in Section 2.3.3 from (Filiatrault et al., 1993). Their study included three cases of pounding between adjacent structures that were analytically investigated. (Filiatrault et al., 1994) study concluded that designers should consider pounding phenomena on a case-by-case basis as pounding can be regarded as complex behaviour, which is not appropriately addressed in the 1990 National Building Code of Canada (NBCC-1990). In addition, when two structures are initially in contact, the time between two impacts corresponds to about one-half the mean period of the building, leading to many interactions between the structures. Lastly, (Filiatrault et al., 1994) concluded that from a floor-to-column pounding, large shear forces in the column above the contact point would be generated compared to pounding of a similar structure with floors of the same elevation, which has been later analytically proven by (Karayannis and Favvata, 2005b) and (Mariam Ehab et al., 2014).

In 1992, an earthquake occurred in Cairo, Egypt leading to catastrophic damages, 350 buildings were entirely destroyed, and 9,000 others were severely damaged, leading to 545 fatalities and 6,512 injuries, resulting in over 50,000 citizens being homeless (Mariam Ehab et al., 2014). Figure 2.3 and Figure 2.4 show examples of structural collapse from the Cairo earthquake. After this destructive earthquake, Egyptian authorities changed their structure's design codes and provisions to account for the modified hazard maps resulting from building collapse and control major

structural elements' damage. Additionally, Egyptian regulations introduced a mandatory gap distance between neighbouring structures for all new constructions to consider the multiple pounding incidents resulting from the seismic events. The first official code towards seismic loading was published by the Ministry of Housing, Utilities and New Communities in 1989 - the Reinforced Concrete Code (ECP 1989). This code alternatively overlooked a more significant number of primary seismic considerations, such as the influence of soil conditions and the dynamic properties of buildings (Abdel Raheem, 2013). The 2004 Egyptian code largely follows the same philosophy adopted in EC8 (ECS 2004; UBC 1997). In some codes such as ECP 203 (2007), ICB (2003), and the UBC (1997), the minimum required Gap Distance ($d_{g,min}$) can be calculated as per Equation (1). Structures built before these new design codes and regulations may have an uncontrolled maximum lateral displacement, leading to an unpredicted pounding behaviour for new structures being designed.

$$d_{g,min} = \sqrt{(\Delta_1)^2 + (\Delta_2)^2} \hspace{3cm} \text{Equation (1)}$$

Where $\Delta 1$ is the maximum displacement for one of the adjacent buildings, and $\Delta 2$ is the maximum displacement for the second building at the same level considered in the first building.

Figure 2.3. Failure of a load-bearing masonry house in Cairo adapted from (Badawi and Mourad, 1994)

Figure 2.4. The complete collapse of a 14-storey reinforced concrete residential building in Cairo adapted from (Badawi and Mourad, 1994)

In another large-scale seismic event, an earthquake occurred in 2011, affecting Christchurch, New Zealand (Cole et al., 2012), where the building damages and failures were reported to be resulting from structural pounding. Building conditions were investigated in their study for local damages and their contribution to the global failures of the structure. A total of 374 buildings were inspected during their research. While the pounding observed was a secondary effect for the structures, over

6% of the total surveyed buildings were detected to have significant or more remarkable pounding damages. There were 51 buildings in the location of the Christchurch earthquake, and it consisted of low-rise structures involving little to no separation gap. Over 65% of the structures were only two stories tall, while 6% were over ten stories. It was also reported that 45% of the structures were made of concrete, 45% were made of unreinforced masonry material, while only 6% were made of steel. Buildings with no separation were observed to be 93% in the pounding incidents, while only 5% ranged from 1-50 mm in separation distance and 51-100 mm there was only one structure involved. Out of the total 374 structures observed, 119 were involved in pounding damages. Within the 119 structures, 26 buildings were ranked as significant damage towards pounding, 18 structures involved were classified as partial collapse, and two of the structures had a total failure. The other 73 structures had minor or no structural damage. Figure 2.5 and Figure 2.6 show structural collapses due to building pounding involved in the 2011 Christchurch earthquake. Table 2.1 and Table 2.2 explain these figures by indicating the damage categories and confidence levels of these building damages. (Chouw and Hao, 2012) prepared another study exploring the multiple structures involved in this earthquake event and compiled a report regarding the buildings that conducted pounding excitation. Structures reported were also involved from a previous main shock back in September 2010, causing several thousand buildings to have already weakened in structure. Further failures occurred following the 2011 Christchurch earthquake, leading to many structures experiencing internal and/or global failures from the pounding of structures and bridges. (Chouw and Hao, 2012) agreed with (Cole et al., 2012) conclusions that pounding due to earthquake excitation can occur to tall structures and relatively low structures such as one or two stories. In addition, unreinforced masonry material buildings were the most

vulnerable to damage from pounding, especially ones with large windows or door openings (Figure 2.7).

Table 2.1. Damage categories based on (Cole et al., 2012)

Icon	Damage level	Description of pounding damage
	0	None: building involved in pounding, however no evidence of damage was found
	1	Minor damage: damage to non-structural elements, or isolated hairline cracking
	2	Damage at contacts: local spalling or crushing damage at the interface between buildings, or substantial damage or collapse of parapets
	3	Significant damage: cracks greater than 1 mm extending along load paths or present in multiple locations on the building
	4	Partial collapse: loss of a facade or similar size component
	5	Complete building collapse: the collapse of a building storey or greater damage

Table 2.2. Confidence levels based on (Cole et al., 2012)

Icon	Confidence level	Description
	Low	Evidence of pounding is present; however, pounding may only be a secondary factor for the observed level of damage. Alternatively, specific details for damage are unavailable because of the collapse of demolition
	High	Damage follows laid paths that indicate building collision or damage patterns are consistent with pounding damaged structures observed in previous earthquakes
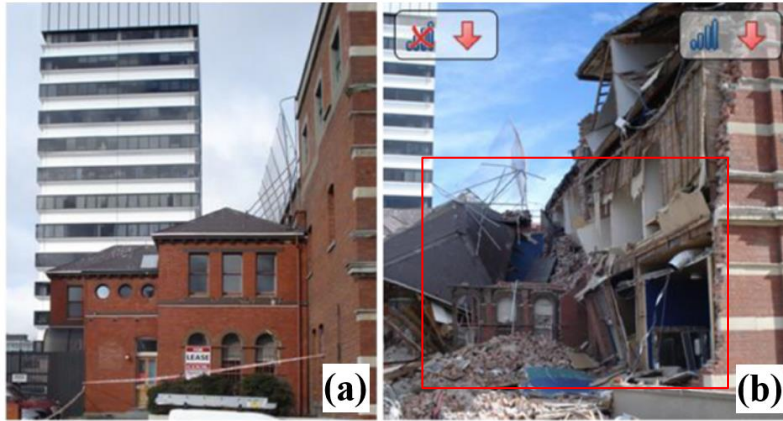
Figure 2.5. Damage to unreinforced masonry buildings: (a) after the Darfield earthquake; and (b) after the Christchurch earthquake, adapted from (Cole et al., 2012)

Figure 2.6. Pounding damage to masonry buildings: (a) damage after the Darfield event (panoramic image); and (b) damage after the Christchurch event, adapted from (Cole et al., 2012)

Figure 2.7. Pounding between unreinforced masonry and reinforced concrete buildings, adapted from (Cole et al., 2012)

2.3.2   Out-of-phase pounding incidents

Structures within metropolitan cities are typically built within proximity and commonly have many different dynamic properties. Adjacent tall buildings can experience out-of-phase vibrations due to the difference in their dynamic properties (Jankowski, 2009; Kasai and Maison, 1997; Maison and Kasai, 1992). During the 1971 San Fernando earthquake, a study from (Jankowski, 2009) examined the pounding failure of the Olive View Hospital main building and one of its independently standing stairway towers shown in Figure 2.8. The seismic joint to separate the stairway tower and main building was insufficient to accommodate the actual lateral displacement during this seismic event. (Mahin et al., 1976) reported that the main building's impact with the tower had a much more significant effect on the subsequent seismic response, in addition to the distributing damage, leading to an out-of-phase occurrence of pounding. The damage reported had appeared to be the consequence mainly of intensive ground motion and partly of the inadequate structural system. The damages reported are believed not to be caused by the foundation failure nor by the defective material used or their installation. Jankowski's results concluded that the

collision led to a significant increase in the response of the lighter stairway. Additionally, it resulted in a substantial increase in the range and intensity of damage at the structure's base because the heavier main building was found to be slightly influenced by structural interaction. With the additional study of (Jankowski, 2012), a similar outcome as previously mentioned (Jankowski, 2009) can be concluded, but for non-uniform earthquake excitation. The study employed the same parameters from the Olive View Hospital main building and stairway tower. It was stated that uncertainty is related to structural interactions during similar earthquakes could come in several other aspects. Lastly, it was reported that the accuracy of the numerical analysis could be increased if additional parameters were taken into consideration. Such considerations can include the concrete confinement, the soil-structure interaction, possible spalling of concrete cover, buckling of reinforced concrete, and slip interfaces between the reinforced steel and the concrete.
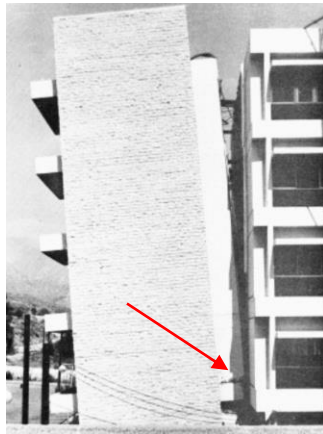
Figure 2.8. Permanent tilting of a stairway tower; San Fernando earthquake, 1971, adapted from (Jankowski, 2009)

(Kasai and Maison, 1997) explored building pounding damage during the 1989 Loma Prieta earthquake, which was an extension of the study by (Kasai et al., 1992). (Kasai and Maison, 1997) examined more than 200 pounding occurrences involving more than 500 building structures. The hypocenter of the 1989 Loma Prieta earthquake was located 19.5 kilometres below the ground surface on the San Andreas Fault and had an earthquake of 7.1 on a Richter scale. Structures

involved in the pounding phenomena were typically constructed prior to 1930 and are primarily multi-storey structures. The buildings built before 1930 that were involved in the investigation mainly were constructed with masonry, either having or not having a steel skeletal vertical load resisting system. The number of modern structures involved in the pounding phenomena was very few at the time of the event. Four divisions were alienated by a ranking of damage, ranging from usable structures with minor damage to nature (Type-4 damage) to typically unusable until the structural damage from pounding is repaired (Type-1 damage). Within the reported 200 pounding incidents involved, 38 (21%) structures were reported as Type-1 damage whereas 144 (79%) were reported as Type-4 damage. The heights of the structures involved ranged from two stories to over 20 stories tall, however, structure heights and building materials ranged drastically depending on the location within the city. Examples of structures involved in the Loma Prieta earthquake were examined in detail. One example observed was a ten-storey structure constructed out of masonry and combined with a steel skeleton that was built before the 1906 San Francisco earthquake and was involved in pounding with a massive five-storey structure built with reinforced concrete. The five-storey structure was eight times the square floor area of the ten-storey building and was seismically upgraded in the early 1980s by adding steel concentric braces to increase its lateral stiffness. The collision of the two structures was located at the sixth level in the ten-storey structure and roof level of the five-storey building, shown in Figure 2.9. The building separation gap was only 1 inch to 1.5 inches as was exceeded mostly from the ten-storey structure during the event of this earthquake, resulting in structural damage for the ten-storey building due to an out-of-phase vibration. Similarly, another ten-storey reinforced concrete structure was built in 1965, which experienced significant structural damage by exceeding a 2-inch separation gap with its neighbouring tower. This structure was in collision with a seven-storey structure made out of

45

reinforced concrete for the lower four stories and steel for the remaining three stories due to out-of-phase pounding vibrations. Many of these examples involved in pounding included at least one structure over ten stories tall. The pounding produces sharp, irregular motions and large high-frequency lateral accelerations, which can result in amplifying the forces in the appurtenances by having high vibration frequencies. Such pounding incidents were analytically proven by (Kasai et al., 1990) and experimentally demonstrated by (Filiatrault et al., 1995).
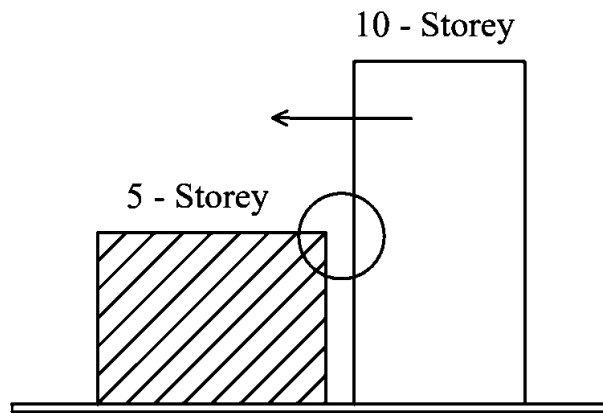
Figure 2.9. Example of pounding damage (Mission Street, San Francisco) adopted from (Kasai and Maison, 1997)

2.3.3　　Pounding incidents developed at expansion joints

The majority of structural pounding incidents have been experienced through the external envelope of the structures, causing global failure. Alternatively, local or internal pounding within a structure may also be produced. For instance, colliding of building parts at the construction or expansion joints can lead to local pounding within a structure. Damages from local pounding incidents such as expansion joints have been numerously reported and thoroughly investigated through multiple studies from the past (Comartin et al., 1995; Pantelides and Ma, 1998; Petronijević et al., 2014; Stewart et al., 1994; Wada et al., 1984). (Wada et al., 1984) investigated the collapse of structures built at proximity, causing pounding excitation due to the existence of expansion joints within the structures. When the structures built with expansion joints are subjected to earthquake excitation,

a collision can occur, and the actual horizontal force produced can be greater than the usually expected magnitudes. The latter study detailed how to properly depict a collision behaviour between adjoining buildings, and indicates that this phenomenon is one of the main reasons for the collapse of structures. (Wada et al., 1984) analyzed past incidents such as the Olive View Hospital and stairway tower that occurred in the 1971 San Fernando earthquake, the Kuju Lakeside Hotel Building and the city hall of the Mutsu Municipal Office during the Tokachi-Oki earthquake in Japan. They concluded that although pounding in such structures is likely to concur with particular seismic excitation, many structural designers usually perform seismic designs without considering specific pounding effects. Namely, when buildings cause these pounding phenomena, large impact forces not foreseen in the design stages can occur and may result in many tragic situations.

Another study from (Kasai and Maison, 1997) mentioned in Section 2.3.2 explored another pounding incident located at 11th Street, Oakland City Center that involved a large modern six-storey steel structure occupying an entire city block. This building was built in 1981 and consisted of three segments separated by 4-inch expansion joints. All segment structures consisted of having steel moment-resisting frame systems. One of the six-storey segment structures was initially designed as a 20-storey high-rise building making the segment much laterally stiffer than the other two segments. Comparatively, large relative displacement can develop between the rigid and flexible segments due to very different vibration periods of the segments (Jeng et al., 1992; Jeng and Kasai, 1996; Kasai et al., 1996), leading to the out-of-phase pounding phenomena due to the structure's existing expansion joints. It was noted that during large-scale earthquake events, structures could contribute towards pounding phenomena in many ways leading to structural disasters or failures (i.e., expansion joints).

Bridges that have experienced damages due to pounding-induced incidents have been concluded in past earthquake events. Such events include the 1971 San Fernando earthquake (Jennings, 1971), the 1988 Saguenay earthquake in Quebec (Tinawi et al., 1990), the 1989 Loma Prieta earthquake (Priestly et al., 1996), the 1994 Northridge earthquake (Moehle, 1995), the 1955 Kobe earthquake in Japan (Bruneau, 1998; Bruneau et al., 1996), the Chi-Chi earthquake in Taiwan (1999) (Lee and Loh, 2000), the 2006 Indonesia Yogyakarta earthquake (Elnashai et al., 2007), the 2008 Wenchuan earthquake in China (Li et al., 2008; Qiang et al., 2009), the 2010 Maule earthquake in Chile (Elnashai et al., 2010; Kawashima et al., 2011), and the New Zealand Christchurch earthquake in 2011 (Chouw and Hao, 2012). A state-of-the-art review of seismic pounding between bridge segments has also been conducted by (Miari et al., 2021) to review previous research studies concerning earthquake-induced structural pounding in bridge structures, the factors that influence it and the recommended mitigation measures. (Filiatrault et al., 1993) studied the case of pounding observed on the cable-stayed Shipshaw Bridge, which crosses the Saguenay River about 10 km northeast of Jonquiere, Quebec, as mentioned earlier in Section 2.3.1 (Figure 2.10). The bridge's deck underwent a longitudinal motion and pounded against both abutments (Kenogami and Shipshaw) during the earthquake, shown in Figure 2.11 and Figure 2.12. The repeated pounding caused massive cracking of the concrete covers at the abutments and local buckling of horizontal bracing members underneath the deck. It contributed to the complete failure of one of four anchorage plates connecting the deck to one abutment. (Filiatrault et al., 1993) first performed a static analysis of the bridge under its dead load to understand its state before the Saguenay earthquake, following dynamic analysis to investigate the stress concentrations under the tensile dead load at each abutment. In conclusion, the results from the study demonstrate that the anchorage plates were already subjected to high-stress concentrations

under dead load only prior to the Saguenay earthquake and this event was the direct cause of the failure of an already locally yielded anchorage plate at the ship show abutment. The ultimate stress of the steel and chemical analysis indicated an increase in the brittleness of the steel near the failure surfaces. The study explained that this cause of failure was conducted in a simplified manner, whereas advanced dynamic analysis can be utilized to obtain the complete response of the bridge under the Saguenay earthquake.

Figure 2.10. Overview of the constructed 1992, double-leg steel cable-stayed Shipshaw bridge of 183 m in length, adopted from (Filiatrault et al., 1993)
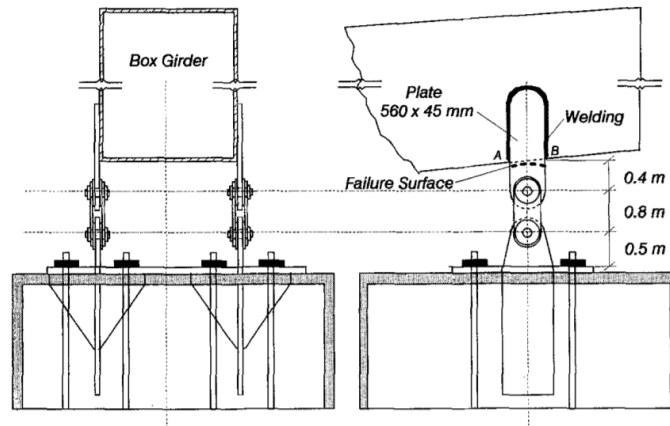
Figure 2.11. Tie-rod assembly at each box girder of Shipshaw abutment, adopted from (Filiatrault et al., 1993)
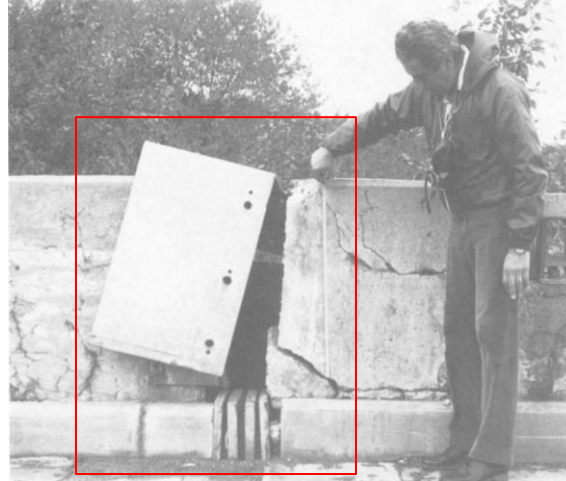
Figure 2.12. Damage to concrete cover at Kenogani abutment, adopted from (Filiatrault et al., 1993)

Additional studies from Earthquake Engineering Research Institute (Schiff, 1999; Stewart et al., 1994) investigated more pounding phenomena due to expansion joints. In 1995 (Schiff, 1999), an earthquake in Kobe, Japan named the Hyogo-Ken Nanbu earthquake caused longitudinal movements along with the elements of the Hanshin Expressway superstructure reaching a displacement upwards of 300 mm, leading to considerable pounding damage located at the expansion joints. In the 1994 Northridge earthquake at the Interstate 5 and State Road 14 interchange located approximately 12 km from the incident of the epicentre, Earthquake Engineering Research Institute (Stewart et al., 1994) found significant pounding damage at the expansion hinges and abutments of the upright portion at a number of bridges.

2.4   Experimental Modelling Towards Pounding

Motivated by the numerous earthquake-induced pounding incidents discussed in Section 2.3, many studies adopted experimental approaches (Chau et al., 2003; Papadrakakis and Mouzakism, 1995; Rezavandi and Moghadam, 2007) and numerical approaches (Anagnostopoulos, 1988; Conoscente et al., 1992; Muthukumar and DesRoches, 2006) to model the structural pounding behaviour during lateral excitation. This section reviews past studies investigating the pounding of tall

buildings using experimental techniques, while the numerical approaches are discussed in the following Section 2.5.

(Rezavandi and Moghadam, 2004) studied different methods of reducing the effect of building pounding during earthquakes with experimental modelling aided by the use of shaking tables. The experimental analysis employed two series of shaking table experiments on small-scale moment-resisting frames subjected to harmonic excitation; in addition, seismic loading was then described. Their study uses a series of experiments regarding some measures to reduce the damping effect of pounding. The criteria used in their experiment included increasing the distance between the buildings, application of impact-absorbing material, and connecting the two buildings. The two small-scale structures consisted of a 1/10 scale size, being individual single-bay moments resisting steel frames. The frames were designed based on the static analysis approach of building codes. The one steel frame was a 6-storey building of 1.5 meters tall, while the other was a 3-storey building of 0.9 meters tall, shown in Figure 2.13. The shaking table utilized three different earthquake ground motion records (i.e., Tabas, Nagham and El Centro). The experiments conducted vibrations of the structures (i) without a pounding phenomenon, (ii) with pounding of structures spaced at 5.0 mm and 10 mm, (iii) with pounding while polystyrene material is installed on the third floor of the 6-storey building, (iv) the two structures are connected just at the third floors, and (v) structures are connected at their first and third floors of the structures. The results from their experimental analysis concluded that, at full-scale, no pounding would occur with spacing as 100 mm between structure and vibration amplitudes of 10 mm neither with vibration amplitudes of 20 mm and frequencies of 1 and 1.5 hertz. It was observed in their study that when the two structures had a spacing of 50 mm, the acceleration decreased with the decrease in vibration amplitude. Additionally, with the increase in distance between the two steel frame

51

structures, if pounding occurs, acceleration response will also increase due to the increase in velocity. Acceleration response, although, significantly decreases when polystyrene is installed. Lastly, they concluded that the maximum responses occur at a frequency equal to 2.5 Hz when the two frames are connected because an increase in the stiffness of the combined structure will occur. Therefore, connecting the two steel buildings will reduce their responses, leading to a lower pounding risk.

Figure 2.13. View of two structures on shaking table, adopted from (Rezavandi and Moghadam, 2004)

(Chau et al., 2003) applied experimental simulations to investigate seismic pounding between two adjacent structures. Shaking tables were used to simulate the earthquake excitation to investigate the pounding between two steel towers. The towers tested were conducted with different natural frequencies and damping ratios. The buildings were subjected to a sinusoidal excitation, in addition to the 1940 El Centro earthquake (Pantelides and Ma, 1998). They were built with four hollow steel columns cross-section being 2 meters in height with steel plates on the top of the structure conducting a size of 1.0 meters by 0.6 meters, shown in Figure 2.14. Their study uses alternating

mass and damping ratios of two towers to investigate different pounding phenomena. It also finds the minimum space gap distance where no pounding can occur between the two structures by establishing a function of the excitation frequency. A total of 190 pounding experiments were investigated by alternating the dynamic characteristics of the tower structure, changing input excitations and lastly, various separation distances between the two structures. Results concluded that either chaotic or periodic pounding occurs non-linearly on the changes in parameters of the two adjacent structures and ground motion characteristics. Namely, gap spacing and ground motion alone can lead to a completely different pounding excitation between two structures. Additional studies were also examined through analytical and numerical predictions from past reports and compared with the experimental analysis.
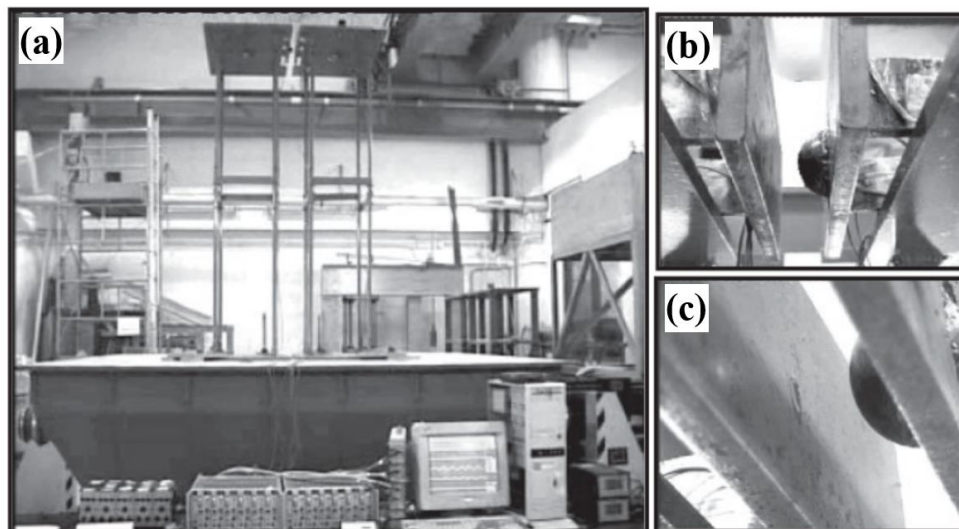
Figure 2.14. Shaking table tests: (a) showing two steel towers on a shaking table for the pounding experiments; (b) showing the contact; and (c) indentation mark after experiments, adopted from (Pantelides and Ma, 1998)

An additional study from (Rezavandi and Moghadam, 2007) employed experimental and numerical studies for the pounding effects and mitigation techniques on adjacent structures. The parameters of their research utilized similar models and shaking table ground motions as the previous study used from (Rezavandi and Moghadam, 2004). The experimental results were

compared to the numerical analysis results. The Finite Element Method (FEM) was conducted to test similar elements and materials for the 2-D structures as the experimental investigation for their numerical analysis. Results from the experimental study concluded that the frame acceleration response was reduced by using impact-absorbing materials. Connecting the framed structures on a floor level will reduce both analytical and experimental responses. However, joining the frames with two levels did not improve the displacement nor acceleration. A significant increase in response can occur by increasing the structure's spacing and still having pounding occurring. Alternatively, insufficient space gaps generally intensified the acceleration responses of the frames. Although there were some sources of error in the experimental practice, both analytical and experimental analysis showed acceptable agreements with respect to in-phase motion and maximum absolute displacement.

(Jankowski, 2010) also used experimental analysis for the earthquake-induced pounding phenomenon. The study aimed to analyze two experiments concerning interactions between elements made of different building materials (i.e., steel, concrete, timber and ceramic) towards structural pounding phenomena. The first experiment includes a weighted ball of different mass dropping from various heights onto a rigid surface. The second experiment involved a comparative shaking table with two adjacent structural models made of different materials to focus on the colliding elements once pounding is applied. With the second experiment, two similar, one-meter tall structure models were designed with different dynamic properties on the top of the building for the experimental testing, as shown in Figure 2.15 and Figure 2.16. The experimental study was conducted under the 1940 El Centro earthquake. A spacing gap size of 40 mm between the modelled structures was conducted, being constant for each different material testing of pounding. The study results from the experimental analysis can confirm that the structural pounding may lead

to the considerable amplification of the response. Additionally, it may also play a positive role by reducing vibration in some cases. The highest increase in peak displacement examined was obtained from the steel structure. At the same time, timber-to-timber pounding was lower in peak displacement, which can be attributed to their lower masses.

Figure 2.15. Overview of the experimental setup of the shaking table and adjacent framed structures with different top-mounted properties, adopted from (Jankowski, 2010)
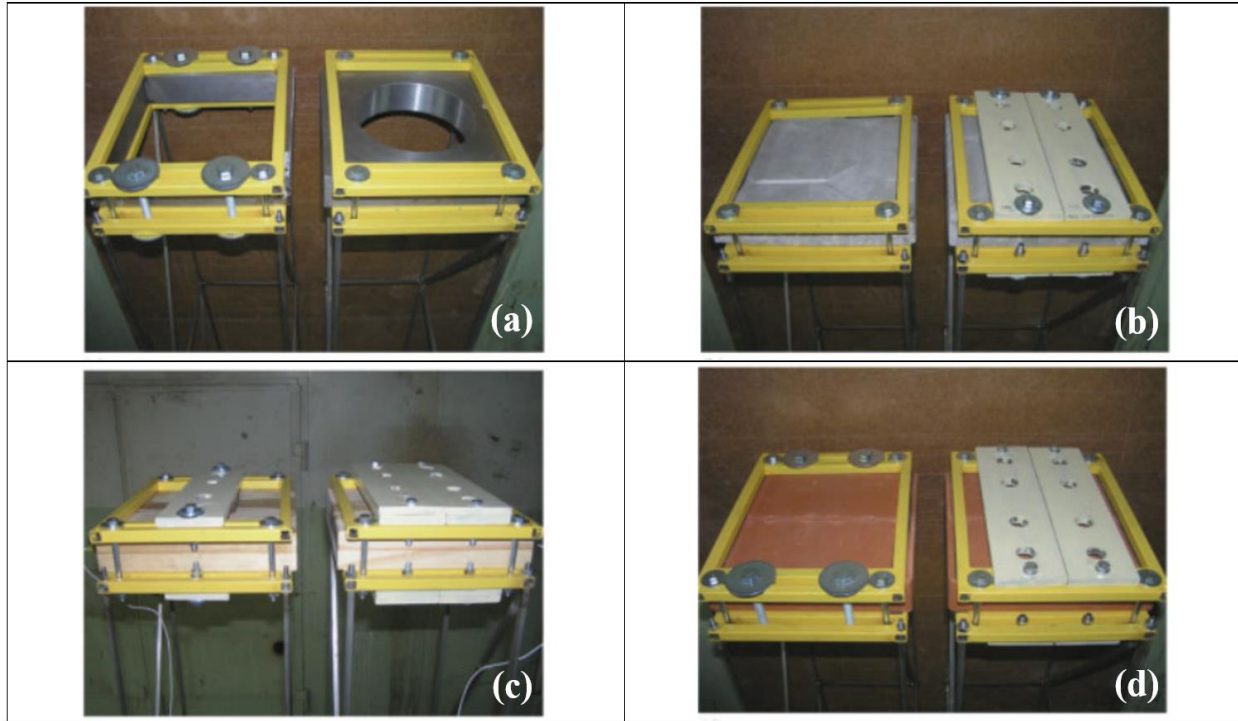
Figure 2.16. Replaceable elements mounted at the top of the towers (with additional weights): (a) steel elements; (b) concrete elements; (c) timber elements; and (d) ceramic elements, adopted from (Jankowski, 2010)

(Favvata et al., 2013) studied a similar research topic relating to concrete and steel structures interactions. Their study showed that the RC structures are more vulnerable in two specific locations. Firstly, more vulnerable at the top columns concerning flexural and ductility demands. Secondly, at the bottom columns regarding the shear and ductility demands. However, the steel structures are affected mainly at the top of the columns regarding flexural and shear demands, whereas the bottom columns are only affected by flexural demands.

Later, (Sołtysik and Jankowski, 2016) compiled a research study related to the collision of adjacent steel structures while subjected to earthquake excitation using experimental and numerical methods. The study aimed to investigate the influence of pounding effects between three insufficiently separated steel model structures due to the structural response under earthquake excitation from shaking tables. Figure 2.17 shows the three adjacent steel structures with different

dynamic properties used for their experimental analysis. Each tower was one meter tall with the addition of skew bracing to prevent the structures from transverse and torsional vibrations. Additional masses on top of each structure were added to obtain different dynamic properties for each tower. The model consisted of two concrete plates weighing 42.4 kg on each external structure, while only one plate was mounted on the middle tower. The shaking table was unidirectional and was under three different earthquake excitations. A scaled-down version of these earthquakes was considered to prevent any severe damages to the analyzed models. Separation spacing between structures was tested at 30 mm and 40 mm. In conclusion, after the experimental and numerical analysis was complete, the studies indicated that the pounding between adjacent structures might lead to a significant change in their response during certain earthquake phenomena. The pounding of structures can increase or decrease depending on the alteration of its peak response. Additionally, while the response is decreased, the effect of interactions may result in considerable damage within locations of structural impact under these earthquake events. This statement also agreed with (Rosenblueth and Meli, 1986) and (Vasiliadia and Elenas, 2002) study.
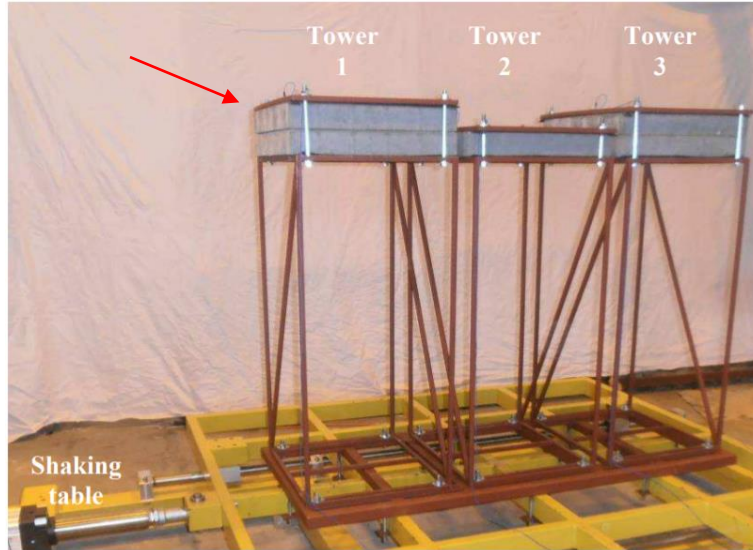
Figure 2.17. Experimental setup of three, 1 meter tall, adjacent models of steel tower structures with different dynamic parameters, adopted from (Sołtysik and Jankowski, 2016)

Although experimental approaches in modelling the pounding phenomena appear to be accurate, they fail short in properly matching the dynamic structural characteristics of the building. In addition, it is difficult to experimentally measure the impacting force developed due to pounding, which may be required to be considered while designing or assessing buildings at proximity.

2.5   Numerical Modelling Towards Pounding

As mentioned previously, this section reviews past reports and studies that have explored and analyzed the pounding of structures through numerical methods. The first part details the use of a single-degree-of-freedom analysis towards structural pounding from past investigations, following part two with similar emphasis, but with the aid of multi-degree-of-freedom analysis. More specifically, both subsections gather evidence from past reports and studies and investigate critical information about how numerical modelling can help depict structural pounding.

2.5.1   Single degree of freedom and one-directional pounding analysis

Studies with the assists of numerical analysis have examined building response from pounding with the use of single-degree-of-freedom (SDOF) systems (Chau and Wei, 2001; Lopez-Garcia

and Soong, 2009; Pantelides and Ma, 1998; Wolf and Skrikerud, 1980) and one-directional research (Bi et al., 2009; Komodromos, 2008; Sarebanha et al., 2018; Sarebanha and Mosqueda, 2017). For instance, (Pantelides and Ma, 1998) explored the behaviour of structural systems once subjected to linear and nonlinear pounding aided with SDOF analysis. They modelled their structural systems as SDOF structures using elastic and inelastic structural assumptions and making the pounding model a Hertz impact force. For numerical evaluation of the seismic structural responses, artificial, actual earthquake excitations and realistic parameters for the pounding model was used. This evaluation was utilized to examine the effects of separation distance and inelastic structural behaviours on the magnitude of the pounding forces applied. Results from numerical simulations concluded that the pounding response is not sensitive to the exact value of the impact stiffness parameter. These parameters are related to the materials of the two structures that proceeded to make contact during the pounding phenomena. Within structures that have different natural periods, the same earthquake excitation can produce different magnitudes of pounding forces and resulting structural responses. If structures are flexible with producing periods longer than 0.3 seconds, a significant reduction of pounding can occur by increasing its effective damping by either utilizing passive or active structural control devices. Without doing so, these flexible structures can lead to more significant failure from such pounding phenomena. It was also found that the seismic separation for the SDOF was less than the seismic gap designed in the Uniform Building Code for earthquake provisions. Meaning the building codes are being conservative with the design of the seismic separation gap.

A study from (Chau and Wei, 2001) employed a non-linear Hertzian impact analysis between two oscillators under harmonic earthquake excitation to model pounding between two adjacent structures. Their findings were further carried out from (Davis, 1992) study that examined the

pounding of two SDOF oscillators with different stiffness, mass and damping ratios, as shown in Figure 2.18. Their numerical simulation was conducted to investigate the applicability of analytical solutions for rigid impacts and the maximum impact velocity. A non-linear Hertzian equation derived from (Davis, 1992) was employed. The impact force applied depended on the 3/2 power of the relative displacement between the oscillators and the relative contract stiffness of the structures. This analysis concluded that their analytical predictions for rigid impacts agreed qualitatively with their numerical simulations for non-rigid impacts. They also established that when two oscillators have the same natural frequency, a more significant difference between the damping ratios of the two oscillators will lead to a larger impact velocity, leading to more chaotic impact behaviour for the oscillators. They also discovered that seismic pounding between adjacent structures might induce unwanted damages even though each structure may have been designed adequately to withstand such an earthquake because of the unwanted period shift of existing structures imposed by new buildings in its neighbouring location, which may lead to unprepared and unexpected damages.
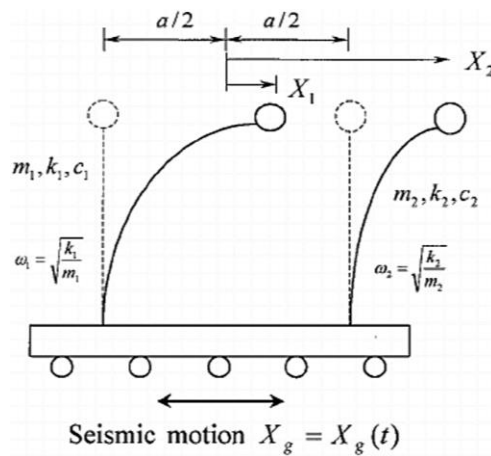
Figure 2.18. Pounding of two adjacent buildings modelled as Hertzian impact of two single-degree-of-freedom oscillators with natural circular frequencies ω_1 and ω_2, adopted from (Chau and Wei, 2001)

(Lopez-Garcia and Soong, 2009) investigated seismic pounding between linear structural systems to acquire adequate separation to prevent these pounding phenomena using modelling SDOF systems. Their study examined the accuracy of the double-difference combination rule in predicting the required separation gap between two structures to avoid the essential pounding from seismic excitation. An earlier agreement was also brought from (Kasai et al., 1992) for using the accuracy of the double-difference combination rule in finding required avoidance seismic gaps. Accordingly, the double-difference combination rule is illustrated as follows:

$$S = \sqrt{X_A{}^2 + X_B{}^2 - 2\rho X_A X_B}$$
Equation (2)

where X_A is the maximum displacement for the first building, X_B is the maximum displacement for the second building at the same level considered in the first building, and ρ is the cross-correlation coefficient commonly used in the complete quadratic combination rule of modal responses of linear multi-degree-of-freedom structures, provided from (Grigoriu, 1981; Kiureghian, 1980).

Although pounding can typically arise when two adjacent structures in proximity develop a lateral deflection, one-direction pounding can also occur when one structure is isolated, making interaction with its adjacent structure considered completely rigid (Komodromos, 2008; Sarebanha et al., 2018; Sarebanha and Mosqueda, 2017). A study from (Komodromos, 2008) uses a numerical simulation to investigate how potential pounding affects the effectiveness of seismic isolation from seismically isolating buildings with adjacent structures. In the study, (Komodromos, 2008) conducted a superstructure as a shear-beam building with lumped masses at the floor levels, which remained elastic during experimental earthquake excitation. At the base level, the modelled structure consisted of using a linearized model with effective stiffness and damping. The moat wall and the floor mass at the isolated level were considered as one-directional pounding impact for a

seismically isolated building. The pounding in the analysis was modelled using a nonlinear Hertzian impact model. (Komodromos, 2008) concluded that in certain locations of a seismically isolated structure, pieces of flexible material with damping properties can be added and used as a shock absorber.

Other studies consisting of one-direction pounding were also involved in expansion joints within structures. Such examples can be found in bridge abutments or in-between bridge decks where complete avoidance of pounding within such structures is often near impossible. As previously mentioned, more considerable separation distances between adjacent structures are needed to avoid pounding completely. However, in expansion joints for bridges, increasing the separation gaps is limited to ensure a serviceability condition for smooth traffic flow. (Chouw and Hao, 2008) found that a few centimetres of a gap size for a conventional expansion joint will not be adequate to eliminate possible pounding occurrences, even if the adjacent bridge decks have the same fundamental period. (Bi et al., 2009) investigated the required separation distance between two adjacent bridge decks and between the bridge decks and adjacent abutments using a modular expansion joint subjected to the influence of spatial variation of ground excitations. This was a further analysis from (Bi et al., 2008; Hao, 1998). In (Bi et al., 2008) analysis, their modelled structure was simplified. The bridge decks were assumed to be rigid with lump masses and connected with one degree of freedom to the model of the bridge, which was considered a six degree of freedom structure. The two bearings located on the abutments and the pier for each deck were assumed to have the same dynamic characteristics. The stiffness and damping characteristics were considered one-directional at such locations for such pounding incidents in their study.

2.5.2   Multi-degree-of-freedom pounding analysis

Other studies have altered their examination for structural pounding with the utilization of multi-degree-of-freedom (MDOF) (Anagnostopoulos and Spiliopoulos, 1992a; Mariam Ehab et al., 2014; Karayannis and Favvata, 2005b; Kasai and Maison, 1997; Lin, 1997; Maison and Kasai, 1990, 1992; Papadrakakis et al., 1996b, 1996a), which was found to provide more reliable matching to the pounding behaviour due to being able to capture the higher-order vibration modes (Ye et al., 2013). (Maison and Kasai, 1990) investigated the dynamic varieties of structural pounding with the formulations and solutions of the MDOF equations for high-rise structures. Assumptions were made in the presence of their study for pounding occurrence as follows. The pounding would occur at a single floor level in the building of interest, and the floor diaphragms are rigid in-plane. Namely, the forces from the pounding were distributed to all the structural elements connected to the singular floor level. The structure of interest dynamically vibrates, and the adjacent structure would be rigid. Therefore, the building of interest would be very flexible and have a relatively low mass. Additionally, the point of contact during the collision coincides with a linear spring that represents the local flexibility of the structure. Lastly, two linear states were idealized for the pounding phenomena, as state one was the structure of interest vibrates by itself, and state two was that the buildings were in contact. A nonlinear problem results as the response oscillates from one linear state to another. The structure of interest was the University of California Medical Center building located in San Francisco, California, as this structure has been the subject of previous studies (Maison et al., 1983; Neuss et al., 1983; Rea et al., 1968). Although this structure is not close to adjacent structures, their analysis uses hypothetical scenarios where the structures are within proximity. The structure examined was a 15-storey steel building that had a moment-resisting frame shown in Figure 2.19. The study was conducted where a non-damped pounding occurred in four different cases. The first case of pounding was at level four, the second

one was at level eight, the third one was at level twelve, and the last one was at the top of the fifteenth level. Within each of those cases, separation distance was also altered. Three levels within each pounding case were conducted. In contrast, the first, second and third level of separation was applied at 90% (18.5 mm), 50% (10.4 mm), 0% (0.0 mm) of the peak displacement from the level in which pounding is ignored, respectfully. After analysis, the conclusion concurs that the storey drifts, shears, and overturning moments in the stories about the pounding elevations will be underestimated. Secondly, extrapolation may be used to assist in the building design process if the physical problem characteristics are similar to those employed, which was indicated in the response behaviour trends from the sample analysis. Lastly, recommendations towards pounding should be evaluated on a case-by-case basis using dynamic analysis. Analytical application tools utilized in their study can be applied to obtain insight into the possible pounding behaviours, provided the formulation presented in their study applies to the particular problem of interest.
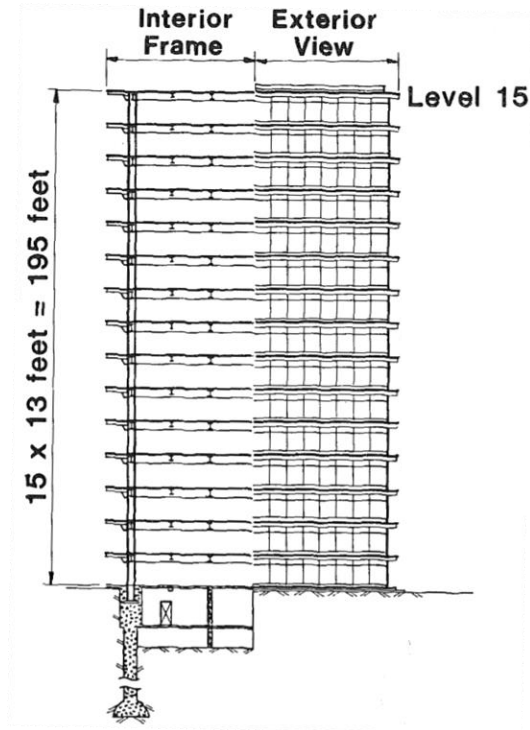
Figure 2.19. 15-storey tall steel building studied with a moment-resisting frame, adopted from (Maison and Kasai, 1990)

Studies for local effects from reinforced structural pounding have also been numerically investigated by past scholars (Mariam Ehab et al., 2014; Karayannis and Favvata, 2005b) through the use of MDOF analysis. The study from (Karayannis and Favvata, 2005b) considered the local effects such as inelastic flexural deformation, the yield of the flexural reinforcement, and ductility requirements of the columns in the pounding area, through the unique purpose elements employed for the modelling towards the columns of their structure. Their study used non-linear dynamic analysis to investigate two adjacent structures made out of reinforced concrete of non-equal heights, ranging in height differences. Additional studies from (Karayannis and Naoum, 2018a, 2017a, 2017b) are also gathered and explained later with a further investigation relating to this study. The structures were modelled as a 2D assemblage of non-linear elements and were connected at the nodes. The contact elements within the simulation were considered special-

purpose contact elements located at the impact locations of the structures examined. The elements would only become active when the corresponding nodes of the two adjacent structures coincide (make contact with each other); otherwise, the contact elements would remain inactive. The contact elements in any investigation is an essential aspect to be considered because it can further determine failures such as local or global effects. Local effects within their study, such as ductility effects within the columns of the contact locations, the yield of the flexural reinforcement, and inelastic flexural deformation, were considered through their special purpose elements employed in modelling the columns. Their analysis also accounted for damping to be considered within the contact elements. Each structure responded dynamically and vibrated independently. The finite element mesh was applied to model each structure and used a one-dimensional element for each structural member. Seventy-Two pounding cases of multi-storey buildings with unequal total heights were examined. The collision of structures occurred between equal heights of the structural floor slabs and was defined as 'Type A' pounding. Accordingly, thirty-six pounding cases of multi-storey buildings with unequal total heights were investigated. The collision of the structures occurred from one structure's floor slab hitting the column of the other structure. Such collision is defined as 'Type B' pounding and is shown in Figure 2.20. The most important remark for 'Type B' pounding was concluded by the local response of the external column of the tall structure. This local failure of the column can lead to a partial or total collapse of the potential tall structure, depending on the severity of pounding that occurs. 'Type B' pounding to the column is also concluded as the most critical condition due to shear action if the pounding exceeds the shear strength of the column. The column appears to be critical due to high ductility demands if the two structures are in contact from the beginning. It was also observed that the ductility demands for

the column that suffers the pounding substantially increased compared to the ones away from pounding.
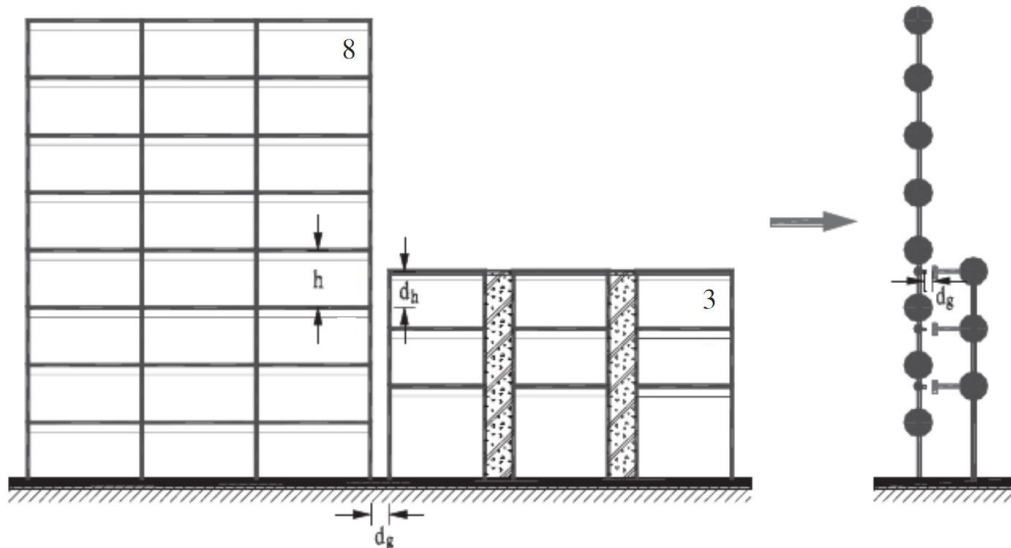
Figure 2.20. The numerical model of the two structures examined having unequal total heights and the heights of the storey levels not being equal, leading to a 'Type B' pounding, adopted from (Karayannis and Favvata, 2005b)

A study from (Papadrakakis et al., 1996b) explored the effect of a pounding phenomenon of two adjacent three-dimensional structures during earthquake excitations with aligned and nonaligned rigid horizontal diaphragms, in addition to linear and nonlinear structural responses. The dynamic contact conditions for the velocities and accelerations in the three-dimensional structures were taken into account from the developed formulations in their report. The contact points were determined geometrically from the displacements of the diaphragm center of mass. After examination, the results were to be compared to those based on the Lagrange multipliers approach. The adjacent structures consisted of two, five-storey tall reinforced-concrete buildings shown in Figure 2.21 subjected to natural earthquake motions from the Kalamata earthquake with elastic and inelastic structural responses. The structures were modelled as MDOF systems with finite elements assuming rigid slab response at each floor. The investigation involved dynamic linear behaviour without pounding, dynamic nonlinear behaviour without pounding, dynamic linear

67

behaviour with pounding and lastly, dynamic nonlinear behaviour with the pounding. In conclusion, the proposed formulation provided an efficient and reliable tool for studying the pounding phenomenon of adjacent buildings during earthquakes while considering three-dimensional simulation and nonlinear structural response. It was also found that buildings may suffer significant rotation when eccentric pounding occurs between the two structures. Lastly, when the induced input energy enters both structures when pounding, the nonlinear response is less than the corresponding generated energy with linear response.
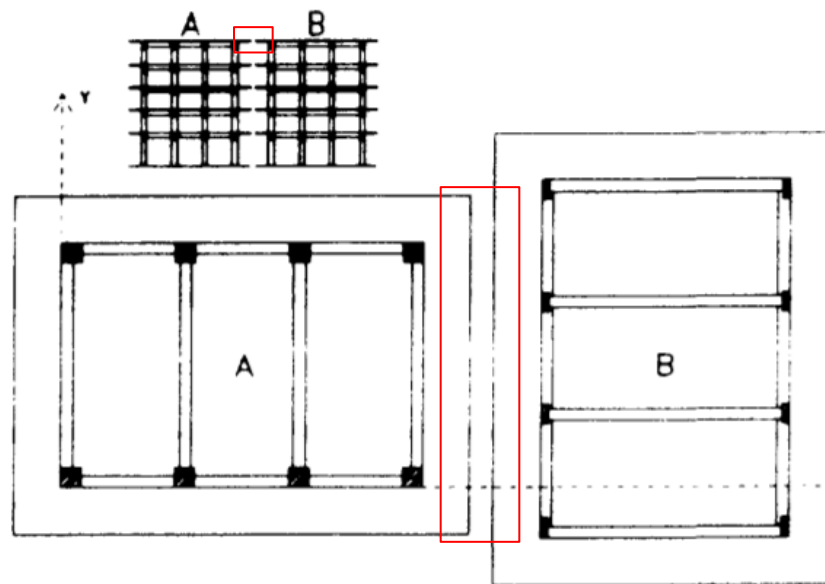
Figure 2.21. The general arrangement of the two adjacent five-storey buildings where building "A" is considered as a stiff structure and building "B" as a flexible structure, adopted from (Papadrakakis et al., 1996b)

A three-dimensional simulation of structural pounding during earthquake occurrences was analyzed from (Papadrakakis et al., 1996a). The three-dimensional model was developed to simulate the pounding phenomenon for the response of two or more adjacent structures during earthquake excitation. Their study used the Lagrange multiplier method for the contact-impact problem. The structures were modelled as MDOF finite element model while accounting for the possibilities towards contact between slabs and columns. The elastic analysis was carried out for

68

El Centro and Kalamata earthquake motions. Three two-storey buildings in orthogonal directions in plan with the aligned floor levels were tested in a dynamic contact problem as shown in Figure 2.22. The building at the corner is considered stiff, while the remaining two structures adjacent to it are considered flexible and have identical dynamic characteristics. The structures are discretized with one beam element for the simulation of columns and beams and four-node rectangular plane stress elements for the simulation of slabs. Four pounding cases were carried out in their study. Case one was considered with two structures pounding, case two employed three buildings by orthogonal pounding, case three utilized two structures pounding with stiffness irregularities in-plan, and lastly, case four applied three-building orthogonal pounding with stiffness irregularities in-plan as well. These cases can be viewed in Figure 2.23 for further understanding. In conclusion, when additional loading to stiff buildings suffers while pounding occurs along with one or two orthogonal directions, pounding is more pronounced when more flexible structures surround them. Results concluded that different arrangements in the two-building pounding cases (e.g., stiff-flexible) could change the amplification factor of up to 200%. A combination of flexible and stiff adjacent structures results in an amplification effect during pounding on the rigid structures for all cases considered. This amplification is particularly when the excitation is near the resonance of the flexible building and in a mitigation effect on the flexible structures in most cases.
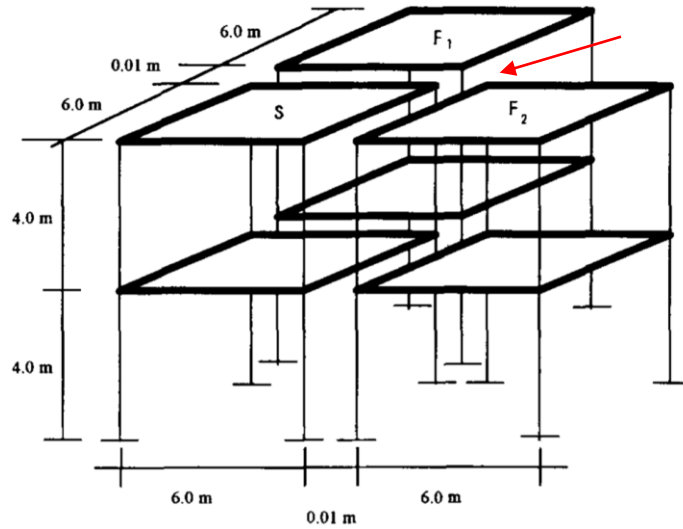
Figure 2.22. Overview model of experiment two and four with three, two-storey adjacent structures with stiffness irregularities: Contact system layout: S = Stiff building; F_1, F_2, = Flexible building, adopted from (Papadrakakis et al., 1996a)
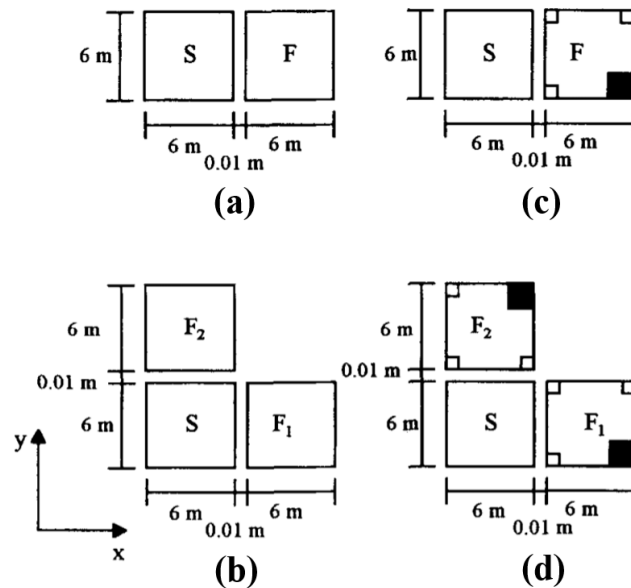
Figure 2.23. Plan view scenarios of adjacent buildings: (a) two-building pounding; (b) three-building orthogonal pounding; (c) two-building pounding with irregularities in stiffness; and (d) three-building pounding with irregularities in stiffness, adopted from (Papadrakakis et al., 1996a)

A further study from (Karayannis and Naoum, 2018a) used a similar model as previously mentioned in (Karayannis and Favvata, 2005b). The study was to analyze pounding cases with torsional effect between structures of equal and unequal storey levels which were partly in contact

70

with each other in a non-symmetric way, additionally having a difference in total heights for the structures examined (Figure 2.24 (a)). Initially, earlier studies from (Favvata and Karayannis, 2009; Karayannis and Favvata, 2005a) examined the behaviours, global and local, of structures subjected to a transverse pounding from floor-to-floor structural interactions (scenario one) and floor-to-column pounding (scenario two). Results found that in scenario one, the columns at the contact area experienced a significant increase in the ductility demands in both buildings. However, this may exceed the available ductility values. Additionally, the initial studies found that in scenario two, floor-to-column pounding, only the columns of the taller structure at and above the contact area also experienced significant increases in the ductility demands. This pounding case was then further examined by (Karayannis and Naoum, 2017a), who investigated the torsional effects from asymmetric pounding due to the adjacent interactive structures of the same storey heights with differences in overall building heights and the differences in storey heights with alteration of the total building heights (inter-storey pounding) (Karayannis and Naoum, 2017b). The structures were modelled and analyzed using a three-dimensional analysis through an MDOF computer program consisting of a yielding check based on a three-dimensional yield interaction surface. More than 100 pounding cases were presented for structures of equal storey levels (Type-A) and 100 pounding cases for the structures of unequal storey levels (Type-B). Each pounding case (Type-A and Type-B) was additionally split into two groups. Case 1 being the pounding with high asymmetry as the interaction between structures occurred only one external column of each structure, and Case 2 referring to the occurrence of pounding that took place between two columns of the 8-storey structure and two columns of the adjacent structure (Figure 2.24 (b)). A reinforced concrete structure of a constant storey level of eight designed to specification under EC2 and EC8 (Eurocode) with a shorter variable structure ranging from one storey height to eight storeys was

71

examined in their pounding cases. The gap distances between the two structures ranged from 0 mm, 10 mm, and 20 mm. Their study was based on a nonlinear seismic step-by-step analysis. The contact elements within the simulation were based on a zero-length spring element at the impact locations. The elements would only become active if, at a time step of the performed analysis, the corresponding nodes of the two adjacent structures coincide (make contact with each other). Otherwise, the contact elements would remain inactive. (Karayannis and Naoum, 2018a) stated that when buildings are in partial and non-symmetric contact, seismic interaction may introduce significant torsional oscillations, also referred to as asymmetric pounding. After numerous simulations, the authors concluded that when the adjacent structures are in contact, they will experience the heaviest significances due to the pounding, compared with the interacting structures that had an initial gap distance between the contact points. In addition to their study, they also concluded that the demand for column ductility will be influenced by the interaction of torsional vibration. This will significantly increase the demand towards the columns in contact due to the inter-storey pounding phenomena between the interactive adjacent structures. When this inter-storey interaction occurs, shears in the columns that experience the pounding are very high in comparison to the columns that do not experience this interaction. Lastly, the demit that occurs in this study is of the difference between the pounding of the slab and the column located at the mid-height or at its lower/upper location since it is no clear result, whereas (Doğan and Günaydın, 2009) concluded that pounding at lower/upper part of the column will result in more significant damage than pounding at the middle of the column which is inconsistent to the work of (Rajaram and Ramancharla, 2012) which concluded that pounding at the mid-height is more significant towards damaged failures (Miari et al., 2019).
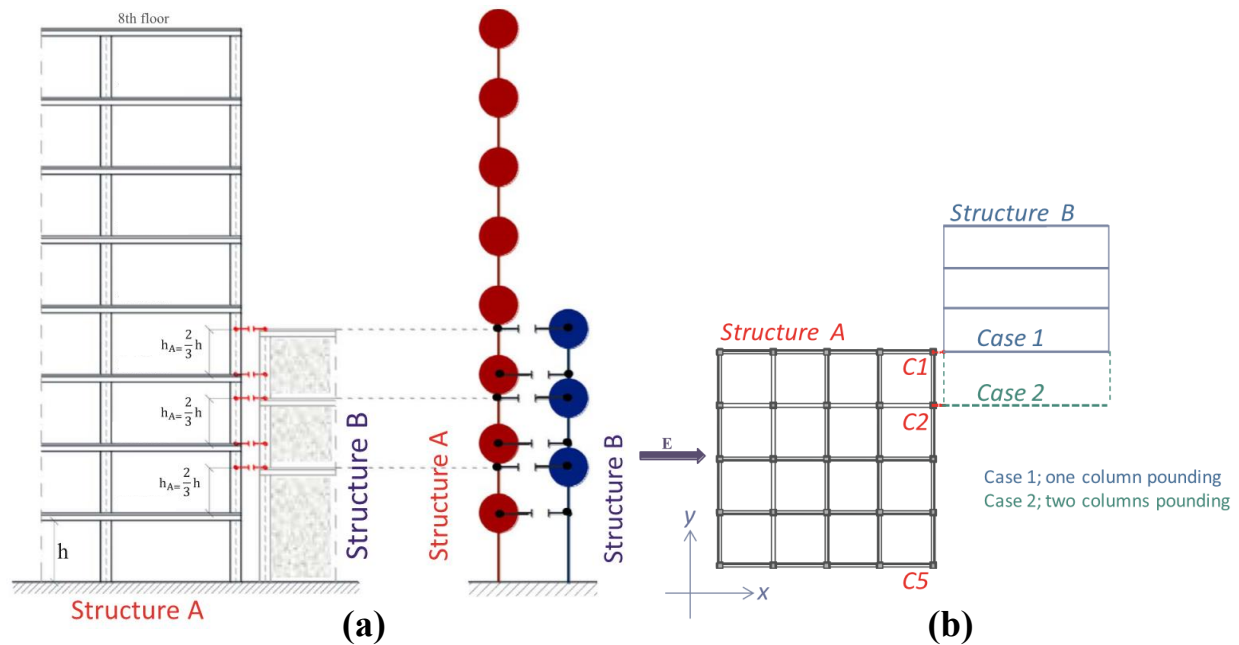
Figure 2.24. The numerical model of the two structures examined: (a) structure B having unequal storey levels ('Type B' pounding); (b) overview of 'case 1' and 'case 2' pounding, adopted from (Karayannis and Naoum, 2018a)

A state-of-the-art method in numerical modelling of structural pounding is being adopted through non-linear FEM analysis, accordingly, while modelling all the structural properties and details of the pounding of structures (Jameel et al., 2013; Jankowski, 2012, 2009; Papadrakakis et al., 1996b; Petronijević et al., 2014; Sołtysik and Jankowski, 2016; Stavroulakis and Abdalla, 1991). The interaction between adjacent structures has been studied from (Jankowski, 2009), as mentioned previously in Section 2.3, using FEM analysis. Jankowski's study examined the earthquake-induced pounding between the main building and the stairway tower of the Olive View Hospital. The structures were modelled in a nonlinear finite element system using precise material properties such as concrete and reinforcing steel. All structural members (i.e., columns, walls, and slabs) of the main building and stairway tower have been modelled by four-node quadrilateral shell elements (Zienkiewicz and Taylor, 2000) with multiple integration points through the thickness. The base of the hospital structure was to be rigidly fixed to the ground, and the soil-structure interaction was not considered in the numerical analysis. The stairway tower structure was initially

modelled with the rocking of its foundation and had been taken into account by introducing rotational springs (Gazetas, 2006). The FEM of the main building consists of 7360 multi-layer shell elements, while the model of the stairway tower consists of 4250 multi-layer shell elements shown in Figure 2.25. A modal analysis was first conducted for the structural models to confirm the dynamic properties. The natural vibration modes of the main structure and stairway tower are shown in Figure 2.26 as a result of the study. The separation gap between the two structures was measured and designed at 101.6 mm (4 in). In Figure 2.27, a displacement time history for the stairway tower and the main building was obtained at nodes 1-4 (see Figure 2.27 (a) for their detailed location). In Figure 2.27, node 1 of the stairway tower and node 2 of the main building come into contact three times during the earthquake, whereas node 3 and node 4's contact occurs only once. After analysis, results concluded that in the cases of analyzing eccentric pounding, which is induced due to torsional vibrations of structures, appropriate numerical modelling is very important to conduct. The study results also indicate that this effect of the overall structural response can play a critical role. The accuracy of the analysis can be increased further if certain conditions are considered in the numerical model. Such effects can include soil-structure interaction, the variation of concrete confinement, spalling of concrete cover or buckling of reinforcement, which these conditions were not considered in (Jankowski, 2009).
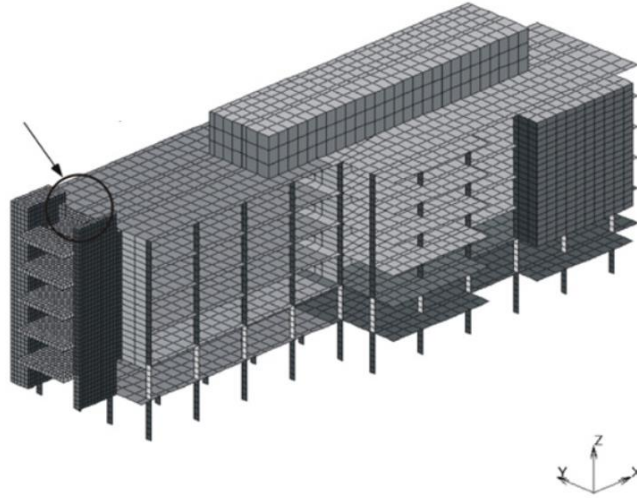
Figure 2.25. Finite element model of the main building (wing C) and stairway tower, adopted from (Jankowski, 2009)

(a)

(b)

(c)

(d)

(e)   **(f)**
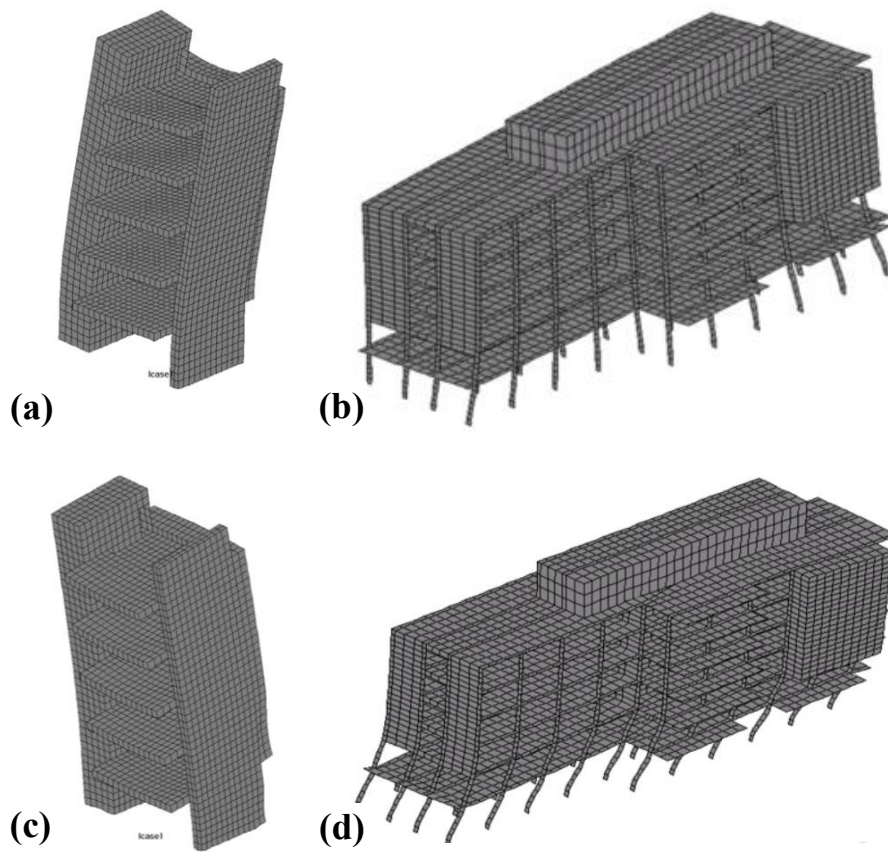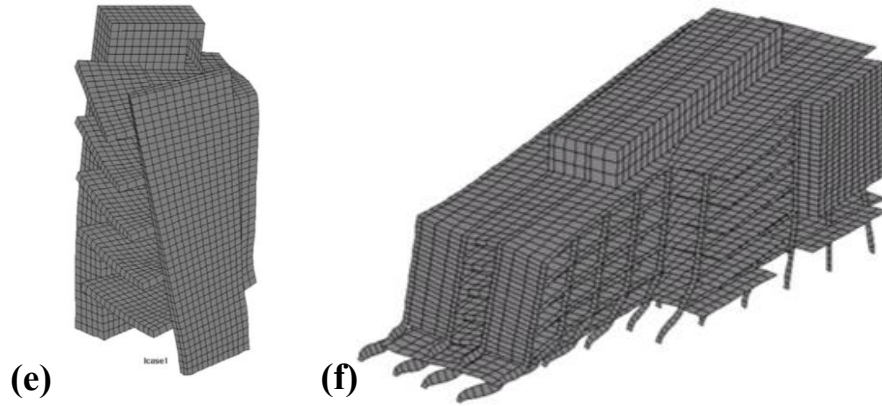
Figure 2.26. First three natural vibration modes for the stairway tower (a, c, and e) and the main building (wing C model) (b, d, and f): (a and b) transverse; (c and d) longitudinal; and (e and f) torsional, adopted from (Jankowski, 2009)

(a)   **(b)**
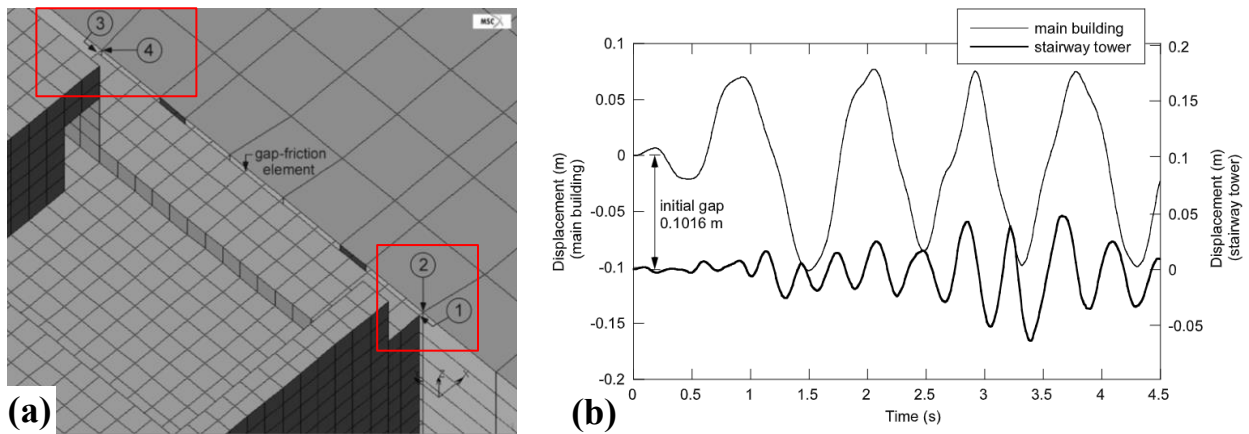
Figure 2.27. (a) Finite element model of interacting stairway tower and the main building detail of the separation gap and (b) displacement time histories for the stairway tower (node 1) and the main building (node 2) in the longitudinal direction, adopted from (Jankowski, 2009)

A study regarding non-linear FEM analysis producing seismic induced pounding between neighbouring multi-storey structures from (Jameel et al., 2013) was also examined. Their study conducted different separation distances between structures to understand and analyze the response behaviour of adjacent buildings with unequal heights under the earthquake-induced pounding using time-domain analysis. The modelling of the structures initially obtained analysis to have no contact of pounding and then were compared to show the importance of avoiding pounding of structures. The numerical investigation of structures includes a four-storey building consisting of

76

16.16 meters in height and a seven-storey structure composed of 28 m in height. The seven-storey building is 18.29 meters in length by 27.43 meters in width, while the four-storey building is 9.14 meters in length by 27.43 meters in width. The structures are built with properties of reinforced concrete for the whole frame structure. Gap elements in the model are linked at four nodes between the structures at the roof level of the lower building in order to simulate contact between two surfaces by generating forces when the two surfaces approach each other. This model's seismic time history function was from the 1940 El Centro earthquake in longitudinal and transverse directions. A total of 20 modes were investigated with the ranging frequency of pounding and no pounding phenomena. Mode 1 is represented in Figure 2.28, which represents both a pounding state (a) and a non-pounding state (b) for the MDOF system structures studied. Additionally, Figure 2.29 is a graphical representation of the maximum displacements at each floor level for the structures in the longitudinal direction for both pounding and non-pounding occurrences. The highest displacement for both pounding and non-pounding cases occurs at the roof level of each structure. The highest roof displacement for no pounding case was concluded to be 137.62 mm for the tall structure. For the maximum displacement movement towards the left, the figure shows the tall structure only to be -111.35 mm towards the no-pounding case. Assumptions were made that this may be due to the flexible nature of the taller structure that causes it to bounce back after pounding occurs. Pounding forces increase when gap distances increase from 25 mm to 125 mm; however, they decrease when gap distances increase from 125 mm to 250 mm. Their results show that adequate gap distances between the structures will significantly reduce pounding damages, reducing the chances of structural failure.
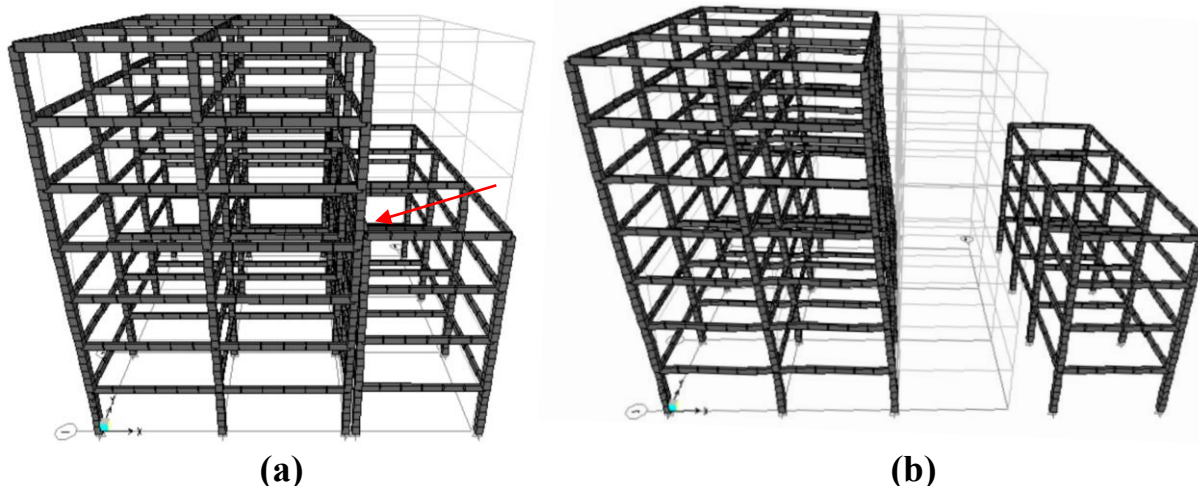
Figure 2.28. Mode 1 of buildings: (a) pounding state; and (b) no pounding state, adopted from (Jameel et al., 2013)
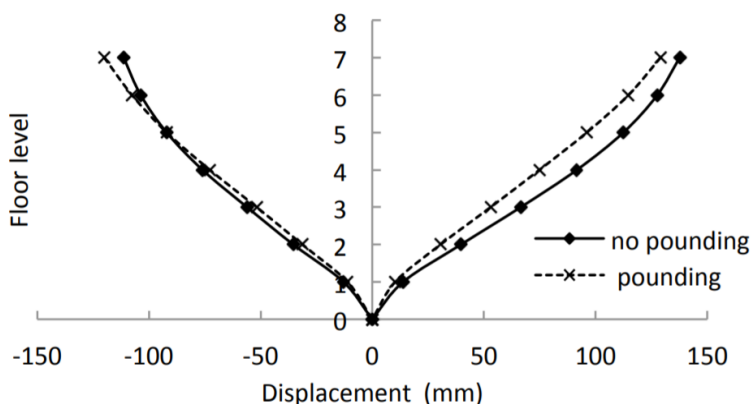
Figure 2.29. Maximum displacement at different floors (longitudinal direction), adopted from (Jameel et al., 2013)

(Petronijević et al., 2014) examined past earthquake incidents due to the thermal expansion joints within a building. Their report investigated two multi-storey structures attached to each other with separation joints designed according to the Serbian regulations and was examined using dynamic analysis (computational MDOF analysis) for pounding excitations due to lateral ground loading. The study investigated structures ranging from three stories to 12 stories in height with different combinations of structural systems and heights of the neighbouring buildings, as shown in Figure 2.30. The parametric analysis employed was conducted implementing finite element analysis and the numerical integration applying Newmark's method for the given accelerograms with 5%

damping as a standard initial value. The soil was modelled as an elastic half-space by 2D shell elements to a depth of 10 m below the foundation level. The loading applied to all modelled structures from the following real earthquake accelerograms: El Centro Earthquake, 1940; San Fernando Earthquake, 1971; Northridge, Pacoima, 1994; and the Bingol Markez Yinderlik ve Iskan Mudurlugu, 2003. It was concluded that structures with separation joints can develop additional colliding loads leading to severe local damages and may result in the global collapse of a structure. This result resonates with the concept of "performance-based design" since assessing the structure after the pounding phenomenon is correlated to its damage level resulting from the pounding impact. Therefore, they concluded that horizontal displacement and the size of the separation joints are considered vital in the design of adjacent structures.
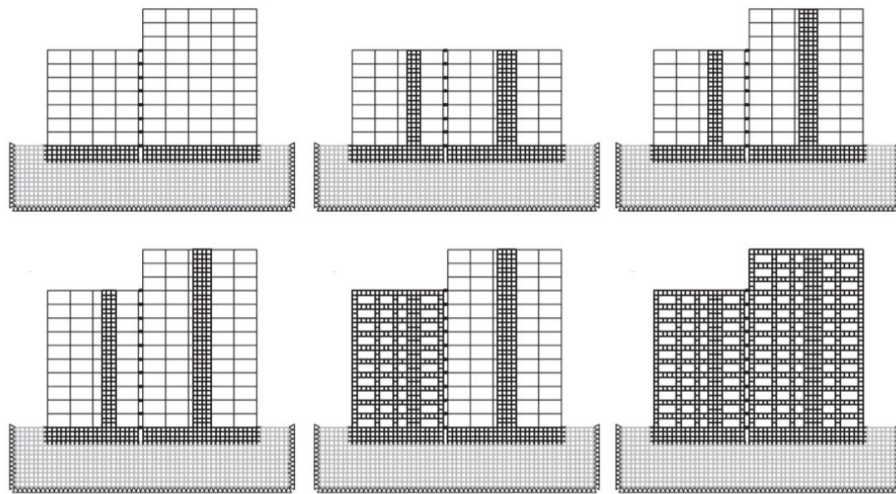
Figure 2.30. Typical cases of considered models, adopted from (Petronijević et al., 2014)

Lastly, a study from (Mariam Ehab et al., 2014) further explored the use of MDOF by using a nonlinear time history dynamic analysis based on the Applied Element Method (AEM) (Meguro and Tagel-Din, 2003, 2001, 2000; Tagel-Din and Meguro, 2000). AEM was proven to efficiently simulate progressive structural collapse (Galal and El-Sawy, 2010; Hartmann et al., 2008) since structural pounding can cause damage such as partial collapse and/or total collapse of the

subjective pounded structures. Their study examined the pounding effect on adjacent reinforced concrete structures subjected to earthquake excitation (KOBE earthquake, Japan in 1995). They utilized six buildings of different loading types, structural systems and floor heights. Each building was 12-stories tall with different live loads and floor heights. Buildings 1-4 are all frame structures, whereas building 5 and 6 are considered shear wall structural systems. Maximum displacement due to earthquake excitation was also specified from Equation (1), as mentioned earlier in Section 2.3. Figure 2.31 illustrates Case 1 with altering spacing gap distances between the two adjacent structures. Results from this study concluded that pounding would take place when the structures experience different modes of vibrations. When the pounding impact occurred, the impact forces acted as external additional lateral forces that changed the mode of vibration of the pounding buildings. Unexpected stress from the case of non-corresponding floor levels in which the slab of one structure hits the mid-height of the column of the adjacent structure because local damage in the collided columns increases the possibility of the building collapse. This result was noted that local damages occurred in the cases of adjacent buildings of different floor levels, possibly leading to global failures (Case 3 and Case 6). Lastly, their study concluded that existing adjacent structures that were not constructed with the code regulations for minimum safe gap distance need to assess potential pounding under horizontal excitations so that necessary strengthening for beams and columns can be carried out.
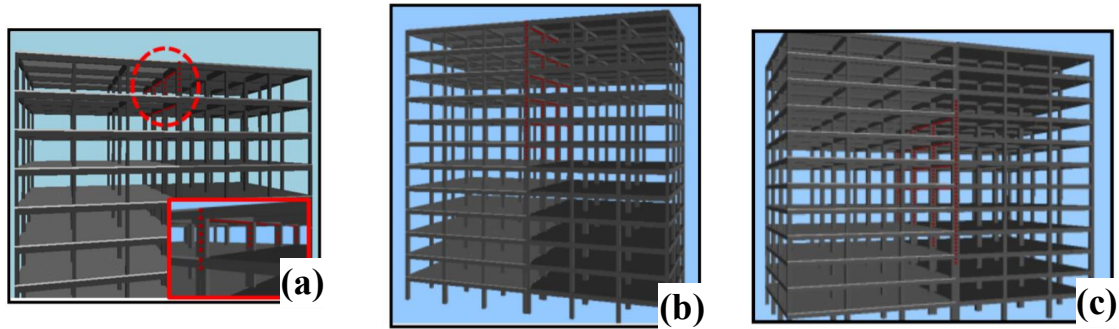
Figure 2.31. Location of collision springs for different gap sizes - Case 1: (a) Gap Distance = 8 cm, Case 1; (b) Gap Distance = 4 cm, Case 1; and (c) Gap Distance = 0.6 cm, Case 1, adopted from (Mariam Ehab et al., 2014)

Following (Mariam Ehab et al., 2014) study, impact forces from the pounding phenomena will be transferred to the colliding structures in the form of different internal forces. These internal forces include normal (beams and slabs), shear (columns), torsion (beams and columns) and bending (beams and slabs). (Mariam Ehab et al., 2014) further proved that the influence of the slabs in the distribution of the impact forces was high, in addition to the case of floor-to-column pounding and the possibility of shear walls and beams in the direction parallel to the direction of the earthquake dispersion was high. Moreover, the dispersion was low in other cases, such as floor-to-floor pounding and shear walls and beams in the direction perpendicular to the earthquake. Therefore, underestimation will have resulted in consideration of frame structures (beam and columns) if taken rather than the "frame + slab" structure (Jameel et al., 2013). Alternatively, the consideration of infills will substantially affect the behaviour of the structures under earthquake excitation, more accordingly, through pounding phenomena. A study by (Favvata and Karayannis, 2013) used a nonlinear dynamic structural analysis program to study the earthquake-induced interaction between adjacent structures with different total heights, taking into account the local response of masonry infilled panels. Frames without infills have a lower stiffness than infilled frames, leading to a more significant impact force when a pounding phenomenon occurs (Elwardany et al., 2017). Infill frames also experience a much smaller displacement than bare frames, concluding that the

81

infilled frames structures require a much smaller seismic gap distance than other frames. Smaller spacing for the infilled frames is because the first mode period is usually dominant for the cases without pounding. In contrast, higher modes are experienced for pounding-involved structural response (Ismail et al., 2017). However, partially or fully infilled frames compared to basic frame structures have a lower first mode period, resulting in an excessive shear and ductility demand for the columns that experience impacts from floor-to-column pounding phenomena (Favvata et al., 2012). Additionally, in a floor-to-column interaction, the column subjected to the pounding of the adjacent slab will still be the most critical case regarding the infilled frame as the ductility and shear demands may exceed the available values (Favvata and Karayannis, 2013).

2.5.3   Numerical impact models

In order to provide valuable knowledge in the assessment of structural pounding, accurate estimation of impact forces during a collision and the prediction of its behaviours are a necessity (Miari et al., 2021). Many different approaches have been developed concerning impact models, where these models mainly focus on two different approaches. The first approach is the stereo mechanical method, and the second is the force-based method (also known as the penalty approach), where the stereo mechanical method uses the law of the conservation of momentum and energy. The force-based method introduces a spring with stiffness that simulates the impact stiffness of the colliding structures, where the spring only activates when there is a positive contact force acting between the interactions of structures.

The first model that utilized the force-based method was based on the linear spring model. The approach is assumed to be an elastic impact that did not consider the energy dissipation and the plastic behaviour when the interaction between structures occurs (Goldsmith, 1960). (Anagnostopoulos, 2004, 1988) used an alternative approach known as the linear viscoelastic

model (also known as the Kelvin-Voigt model). This impact model uses a damper in parallel with the spring to characterize the energy dissipation during collisions. Alternatively, this approach considers uniform dissipation of energy and restitution phases of the collision. Another technique from the force-based method is called the nonlinear Hertz model, which has been used in several studies and has been previously mentioned in Section 2.5.1 (Chau et al., 2003; Chau and Wei, 2001; Davis, 1992). Additionally, a further approach considered in the force-based method is called the Hertzdamp model. This model was introduced by using the nonlinear damping to the nonlinear Hertz model (Muthukumar and DesRoches, 2006). Moreover, (Jankowski, 2006a, 2005; Pratesi et al., 2014) developed a nonlinear viscoelastic model to include the nonlinear response in the impact modelling. Other impact force models have also been developed (Bamer and Markert, 2018; Bi et al., 2011; Bi and Hao, 2013; Guo et al., 2011; Liu et al., 2014; Xue et al., 2016a; Zhu et al., 2002), such as the viscous elastoplastic impact model (further modification from the nonlinear viscoelastic model) to include the elastoplastic behaviour developed from (Khatiwada et al., 2011).

In comparison to all the studies that have focused on the effectiveness of pounding models, each case study used a unique approach that was adequate for their investigation. For instance, (Komodromos et al., 2007) addressed that his outcomes, not including the numerical model used, correlated similar results found from (Anagnostopoulos, 1988) and (Jankowski, 2005). Regarding the nonlinear viscoelastic model, (Favvata et al., 2013; Jankowski, 2010; Vasiliadia and Elenas, 2002) determined that the model has greater precision in assessing the impact force than the nonlinear elastic Hertz model, Hertzdamp, and the linear viscoelastic model. The nonlinear viscoelastic model has lower accuracy than the Hertzdamp model regarding estimating the impact velocity. However, a study from (Khatiwada et al., 2013) indicated that the Hertzdamp model

shows less accurate results for the impact forces compared to the other models (i.e. the linear viscoelastic model, the modified Hertzdamp model and the nonlinear viscoelastic model), which were more precise in this context. (Pant et al., 2010) analysis found their modelled method in estimating the impact force and the inter-storey drift to be more rational in comparison to (Komodromos et al., 2007) and (Ye et al., 2009) model. Moreover, a research analysis from (Mavronicola et al., 2016, 2015) compared the effectiveness of five models described in the works of (Anagnostopoulos, 1988), (Komodromos et al., 2007), (Ye et al., 2009), (Mahmoud and Jankowski, 2011) as well as by (Pant et al., 2010). (Mavronicola et al., 2016, 2015) results concluded that the precision of models is governed by the coefficient of restitution and the impact stiffness taken into consideration in the analyses. In general, (Miari et al., 2021)stated that no decision regarding the most accurate model was reported. Therefore, further research on impact models and their accuracies may be considered.

2.5.4   Codes and provisions

In order to preclude a pounding event between adjacent structures, the standard measures for modern codes specify a sufficient separation distance between structures (2, 1991; 8, n.d.; ACI Committee, 1995). Some factors, however, make these codes and provisions not consistently effective or applicable, as previously mentioned in Section 2.1 (Background). A counterargument can be made that weak structures in contact with stronger buildings in dense city locations may benefit from that contact, provided that the pounding phenomena will not cause any severe local damage, leading to possible failures (Anagnostopoulos, 1995; Athanassiadou et al., 1994). Alternatively, measures against structural pounding have been previously proposed, such as filling of the gap between adjacent structures with shock-absorbing materials (Anagnostopoulos, 1988), the use of permanent connections between the adjacent structures (Westermo, 1989), and lastly,

the new Hellenic Code for seismic design of structures and Eurocode 8 proposed the use of stiffened strong shear walls in the prevention of structural pounding (Karayannis and Favvata, 2005b).

The aim to avoid structural interaction under the maximum inelastic response of each adjacent structure has current separation guidelines in current seismic codes and provisions. Eurocode 8 and ASCE 7-16 require that the maximum inelastic deformation of each building "shall be determined at critical locations with consideration for translational and torsional displacements of the structures including torsional amplifications, where applicable", referred to as δ_{M1} and δ_{M2}, and that the total separation distance between the buildings should be greater than the $d_{g,min}$ as explained in Equation (1). Despite their simplification and conservative approach, these guidelines do not guarantee a collision-free response due to the large ground motion and building response uncertainties. Therefore, structural interaction in dense urban locations will be probable in the continuing future earthquakes and problematic wind affairs (Langlade et al., 2021).

The required separation distance to be provided can be simply calculated as the absolute sum of the peak displacements of both buildings when they vibrate separately (Miari et al., 2019). This required separation distance calculation can be found in multiple codes and provisions, including the UBC (1997). This distance is overestimated and, therefore, will be conservative as the probability for both structures to have their max displacement taken into account at the same instant of time will be very low (Miari et al., 2021, 2019). Accordingly, (Anagnostopoulos, 1988) suggested the use of the square root of the sum (Equation (1)) of the peak displacements of both buildings vibrating separately. This equation will be adequate for the seismic and wind separation distance as several other studies have shown that this formula is conservative for the adequate separation gap distance (Kumar and Kumar, 2015; Pantelides and Ma, 1998). The UBC 97 later

then adapted this formula into their code. This formula, however, will not be conservative when structural interactions (pounding) occur with different structural systems (Mariem Ehab et al., 2014), when the nonlinear response is considered (Jamal and Vidyadhara, 2013), or in the near-collapse limit state when the peak response is due to the ground motion is analyzed (Favvata, 2017; Miari et al., 2019). Therefore, a study from (Van et al., 1992) proposed a different equation known as the double-difference combination or the complete quadratic combination method (Equation (2)) based on the spectral difference method. Although the double-difference combination formula requires evaluating the correlation factor, ρ, which represents the uncertainties in the pounding phenomenon, this formula is considered to be more accurate than Equation (1), square root of the sum. The Taiwan Building Code (*Taiwan Building Code. Construction and planning administration Ministry of Interior, Seismic provisions*, 1997) takes into account the plastic deformations in the required seismic gap formula by multiplying the sum of the allowable plastic displacements of both buildings by a reduction factor of 0.6. The allowable plastic displacements are calculated by an over-strength factor, 1.4, the allowable ductility factors, the first yielding amplification factor, and lastly, the elastic displacement due to the seismic forces. (Lin, 2005; Lin and Weng, 2002) proved that this formula is conservative and overestimates the gap. In addition, the minimum required separation based on the ASCE 7–05 code (American Society of Civil Engineers, 2006) is determined from the multiplication of the total deflection amplification factor and the maximum elastic displacement, then divided by the importance factor. The Australian code (AS1170.4–2007) (Australia Standard, 2007) and others suggest that the required seismic gap should be calculated by relating it to the building's height, such as 1% of the total height of the taller building (i.e. $S = 0.01*H_{max}$). It was concluded by several studies and verified this formula is a conservative approach (Hao, 2015) and will overestimate the required seismic gap (Naderpour et

al., 2017). The absolute sum of the peak displacements and sum of the squares methods, as well as the formula described in the Australian seismic code, will conclude inaccurate results due to the fact of ignoring the in- and out-of-phase vibrations, which is similar to Equation (2) as the correlation factor, ρ, can be substituted with the separation factor, which depends on the periods of both structures.

The formulas described above are for the seismic gap distances between two adjacent structures that concern fixed-base buildings. Flexible-based buildings, however, require more considerable separation distances to be provided as past evidence states that the sufficient gap in the case of soft soil structures may exceed three times larger than the recommended one (Ghandil and Aldaikh, 2017a; Li et al., 2017; Naserkhaki et al., 2013).

2.5.5 Performance-based design

A further evaluation of the characteristics of structural interaction (pounding) can also be assessed by investigating a performance-based approach. Many studies have concluded that existing design procedures for determining the separation distance between adjacent structures subjected to a pounding phenomenon are achieved based on the building's relative peak displacement. These risk procedures are characterized by unknown safety levels and are not entirely suitable for use within a performance-based earthquake engineering framework (Barbato and Tubaldi, 2013; Flenga and Favvata, 2021; Tubaldi et al., 2012; Vega et al., 2009; Wu et al., 2020). A study from Vega et al. (Vega et al., 2009) used the Pacific Earthquake Engineering Research Center framework formula to assess the reaction forces produced by pounding towards determining the mean annual rate of pounding forces exceedance. The studied structure was of a bridge, where the bridge's deck was supported by either sliding or elastomeric bearings, which was used for the longitudinal dynamic behaviour of the bridge. These two types are commonly found in locations of mid-seismicity. The

bridge deck in the study was considered continuous, and pounding was only possible between the deck and abutments because of the insufficient seismic gap to simplify the problem. Results concluded that their selection of intensity measures and engineering demand parameters, which was an a priori selection, have led to similar systems with the same relative intensity to have proportional responses with only an alter in parameters, such as differing only the gap size or scalar factors while enduring similar actions. Both intensity measures investigated in the study were proved to be sufficient and the scaling of records produced no bias in estimations. Additionally, the second intensity measure was more efficient than the first, which is because it led to a lower non-explained variability. Lastly, they concluded that the pulse-type records should be separately treated when estimating engineering demand parameters conditions to intensity measures.

(Barbato and Tubaldi, 2013) proposed a new reliable-based methodology for defining the separation distance between adjacent structures corresponding to a target level of the seismic pounding probability. The method in their study overcomes the limitations of the current critical separation distance design approach. This approach is determined by assuming the separation distance equals the peak relative displacement computed at the most likely pounding location. A corresponding site-specific seismic intensity is considered by finding the separation distance that resembles the target value of the pounding probability during the building design life for a continuum of hazard levels. Their study performed the critical separation distance by recasting an inverse reliability problem described as a zero-finding problem. Accuracy and computational costs altered the solution algorithms, which were proposed and compared. Considerations towards the design of the gap distance between the structures, which were modelled as linear elastic systems subjected to Gaussian excitations, were illustrated for the capabilities of the proposed methodology. Only the seismic input uncertainty was explicitly taken into account because of

space constraints and for the sake of clarity in their study. Additionally, the uncertainty affecting the parameters describing the structural model was not considered in their analysis. The proposed probabilistic performance-based methodology was later applied to determine the separation distance between the structures modelled as a linear MDOF system. Lastly, they used the same methodology to determine the design separation distance between the two structures modelled as equivalent SDOF systems with nonlinear hysteretic behaviour for a wide range of nonlinearity levels. In conclusion, many observations were noted by comparing the separation distances obtained using the proposed methodology with the hybrid algorithm and the modern seismic design procedures. Firstly, the comparison between the proposed design methodology to find the pounding probability for an adequate gap distance and the targeted pounding probability was very close in comparison. Next, the separation distance within the seismic code procedures resulted in being inconsistent and potentially not conservative towards the problematic pounding phenomena. Additionally, having a larger lifespan of a problematic failure is very sensitive to variation in the separation distance (e.g., 50-year probability of failure). A slight variation in separation distance can result in significant variations for the possible pounding probabilities. By modelling the structures as a linear MDOF system, the simplified method appeared to have very close results following the newly proposed general methodology, which provided very low computational costs. Regarding the modelled SDOF systems, it was observed that the more conservative values were concluded using the linear behaviour approximation.

A study from (Wu et al., 2020) used a similar approach to (Barbato and Tubaldi, 2013) study using a probabilistic performance-based assessment for the critical separation distance between adjacent buildings. This was for the structures corresponding to the targeted collision probability within the deterministic design life. Their study treated the seismic collision as a single-obstacle reliability

problem. The pounding event was first expressed as a first-passage reliability problem of a single potential barrier, based on random vibration and reliability theory. Different ground motion intensities were derived for the conditional failure probabilities of the structural systems. The critical separation distance is then calculated, extending the single structure to the adjacent structure, as an inverse reliability problem by the seismic pounding brittleness of the adjacent structures. Their study then analyzed different parameters based on their proposed algorithm. Their results had very similar conclusions as (Barbato and Tubaldi, 2013) study. Using the proposed design methodology based on their three analytical approximations, an accurate estimation of critical separation distances with the target 50-year pounding probability, which had similar agreeance to (Barbato and Tubaldi, 2013) conclusion. Pounding risk levels were consistent for adjacent buildings with different rations of natural periods, floor numbers and site hazard curves from the use of the proposed algorithm to determine the critical separation distances with alteration of different parameters that were analyzed. Lastly, (Wu et al., 2020) stated the Code for Seismic Design of Buildings in China needs a significant revision regarding the seismic joint width. A modification can include the minimum seismic joint width to include a certain pounding probability during the lifespan of the adjacent structures.

(Flenga and Favvata, 2021) aimed to incorporate the local inelastic demands of a multistory RC frame structure for the first time in the problematic seismic assessment of the pounding risk. Floor-to-floor structural pounding and floor-to-column structural pounding were considered. Additionally, incorporating local and global probabilistic seismic demand models in assessing the seismic performance of the buildings subjected to pounding. Linear and bilinear regression models were used for this reason. The study then developed fragility curves of the examined multistory RC frame structures against structural pounding at different performance levels, which was

achieved as a function of gap distances between the adjacent structure, global seismic performance, and the local seismic performances. Their final part then introduces a process that incorporates the capacity levels of global and local engineering demand parameters of subjected pounding structures and the separation distance between the adjacent structures. A few remarks were concluded from their study. Flexural and shear responses of the columns were proved to be a crucial demand parameter for the probabilistic assessment on evaluating the pounding risk from the local performances. Floor-to-floor and floor-to-column pounding will alter the results of the probabilistic assessment in terms of local or global performance. At a given value of intensity measures (peak ground acceleration), the probability of an 8-storey RC frame to exceed a specific local or global performance level is increased due to the pounding phenomena. Due to an inter-storey pounding impact, the shear capacity is proven to be a more significant performance level for an accurate probabilistic assessment of the shear failure of columns. Lastly, by evaluating the compounded fragility-based evaluation of the pounding risk, a clear indication that the 8-storey RC frame has exceeded the examined performance level at a lower value of peak ground acceleration when subject to pounding than the corresponding case without pounding. The most valuable technique to estimate the minimum gap distance between the adjacent buildings when local and global performances are incorporated in the fragility assessment process was aimed at a performance level threshold.

2.6   Summary

This chapter comprehensively demonstrate multiple aspects related to pounding between structures due to lateral excitations (e.g., earthquake and wind). Structural pounding typically transpires when adjacent structures (e.g., buildings or bridges) are at proximity while encountering extensive lateral motion causing these structures to develop an unexpected colliding force to the structural system, which may result in local or global damages. The risk of pounding is expected

to be magnified when the adjacent buildings are placed with a separation distance that is less than the suitable gap space or the structural system can not withstand the additional colliding load.

Pounding incidents have been reported in many cases, such as large city-scale earthquake occurrences, out-of-phase vibrations leading to the pounding of adjacent structures, and within the same structure that has expansion joints. Motivated by the numerous pounding incidents, several studies have adopted experimental and numerical approaches to model structural pounding behaviours and possible damages during past earthquake phenomena, such as models conducted through shaking tables, single-degree-of-freedom, multiple-degrees-of-freedom, finite element method or applied element method analyses. Wind-induced structural pounding has been implemented for the next 2 chapters. Chapter 3 formulates mathematical equations for estimating the required minimum separation gap distance based on the structural parameters. Chapter 4 presents a determined pounding force formulation for two tall structures subjected to wind.

3 Chapter 3 – Separation Distance for Structural Pounding

3.1 Background

Buildings are constructed within dense metropolitan locations, ultimately in proximity to surrounding structures due to limited available land space and the increase in population. With the design of new, tall, and slender buildings, the term pounding has become an important objective when a structure is built within proximity. Pounding of structures has been defined by past scholars (Anagnostopoulos and Spiliopoulos, 1992b; Efraimiadou et al., 2013; Kasai and Maison, 1997; Maison and Kasai, 1992, 1990) as the interaction between two or more adjacent structures in proximity, causing a collision resulting from a lateral load. Furthermore, a pounding can increase in probability due to the structures in proximity conducting an out-of-phase vibrating due to the difference in their dynamic properties (e.g., stiffness and mass) (Jankowski, 2009), which can occur during high-velocity wind events (Abdullah et al., 2001b). Pounding can be considered as a major risk to tall structures; for instance, (Rosenblueth and Meli, 1986) explored a historical earthquake event resulting in many structural pounding occurrences. They concluded that pounding damages can range from minor to major structural damages to the extent of global structural failures. The most recorded pounding events have been initiated during earthquake appearances due to induced ground motion transferring to the structures (Anagnostopoulos, 1995, 1988; Jankowski, 2012, 2009; Kasai and Maison, 1997; Kaushik et al., 2006; Maison and Kasai, 1992; Rosenblueth and Meli, 1986). A pounding occurrence can also be produced when the structures involved are subjected to extreme wind events (Brown and Elshaer, 2022; Huang et al., 2012). Extensive literature reviews on structural pounding have been presented by (Brown and Elshaer, 2022; Miari et al., 2021).

As tall structures are increasing in both height, flexibility and slenderness, buildings are becoming more sensitive to wind load (Huang et al., 2012; Lam et al., 2009), as wind is typically the

governing load for the new generation of tall buildings (Bobby et al., 2014; Ding et al., 2019; Elshaer and Bitsuamlak, 2018; Irwin et al., 2008; Irwin, 2009). It was also indicated that there is a need to lower the building weight to ultimately reduce the gravity loads to control the inertial forces from earthquake events. This further contributes to an enlargement in the wind-induced forces and motions, resulting in wind-induced loads and motions becoming the typically governed applied load for the design of the lateral load resisting systems in tall structures (Elshaer et al., 2017; Irwin et al., 2008; Irwin, 2009) compared to seismic loads since the forces are inertial due to ground motion (Rahman et al., 2012). A further examination from (Aly and Abburu, 2015) used tall structures under multi-hazards events (i.e., wind and earthquake) with similarities in structural properties and geological location to compare the dynamic responses of the structure investigated (i.e., lateral deflection, inter-storey drift, acceleration). In comparison to an earthquake, the same structure under wind loading can develop a more considerable lateral deflection and inter-storey drift magnitudes within an exact geological location (e.g., eight times larger in lateral deflection and 2.5 times more prominent in inter-storey drifts). (Stafford Smith and Coull, 1991) stated that such lateral load could develop intensive structural sway and strong vibrations throughout the structure. Over time, it is becoming more challenging to meet the serviceability requirements (i.e., maintain an adequate lateral deflection or control the extensive vibrations on tall structures) compared to meeting the strength and capacity requirements within a structure (Bernardini et al., 2015; Chan et al., 2009b; Elshaer and Bitsuamlak, 2018; Kwon and Kareem, 2013). Due to structural sway in tall buildings, lateral deflection can damage non-structural elements (i.e., cladding and partition) and main structural components to the extent of damaging possible adjacent structures (Chenna and Ramancharla, 2018; Rahman et al., 2012; Wolfgang, 1977). Large deflection in tall structures can be mitigated appropriately through structural design measures or

94

by introducing external deflection mitigation systems (e.g., dampers) (Malhotra et al., 2020; Tse et al., 2012, 2007).

Thorough studies have been performed to improve safety precautions to avoid pounding risk. Such precautions evaluated and developed an adequate separation distance between possible pounding structures to prevent contact during potential extensive lateral load occurrences (Favvata, 2017; Jankowski, 2005; Jankowski and Mahmoud, 2015; Lopez-Garcia and Soong, 2009; Penzien, 1997; Van et al., 1992). Additionally, when designing and planning for newly constructed structures, pounding risk can be assessed for existing structures to avoid the occurrence of structural pounding. However, many pre-existing structures already in proximity have been built with an insufficient separation distance due to old design codes and previsions, leading to pounding damages (Jeng and Tzeng, 2000; Kazemi et al., 2021). The majority of structural building codes identify the requirements for building deflections. A limited selection of structural building codes fails to identify a required minimum separation distance for possible structures located in proximity during hazardous wind events. Alternatively, other mitigations can be justified to limit damages from structural pounding if insufficient or no separation distance between such adjacent structures can be enabled. Despite rigorous research scholars relating to structural pounding, an adequate separation distance was not correlated to the adjacent structures' dynamic properties or the lateral loads (Chau and Wei, 2001). Such deflections depend on the structure's height, modal period, and the applied lateral load. The applied lateral load (e.g., wind events) can lead to out-of-phase vibrations arising from the possible structural pounding.

Accordingly, this chapter aims to examine a case study of two structures in proximity with varying wind intensity, height, and flexibility to systematically estimate the required minimum Separation Gap Distance ($d_{g,min}$) to mitigate the arising risk of damages and failures due to wind-induced

structural pounding. First, the study conducts a series of Computational Fluid Dynamic (CFD) simulations while altering the applied mean wind velocities to determine wind forces acting on two adjacent tall structures. Then, the extracted wind forces are applied to structures using Finite Element Method (FEM) models to determine the developed deflections for the two adjacent structures. After that, the responses of each structure are then used to determine its lateral deflections while maintaining a large enough $d_{g,min}$ between structures not to conduct possible structural pounding. Finally, once results are conducted and recorded, a Genetic Algorithm (GA) is then utilized to formulate the most accurate mathematical formula for estimating the required $d_{g,min}$ based on the structural natural frequency, building heights, and the applied wind.

This study is divided into five major sections. The first section (3.1) introduces the terms and components of structural pounding and possible arising mitigations, along with the most relevant literature about structural pounding. The second section (3.2) presents the adopted methodology used to generate the training data for the developed mathematical formula; Section 3.2.1 establishes the numerical Large Eddy Simulation (LES) produced in the adopted CFD wind analysis. To determine the structural response when subjected to wind loads, a FEM model is developed and validated in Section 3.2.2. In Section 3.2.3, a description of the developed mathematical formula is presented to determine an adequate $d_{g,min}$. Wind forces are then collected and produced in a FEM model to determine the dynamic response of the adjacent structures based on their structural properties and applied mean wind velocities. These lateral results enabled the determination of lateral deflections of tall structures for various building heights, building flexibilities and wind speeds, which is described in Section 3.3 (Results and Discussion). Section 3.4 correlates the lateral deflections using mathematical formulas to determine the sufficient

minimum separation Gap Distance ($d_{g,min}$) to the building parameters controlling the lateral deflection.

3.2   Mathematical Estimation for Required Minimum Separation Gap Distance ($d_{g,min}$)

The current study aims at deriving a mathematical formulation to determine the required minimum separation Gap Distance ($d_{g,min}$) between two tall adjacent structures in proximity subjected to wind to avoid structural pounding. The adjacent structures will vary in height, natural frequencies, and applied wind loads. The study first conducts a series of LES to determine the applied wind forces acting on the adjacent two structures. Once all wind forces are evaluated, a FEM analysis is performed and validated to determine the dynamic responses of the simulated structures. The structures in the FEM analysis are modelled as elastic material. The beam-to-column connections are rigid, in addition to each columns base being a fixed connection. Each beam and column are considered as line frame elements. The diaphragm for each storey is considered as rigid where the torsion of the floor diaphragms is ignored. The floor framing for both structures is assumed as doubly symmetric in the FEM analysis. The deflection time histories for both adjacent structures will be recorded throughout the applied wind. An adequate $d_{g,min}$ is determined where no structural pounding occurs. Once identified, the smallest $d_{g,min}$ is determined through the FEM analysis based on the structure's height, natural frequency and applied mean wind velocity. These input values are used by a GA to formulate a reliable mathematical formula for determining an adequate $d_{g,min}$ between two structures at proximity. Figure 3.1 summarizes the procedure for determining the required $d_{g,min}$.
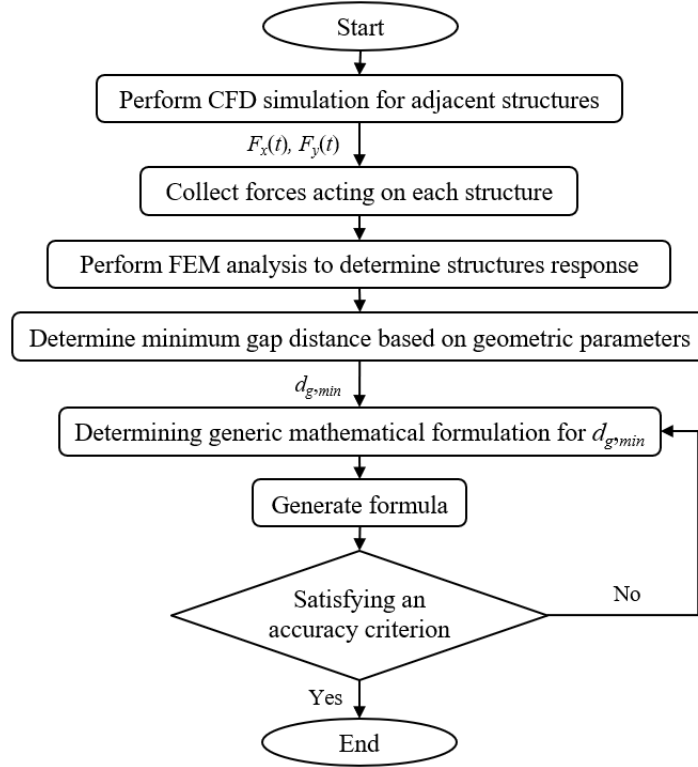
Figure 3.1: Flowchart of the procedure to determine the required minimum separation gap distance ($d_{g,min}$)

3.2.1 Extracting Wind Load Time History Using Computational Fluid Dynamic

In order to accurately model a required $d_{g,min}$ to avoid structural pounding between two adjacent tall structures in proximity, a numerical model must be precisely developed. A high-fidelity CFD model is generated while considering all required fluid properties and structural details. The current study's initial structure considered is the Commonwealth Advisory Aeronautical Research Council (CAARC) structure. The CAARC structure has been an optimal ongoing benchmark in many experimental and numerical wind-related studies (Braun and Awruch, 2009; Melbourne, 1980). Once adequately modelled in the numerical FEM, various building heights are simulated (e.g., 180 m, 140 m, 100 m, and 60 m) while adjusting the sizes of the used steel sections (see Section 3.2.2) to maintain an accurate design according to the AISC steel code (Chan et al., 2009b; Huang, 2017) for the purpose of determining the required $d_{g,min}$. The structure's full-scale

geometric shape is 180 m in height, 45 m in width, and 30 m in length. In the CFD simulation, all aerodynamic characteristics are adopted as per (Elshaer et al., 2016). Then, the FEM analysis uses specific structural attributes in accordance with the studies (Chan et al., 2009a; Huang, 2017). The most unfavourable incident wind direction is considered acting on the longer side of the structures (i.e., zero wind angle of attack along the y-axis), which was deemed in the dynamic response from (Chan et al., 2009a; Huang, 2017).

3.2.1.1 Description of CFD physics and boundary conditions

A CFD simulation from (Dagnew and Bitsuamlak, 2013; Franke, 2006; Franke et al., 2011) employs an LES model with computational domain dimensions shown in Figure 3.2 (a). The computational domain consists of four different types of boundary conditions, which are as follows. The non-slip wall boundary condition is assigned to all ground and walls of the studied structure. Symmetry boundary conditions are considered for the sides and top faces of the computational domain to mirror velocities and pressure characteristics across these surfaces. The inflow boundary condition is located at the front surface of the computational domain to utilize a database for each velocity component depending on both its location and time (e.g., u_x (x, y, z, and t)). This has been previously generated using a Consistent Discrete Random Flow Generator (CDRFG) technique developed by (Aboshosha et al., 2015; Elshaer et al., 2016; Khaled et al., 2021). The outlet is the rear surface of the computational domain to model the outflow, consistent with the CDRFG inflow shown in Figure 3.2 (b) (Aboshosha et al., 2015). The conducted LES uses a dynamic sub-grid scale with a commercial CFD package (STAR-CCM+ v.15.04.008) (Germano et al., 1991; Smagorinsky, 1963). The structure's reference height is of 0.4562 m in the model scale with an exposure factor as an open terrain environment. Each simulation is a total of 14000-time steps to represent a total time of 7.0 seconds in model scale (i.e., 11.5 minutes full-

scale); a time step equal to 5 milli-seconds allowing the Courant Friedrichs-Lewy (CFL) to be maintained less than 1.0 to ensure wind solution's accuracy and convergence (i.e., maximum $CFL = 0.5$ at the top of the studied structure). The turbulence intensity reference in the x, y, and z directions are 0.197, 0.167 and 0.145, respectively. The turbulence length scale in the x, y, and z directions are 0.563 m, 0.147 m, and 0.186 m, respectively. To conduct the CFD simulations, simulations are performed using the (SharcNet 2022) high-performance computer (HPC) facility. The duration required for performing one CFD simulation was sixty hours, which took place on ninety-six processors.
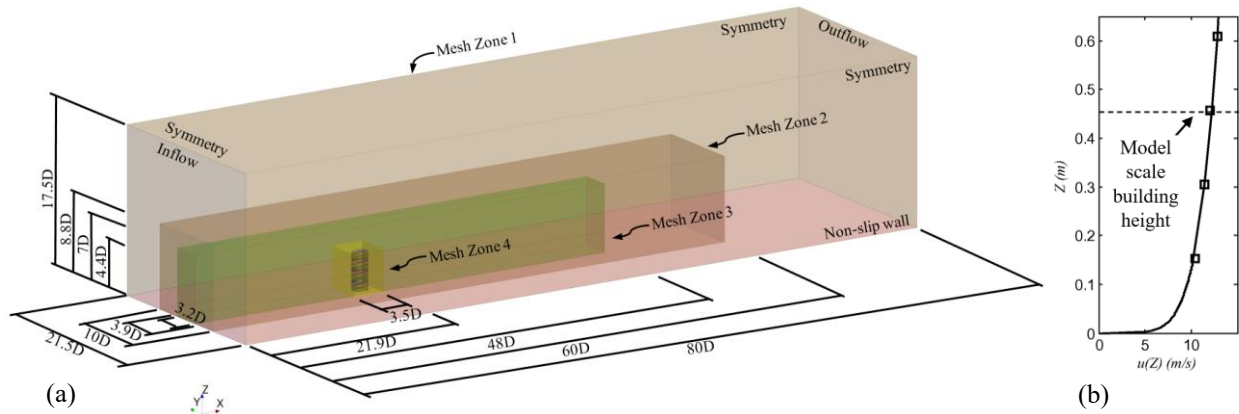
Figure 3.2: (a) Computational domain dimensions and boundary conditions, (b) velocity profile in model scale at the building location

3.2.1.2   Computational domain discretization

Within the computational domain, a grid discretization must be considered, where hexahedral meshes are used. Table 3.1 summarizes the grid resolution and properties for the isolated CAARC structure. The grid used in the computational domain is divided into four zones, as indicated in Figure 3.3. Starting from the furthest away from the structure of interest, Zone 1 is considered with the largest grid. As getting closer to the structure, Zone 2 and Zone 3 are deemed to have medium-sized grids. The last zone, Zone 4, is considered closest to the building of interest, having the smallest grid size. Compared to the other three grid zones, a decrease in grid size will capture

essential flow details around the structure in the wake zone and from the zones between the inflow boundary condition (as previously mentioned) and the structure of interest. Grid zones are chosen based on (Aboshosha et al., 2015; Elshaer et al., 2016) studies and are validated with similar comparisons shown in Figure 3.4 (a) and (b). A total number of $1.75 * 10^6$ mesh cells are considered.

Table 3.1: Parameters for the generated wind flow velocity field

Mesh Zone	Zone 1	Zone 2	Zone 3	Zone 4
Mesh Size	91.2 mm (H/5)	45.6 mm (H/10)	18.2 mm (H/25)	6.91 mm (H/65)
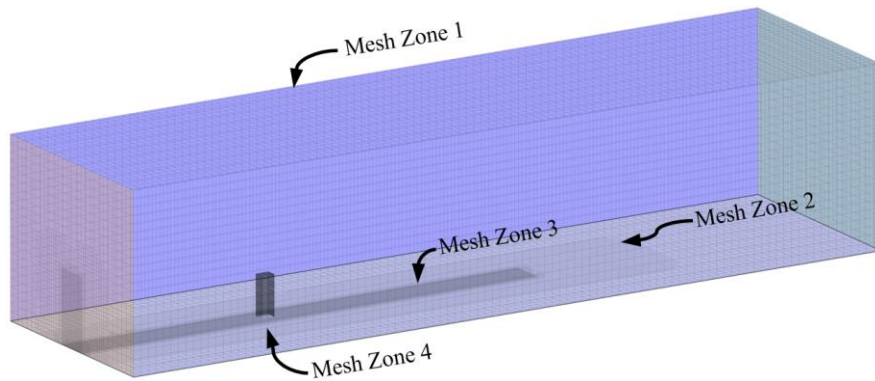
Figure 3.3: Mesh grid resolution utilized in the CFD simulation

3.2.1.3   CFD model validation

An experimental wind tunnel study by (Dragoiescu et al., 2006) is used as a validation benchmark for the CFD simulation in the current study. The study uses a time and length scale of 1:400 and 1:100, respectively. Figure 3.4 (a) shows the comparison of the mean Pressure Coefficient (C_p) from the developed LES model simulation to those from previous wind tunnels and numerical simulations (Melbourne, 1980). Similar comparisons for the Root Mean Squared (RMS) C_p are shown in Figure 3.4 (b). The current CFD model showed comparable results to the wind tunnel and numerical simulations (Dragoiescu et al., 2006).

101
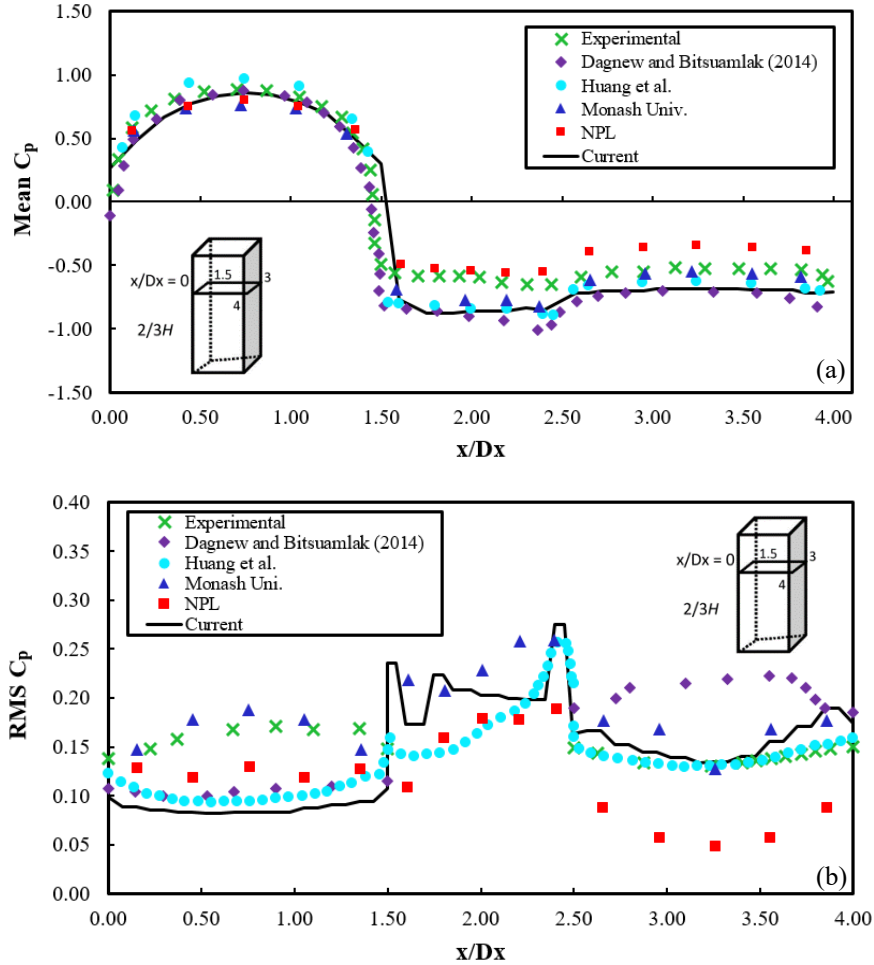
Figure 3.4: (a) Mean and (b) RMS Pressure Coefficient at 2/3 reference height of the CAARC building

3.2.1.4 Determination of wind forces on the study buildings

A time history of forces acting on each storey of the structure is obtained from the LES simulation in order to be used for determining the structural response using FEM simulations. Using LES, two equal-sized buildings are examined to represent two CAARC structures. Each structure is divided into forty-five equal levels to represent the 45 storeys. Figure 3.5 shows all divided storeys (highlighting the 25th storey on the upstream (first) building) on both structures. The forces in the x, y and z directions in each storey are integrated over their surfaces and monitored over time. Figure 3.6 (a-d) show samples of the wind force's time history acting on the 45th storey for each structure in the x and y directions in full-scale. Similar time-history forces are conducted for

buildings of heights of 140 m, 100 m, and 60 m. Similar simulations are performed for different inflow with mean along-wind velocities of 20, 30, 40 and 50 m/s, which will be further discussed in Section 3.2.2.2. The first 50 seconds are not captured in the CFD analysis to allow for the initial converging of the wind flows.
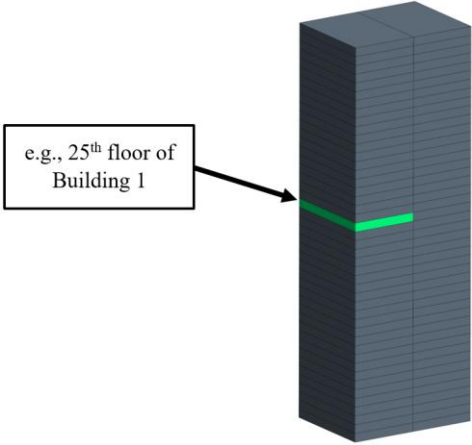
Figure 3.5: Tributary areas used for wind load time history determination
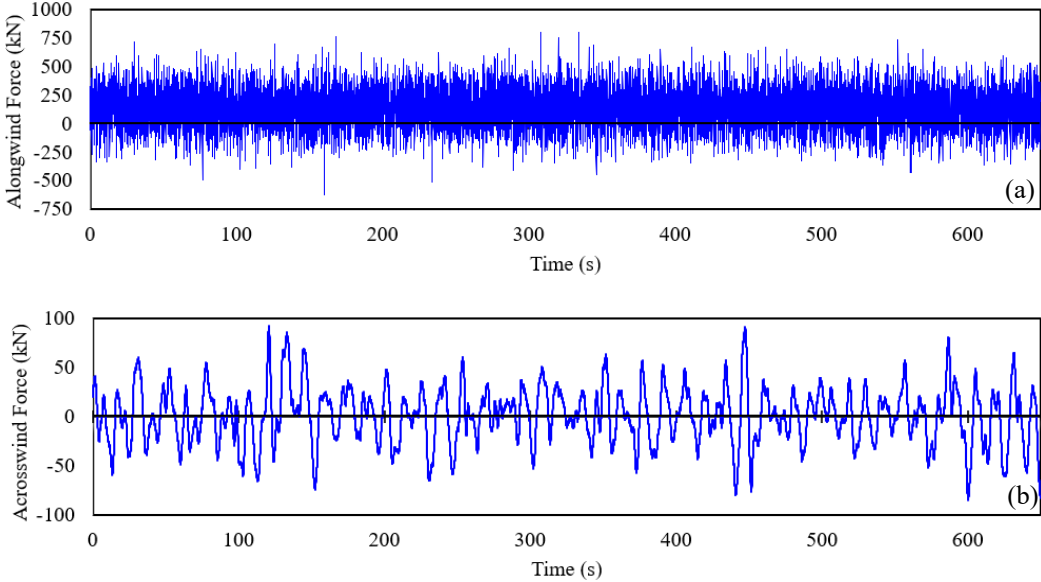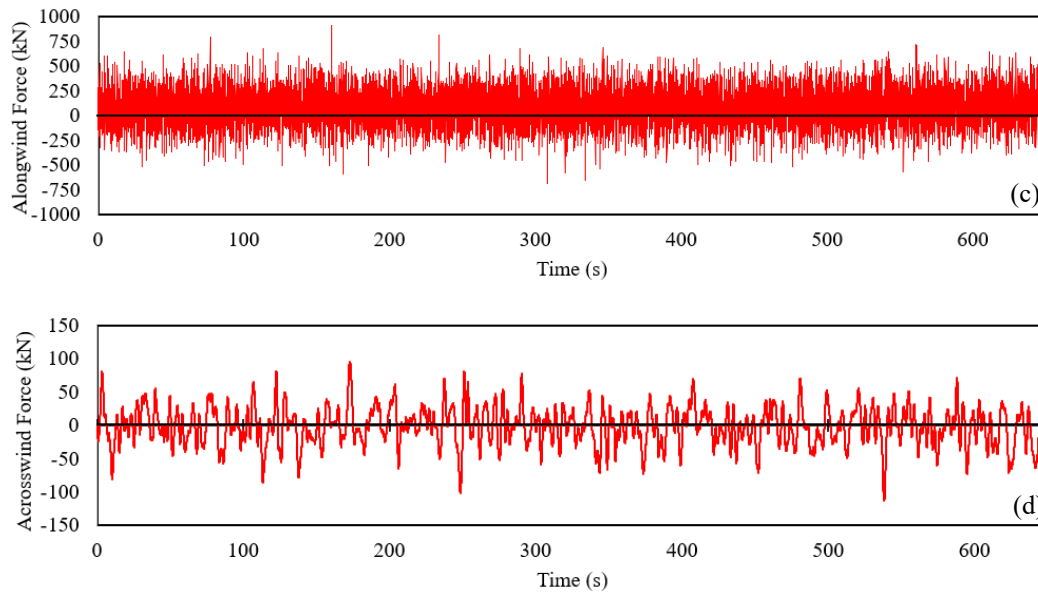
Figure 3.6: Forces time history on the 45th storey of structure for (a) along-wind (x-direction) upstream building, (b) across-wind (y-direction) upstream building, (c) along-wind downstream building, and (d) across-wind downstream building (Full-scale)

3.2.2 Modelling of Structural Response of the Colliding Buildings Using FEM

A 180 m, 45-storey tall steel rectangular skeletal structure (i.e., 30 m by 45 m long, respectively) is used as the initial validated structure for the FEM analysis (i.e., CAARC structure). Once the simulated steel skeletal structure is in good agreement with the validation model, other simulations (e.g., 140 m, 100 m, and 60 m tall buildings) are then calculated per the preliminary strength check for the AISC. The gathered time-history wind loads from the numerical LES modelled analysis are then scaled to full-scale and applied to the two adjacent steel structures in proximity in the FEM model. The identical adjacent tall structures in proximity are examined to determine an adequate $d_{g,min}$ where no structural pounding occurs. This $d_{g,min}$ will be used in the later sections to determine mathematical equations for mitigating wind-induced pounding.

3.2.2.1 Finite element model validation of CAARC building

The full-scale CAARC structure is 180 m tall, having 45 similar storeys' (each storey is 4 m in height), with a 10-bay by 15-bay steel rectangular skeletal framework, as seen in Figure 3.7 (a).

104

Each bay consists of being 3 m wide. The validated CAARC structure's steel size members are based on (Chan et al., 2009a; Huang, 2017) analysis, designed based on a preliminary strength check according to the AISC steel code (2001) to accurately replicate the validated model, as previously mentioned in Section 3.1. The steel columns and beams are selected based on the W14 and W30 sizes, respectively. The remaining structures (e.g., 140 m, 100 m, and 60 m) will be designed similarly to maintain the preliminary strength check (see Table 3.2). The structure acts as a moment-resisting frame, as the lateral forces are taken down into the fixed ground connections. The steel structures' modal damping ratios are equal to 2% to calculate the dynamic drift responses. The density of steel is considered as 7850 kg/m^3 with a Young's Modulus and Poison's ratio of 200,000 MPa and 0.25, respectively. The first, second and third modes are found to be at 0.198, 0.281, and 0.361 Hz, respectively. The mass of each stories floor is determined based on the natural frequencies previously mentioned from (Chan et al., 2009a; Huang, 2017). Based on their height and applied time-history mean wind velocity, all examined structures produced different natural frequencies. Twelve additional structures corresponding to the same structure's height used the same steel and columns selected as the structure subjected to an applied mean wind velocity of 40 m/s, which examined a total of twenty-eight structures. Table 3.3 presents the design along-wind and across-wind base shear forces, the torsional base torque from the wind-induced structural loads at a velocity of 40 m/s acting on a CAARC structure of 180m, 140 m, 100 m, and 60 m height. In the FEM analysis, the structure is considered in a dense, metropolitan location to have multiple structures in proximity. As previously mentioned in Section 3.2.1.3, the overall applied wind loading was acquired using the numerical LES analysis. The across-wind direction (x-direction) of the analyzed structure is found to have a more significant displacement and drift than the along-wind direction (y-direction) response of the structure under a 0° wind angle of attack, see Figure

3.7 (a). Figure 3.7 (b) and (c) show a comparison of the maximum top lateral deflection and inter-storey drift along the x-direction at the most critical instant, respectively. The study by (Chan et al., 2009a; Huang, 2017) concluded that the initial member sizes chosen for their analysis exceeded the maximum deflection and inter-storey drift limit ratios of H/400 and 1/400, respectively. It is considered since the initial member sizes are initially based on the preliminary strength check, as mentioned in Section 3.1. The structural system's intended use is evaluated in a structural optimization study to maintain drift and deflection strains.

Table 3.2: Steel sections for all the examined structures

180 m tall CAARC structure					
Storey levels	Beam size	Column size			
		$v = 20\,m/s$	$v = 30\,m/s$	$v = 40\,m/s$	$v = 50\,m/s$
1 - 9	W30 x 357	W14 x 342	W14 x 398	W14 x 550	W14 x 730
10 - 18	W30 x 326	W14 x 283	W14 x 342	W14 x 500	W14 x 550
19 - 27	W30 x 292	W14 x 193	W14 x 233	W14 x 370	W14 x 398
28 - 36	W30 x 261	W14 x 132	W14 x 159	W14 x 257	W14 x 283
37 - 45	W30 x 211	W14 x 82	W14 x 99	W14 x 159	W14 x 176

140 m tall structure					
Storey levels	Beam size	Column size			
		$v = 20\,m/s$	$v = 30\,m/s$	$v = 40\,m/s$	$v = 50\,m/s$
1 - 9	W30 x 235	W14 x 233	W14 x 311	W14 x 398	W14 x 500
10 - 18	W30 x 211	W14 x 159	W14 x 211	W14 x 283	W14 x 370
19 - 27	W30 x 191	W14 x 109	W14 x 145	W14 x 193	W14 x 257
28 - 35	W30 x 148	W14 x 68	W14 x 90	W14 x 120	W14 x 159

100 m tall structure					
Storey levels	Beam size	Column size			
		$v = 20\,m/s$	$v = 30\,m/s$	$v = 40\,m/s$	$v = 50\,m/s$
1 - 9	W30 x 132	W14 x 159	W14 x 193	W14 x 257	W14 x 311
10 - 18	W30 x 124	W14 x 109	W14 x 132	W14 x 176	W14 x 211
19 - 25	W30 x 116	W14 x 74	W14 x 90	W14 x 120	W14 x 145

60 m tall structure					
Storey levels	Beam size	Column size			
		$v = 20\,m/s$	$v = 30\,m/s$	$v = 40\,m/s$	$v = 50\,m/s$
1 - 9	W30 x 99	W14 x 99	W14 x 120	W14 x 145	W14 x 176
10 - 15	W30 x 90	W14 x 68	W14 x 82	W14 x 99	W14 x 120

Table 3.3: Design wind loads for Building 1 subjected to a design mean wind velocity of 40 m/s

Structure height (m)	Along-wind base shear (kN)	Across-wind base shear (kN)	Torsional base torque (kN.m)
180 (CAARC)	18826	28238	688307
140	13569	20354	496129
100	8752	13128	319986
60	4495	6742	164333

Figure 3.7: (a) FEM CAARC model dimensions, (b) maximum deflection of storeys, and (c) maximum inter-storey drift in the along-wind direction

3.2.2.2   FEM modelling of time-history wind load and determination of the adequate separation distance

As mentioned in Section 3.2.1.4, the two adjacent structures are numerically modelled through the CFD wind simulation to capture forces acting on each structure, then applied to a full-scale FEM model as a time-history analysis to determine the dynamic responses of both adjacent structures. The applied wind load and adjacent structures can be seen in Figure 3.8. The applied wind forces acting on the structure function as a singular wind force, per x and y directions, located at the center of each floor's diaphragm, as mentioned in Section 3.2.1.4. All wind forces are scaled to the full-scale mean wind velocity, varying from 20 m/s to 50 m/s in the along-wind direction. The total

duration of the FEM simulation is 11.5 minutes. The results for the validated CAARC adjacent structures are as shown in Figure 3.9 (a-c), representing the displacement, moment, and shear force-time history for both building 1 and building 2, respectively, for an applied mean wind speed of 40 m/s.

After simulating the structures in proximity using FEM, the $d_{g,min}$ between structures can be determined. If the provided or enabled d_g is less than the required $d_{g,min}$ between the two adjacent structures, and the summation of both the structural lateral displacements exceeded the provided d_g, an interaction (pounding) will occur. This interaction will be discussed in the following section, Section 3.2.2.3. To pursue such an event, each structure will consist of having an independent dynamic response and vibration. Each structure is modelled as an elastic, multi-degree-of-freedom system and will act as a moment-resisting frame. If pounding occurs, both longitudinal and transverse forces will be captured. The influence of the $d_{g,min}$ on the pounding effect from the two colliding structures is parametrically examined in this investigation. The point of contact, if pounding occurs, will occur between the stories floor diaphragms (among the storey masses). This assumption is believed to be suitable because the studied structures have identical storey heights and overall building heights.
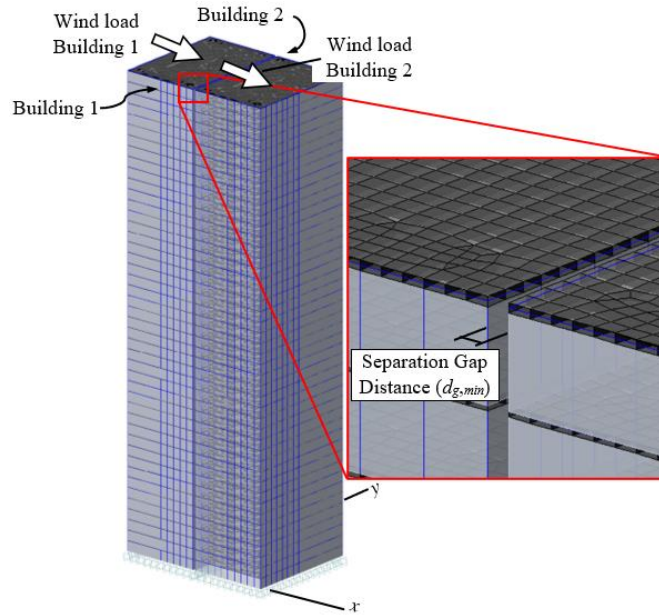
Figure 3.8: Three-dimensional view of the two CAARC structures with a separation distance of $d_{g,min}$
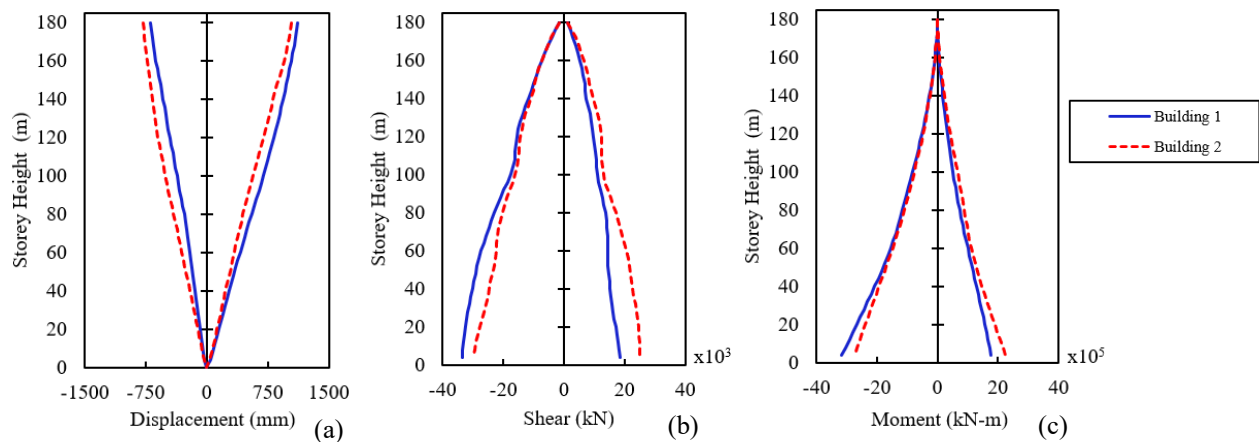
Figure 3.9: Maximum (a) displacement, (b) base shear force, and (c) base moment for building 1 and building 2

3.2.2.3 FEM modelling of the compression gap element

In order to accurately capture forces of the two adjacent structures during pounding, a compression-only gap element in the FEM analysis is considered, see Figure 3.10 (a). The compression gap element considers a specified "gap distance," resembling the separation distance between the two adjacent structures. When this specified gap distance reaches a value of zero, only then the gap element will perform as a compression spring. This will record the compression values

throughout the applied time-history wind analysis and monitor each structure if any part of the structure comes into contact with the adjacent building (i.e., beams, columns or slabs) (Karayannis and Favvata, 2005a, 2005b), as shown in Figure 3.10 (b). As this study examines the necessary $d_{g,min}$ required to mitigate pounding, the local effects and progressive collapse on the structure's columns, beams and slabs are not considered for this modelled analysis as it only affects the performance of the structure during and after the pounding effects.

When examining the adjacent structures at proximity subjected to a time-history wind analysis, the contact gap elements will comply in two scenarios. The first instant considers when the initial separation gap distance (d_g) is larger than the summation of the structure's lateral displacements, which is represented as a position gap opening (δ), see Figure 3.10 (b). Without the summation of the structures lateral displacements being greater than the d_g, the gap element in this scenario will act as a non-active as no contact (pounding) between the two structures has occurred (see Figure 3.11 (a)). The second scenario occurs when the summation of both structures' lateral deflection exceeds the d_g between the adjacent buildings. This will produce a positive compression value from the contact (i.e., structural pounding) between the examined structures, ultimately leading to an active compression spring force, allowing the gap element to monitor the pounding forces over the allocated period (see Figure 3.11 (b)).
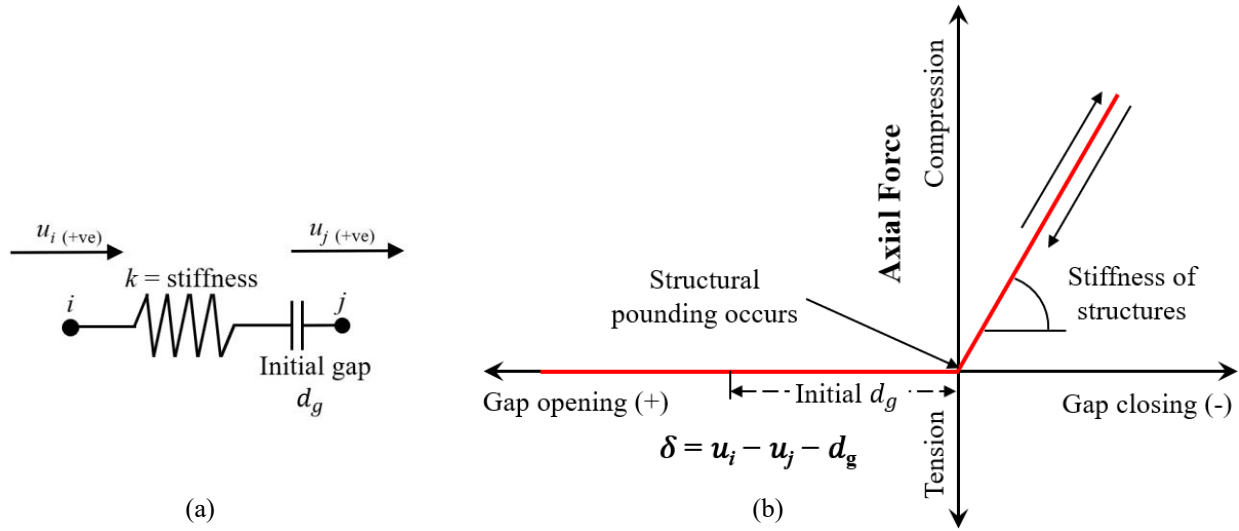
Figure 3.10: (a) Replicated gap element and (b) response of gap element
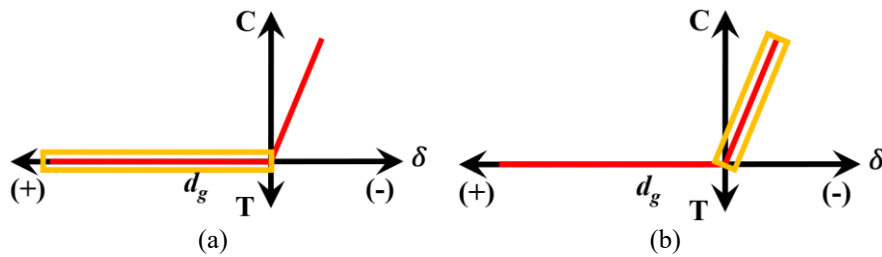
Figure 3.11: Response of compression gap element in all pounding scenarios for (a) Scenario 1 $(\Delta_1 + \Delta_2 < d_g)$, and (b) Scenario 2 $(\Delta_1 + \Delta_2 \geq d_g)$

To monitor the compression forces when pounding occurs, the spring stiffness (k) in the gap elements must be chosen appropriately. It was reported that the k is considered relatively large when pounding transpires (Anagnostopoulos, 1988; Karayannis and Naoum, 2018b; Mahmoud et al., 2013). A constant value of k is uncertain due to the unknown geometric impact surface, materials involved during the pounding impact from its uncertain structural properties, despite variable impact velocities. A study by (Ghandil and Aldaikh, 2017b) found that when k values are more significant than 10^{10} N/m, the pounding-involved response is insensitive to the impact stiffness. On the other hand, the impact stiffness coefficient should be between 50 and 100 times larger than the lateral stiffness of the structure involved in pounding (Naserkhaki et al., 2012).

These values cannot be generalized since they are applicable to the specific numerical and experimental studies (Miari et al., 2019). However, past literature (Anagnostopoulos and Spiliopoulos, 1992; Karayannis and Naoum, 2018; Kim et al., 2000; Maison and Kasai, 1992) mentions that the structural response is not remarkably sensitive to the alteration of k when considered at relatively high values (i.e., amplifying by a factor of one hundred). Therefore, a pounding stiffness model is implemented in this studied model as a linear elastic model (Jankowski, 2008b, 2006b, 2005; Miari et al., 2019). Once the gap element is activated (i.e., pounding occurs), a pounding force impact (F_I) is captured at the location of impact, which is expressed in Equation (3)

$$F_I = k\delta \qquad\qquad \text{for } \delta = u_i - u_j - d_g \qquad\qquad\qquad \text{Equation (3)}$$

where δ is defined as the relative displacement between the pounding structural elements. The spring stiffness (k) is only activated when pounding of adjacent structures occurs in Scenario 3 (see Figure 3.11 (b)). u_i, u_j are the displacement of the element nodes i and j, respectively.

To determine k for the gap element, the examined models' structural stiffness needs to be evaluated (Naserkhaki et al., 2012). Therefore, the structure's stiffness (k_T) is obtained from determining a shear force (V) from an applied load acting on the examined structure, as per Equation (4).

$$V = k_T * \Delta u \qquad\qquad\qquad\qquad\qquad\qquad\qquad\qquad \text{Equation (4)}$$

where V is defined as the structure's shear force, which represents the summation of applied forces in a given direction. k_T and Δu are defined as the overall structural stiffness and lateral displacement of the structure, respectively.

V, k_T and Δu are shown in Figure 3.12 to represent a 10-storey skeletal frame structure with applied wind force, V. Equation (4) is then re-arranged to determine k_T in order to determine k for the gap element. Once the k_T is defined, a multiplication factor of 50-100 times is applied (Naserkhaki et

al., 2012). Therefore, a single applied force, V, of 10^6 N is considered to act only on the top storey diaphragm of the 45-storey structure, perpendicular to the longest side of the building (i.e., 45 m long side). This is equivalent to the base shear force of the structure. A maximum lateral displacement (Δu) of 82.64 mm was determined, meaning the overall stiffness of the structure (k_T) is approximately $12.1 * 10^6\ N/m$. A compression gap element stiffness (k) per storey of $12 * 10^8\ N/m$ was determined from k_T*100. To assure that the acquired k is sufficient for all examined structures, a comparison with altering k (i.e., 6.6k, 5k, 3k, 2k, 1.66k, 1.33k, k, 0.66k, and 0.33k) was performed. It is found that the FEM captures an average pounding force of 12,800 kN for various gap element stiffnesses, k, as shown in Figure 3.13. Therefore, a $k = 12 * 10^8\ N/m$ is determined to adequately capture the average pounding force for all the examined models.
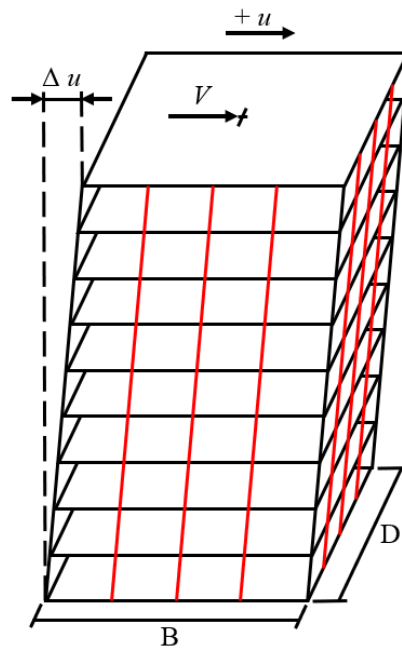
Figure 3.12: Deformation of structure from applied force (V)
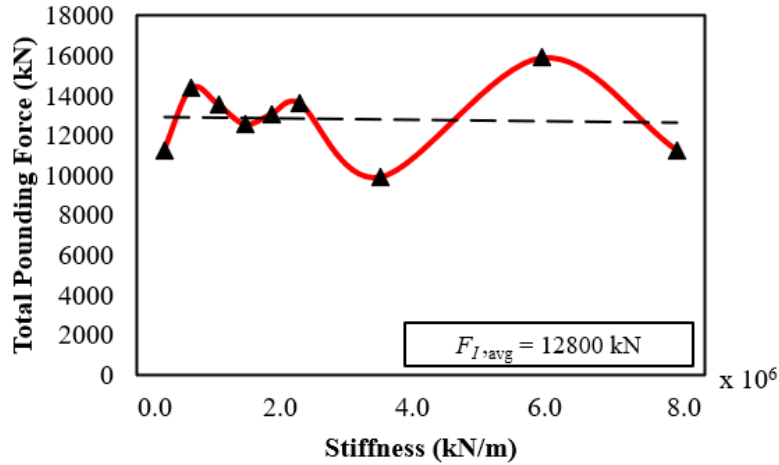
Figure 3.13: Pounding force of structures for different gap element stiffness (k)

A sensitivity analysis is performed to determine the required number of gap elements. In the examined pounding model, results have shown pounding to occur only in the top three floors, depending on the separation gap distance. Therefore, a total of ten floors are modelled with gap elements. Since there are a total of fifteen bays in the longitudinal direction of the structures (i.e., 45 m long side), a total of sixteen columns-to-beam connection locations would be used for locations of the gap elements. A compared analysis of 1, 4, 9 and 16 gap elements are studied, shown in Figure 3.14, having the summed F_I at the time instant of impact. Altering the number of gap elements to capture the total F_I, the most considerable difference in F_I is between 1 and 9 gap elements per storey, having a difference of 2.42%. It is determined to accurately capture and monitor the pounding of structures; four gap elements being evenly spaced out among the longest side of the adjacent structures were considered. The value k is considered to be equal to $3*10^8$ N/m per compression gap element throughout all examined structures. Each storey consists of the four gap elements, having a total of forty gap elements monitoring the pounding forces acting on the colliding structures. Figure 3.15 shows the locations of the gap elements on the adjacent structures.
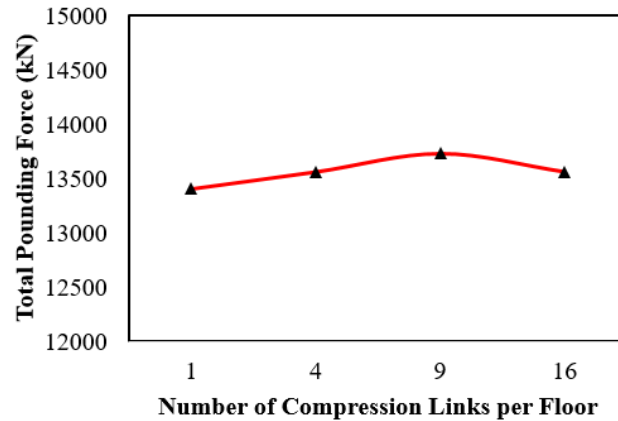
Figure 3.14: Pounding force with alteration of the number of gap elements
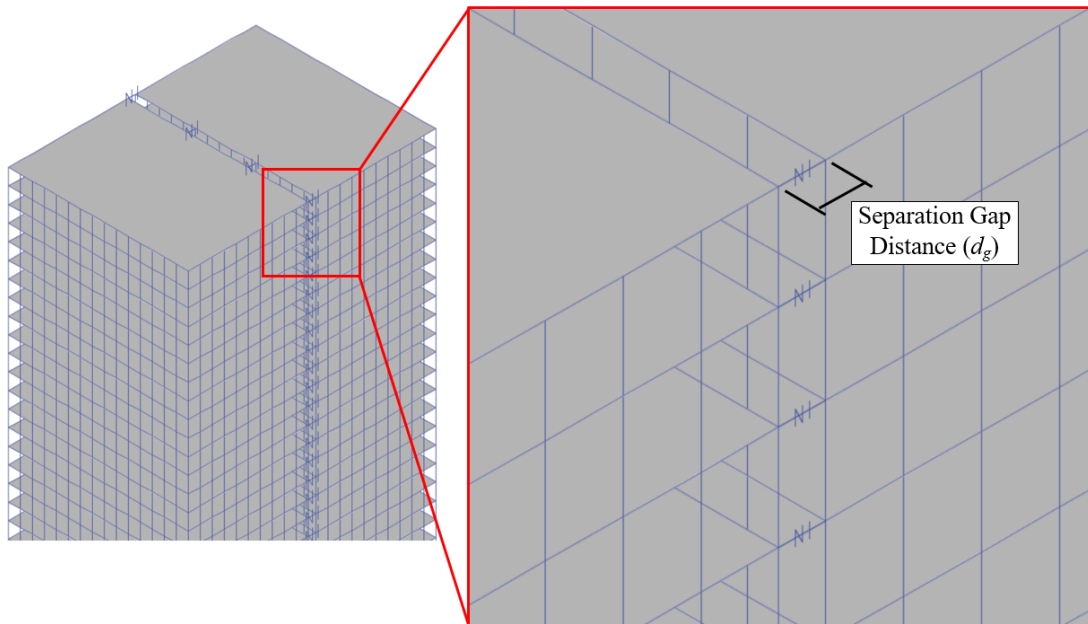
Figure 3.15: Gap element locations on CAARC structure

3.2.3 Development of Mathematical Formulas to Determine Minimum Separation Gap Distance ($d_{g,min}$)

The mathematical formulation can be determined for the required $d_{g,min}$ by examining various input properties relating to the structure's lateral deflection. Such parameters can include the structure's Natural Frequency (F_n), building Height (H), and applied mean wind velocity (v). The mathematical formula aims to determine the required $d_{g,min}$ between two adjacent structures in

proximity to mitigate pounding interaction. A genetic algorithm (GA) is adopted in this study to optimize the numerical formulation. The adopted GA (Edwards, n.d.; Keim, n.d.) was developed at the Computational Synthesis Lab at Cornell University (Schmidt and Lipson, 2009) from a numerical package called "Eureqa". The GA technique involved many numerical simulations of the objective function association to several initial entries (i.e., a combination of different variables over multiple generations) (Elshaer et al., 2017). The process of determining the objective function can become extremely costly if the objective function is to be evaluated directly using the CFD and FEM numerical simulations.

The GA uses design variables, which are coded as real numbers, and is adopted for the optimizing formulation. For detecting equations and hidden mathematical relationships in raw data, the GA uses a symbolic regression (Dubčáková, 2011). One key advantage of GA is its ability to find the global extreme value without being confined to a local extreme value (i.e., maximum or minimum extreme value). The GA process initiates from a search process, including multiple raw data points in the search space. In addition, it will include mutation operators that will generate search points away from the high fitness region. This will help avoid any search points being trapped within a local extreme value (Elshaer et al., 2017). The GA has been reported by past scholars (Ansary et al., 2011; Elshaer et al., 2017; Zhou and Haghighat, 2009) to be efficient in determining the optimal solution in similar complex engineering optimization problems, and more information regarding the GA can be seen in (Davis, 1991; DE Goldberg, 2013).

The GA uses combinations of different design parameters labelled as the "candidate" and represents other dynamic variables. The GA starts its optimizing process by initiating the search using the initial candidate, also known as the "initial population." Within the initial population, the objective function is evaluated for each candidate. This will sort the candidates according to

their own fitness (i.e., lowering or elevating the value objective function). To produce better candidates (offspring), the crossover and mutation operators must be applied to the current population. The crossover operators will be applied to the candidates (parents) with higher fitness to seek for better performing offsprings. Additionally, the mutation operators are applied to the parents with lower fitness to explore the possible different regions within the search space and help avoid any stagnation in local extreme values (Elshaer et al., 2017; Mengistu and Ghaly, 2008). The GA process towards applying the operators and producing new generations will maintain optimization until there are no substantial improvement over generations. Therefore, the last generation for the highest fitting candidate is considered the GA optimal solution.

In the current study, the GA will aim to find the dg,min needed to mitigate structural pounding from two adjacent structures in proximity. The objective function is set to be the minimum separation gap distance (dg,min). For each combination of design variables (candidate), the objective function is evaluated for four increments of mean along-wind velocities (v) at the reference building height (i.e., 20 m/s, 30 m/s, 40 m/s, and 50 m/s). The design variables, H and Fn, represent the structural height and its overall mass and stiffness, respectively, where Fn is defined in Equation (5).

$$F_n = \frac{1}{2\pi} \sqrt{\frac{k}{m}} \, \text{(Hz)} \qquad\qquad \text{Equation (5)}$$

where m is the mass (kg), and k is the stiffness (N/m) of the structure.

Table 3.4 summarizes all the examined training samples used to train the mathematical formulas. In the presented study, the lower and upper bounds are set to 60 m and 180 m for H, respectively, while the lower and upper bounds for F_n are set to 0.148 Hz and 0.416 Hz, respectively. These parameters are applied throughout the FEM analysis.

Table 3.4: Initial design variables

Building Height (H) (m)	Applied Mean Wind Velocity (v) (m/s)	Natural Frequency (F_n) (Hz)
	50	0.211
	50	0.198[a]
	40	0.198
180	30	0.166
	30	0.198[a]
	20	0.148
	20	0.198[a]
	50	0.249
	50	0.222[b]
	40	0.222
140	30	0.197
	30	0.222[b]
	20	0.195
	20	0.222[b]
	50	0.302
	50	0.277[c]
	40	0.277
100	30	0.239
	30	0.277[c]
	20	0.209
	20	0.277[c]
	50	0.416
	50	0.381[d]
	40	0.381
60	30	0.308
	30	0.381[d]
	20	0.281
	20	0.381[d]

[a] properties from 180 m structure for $v = 40\ m/s$
[b] properties from 140 m structure for $v = 40\ m/s$
[c] properties from 100 m structure for $v = 40\ m/s$
[d] properties from 60 m structure for $v = 40\ m/s$

3.3   Results of the Performed Parametric Study

Twenty-eight examined structures in proximity with equal height involved in an extreme wind-induced occurrence to determine the required $d_{g,min}$ is examined and discussed. The parametric study used FEM analysis to calculate the lateral deflections of two adjacent tall structures in order to determine the adequate $d_{g,min}$ to avoid wind-induced pounding. A graphical comparison of the two adjacent structures is shown in the following figures representing their lateral displacement responses (sufficient $d_{g,min}$ for preventing a pounding event). Figure 3.16 shows the time history of the two adjacent 180 m tall structures (acting on the 45th storey for their lateral deflection)

subjected to a synoptic wind with a mean velocity of 40 m/s at building height with a d_g at 2000 mm. A $d_{g,min}$ required to prevent a collision for this scenario at the top of both structures is 1898.64 mm. It can be noted from Figure 3.16 that at the time instant of 628 seconds, both structures have a significant spike in their lateral sway. Such lateral deflection based on the structure can occur due to the natural sway frequency of a building having a similar natural frequency of the vortex shedding acting on the specific structure from to the applied mean wind velocity. This will cause the structure to have a dramatic spike in its sway with lower mean wind velocities than the deflections of a structure with higher applied mean wind velocities. Figure 3.17 (a) shows the collision (i.e., pounding) of the two 180 m tall adjacent structures with a d_g equal to 1800 mm. As shown in Figure 3.16, the d_g between structures is 2000 mm and came into proximity at 628.17 seconds; however, no collision of structures occurred. Since the gap elements are not activated, no forces were produced because the structures did not come into contact. Therefore, Figure 3.17 (a) came into contact at the same instant since the d_g is reduced to 1800 mm, even though the required $d_{g,min}$ was concluded to be 1898.54 mm. Figure 3.17 (b) and (c) display the pounding forces acting on the two structures when a collision occurs ($t = 628.17\ seconds$). Figure 3.17 (c) compares the forces applied at storey 45, 44, and 43 when the pounding of structures occurs.

For a pounding force where the determined $d_{g,min}$ is violated, a similar mathematical formula can be developed to estimate the expected pounding force as a function based on certain preliminary factors (i.e., H, v, F_n and $d_{g,min}$). The pounding force under this scenario is recorded with the compression gap element, as described in Section 3.2.2.3. In Figure 3.18-Figure 3.21, a similar time-history comparison was conducted, as shown in Figure 3.16. The applied time-history velocity in Figure 3.18 is 50 m/s on two adjacent 180 m tall structures. Figure 3.19, Figure 3.20, and Figure 3.21 show that the applied mean wind velocity is 40 m/s on two adjacent 140 m, 100

m, and 60 m tall structures, respectively. The initial separation distance utilized in Figure 3.18-Figure 3.21 are stated in the figures (i.e., 3000 mm, 1000 mm, 500 mm, and 400 mm, respectively). Figure 3.22 compares the determine $d_{g,min}$ required for all twenty-eight FEM models, depending on the structure's height, natural frequency and applied mean wind velocities. As noted, tall and slender structures are more susceptible to more significant structural sway, even with lower applied lateral load.
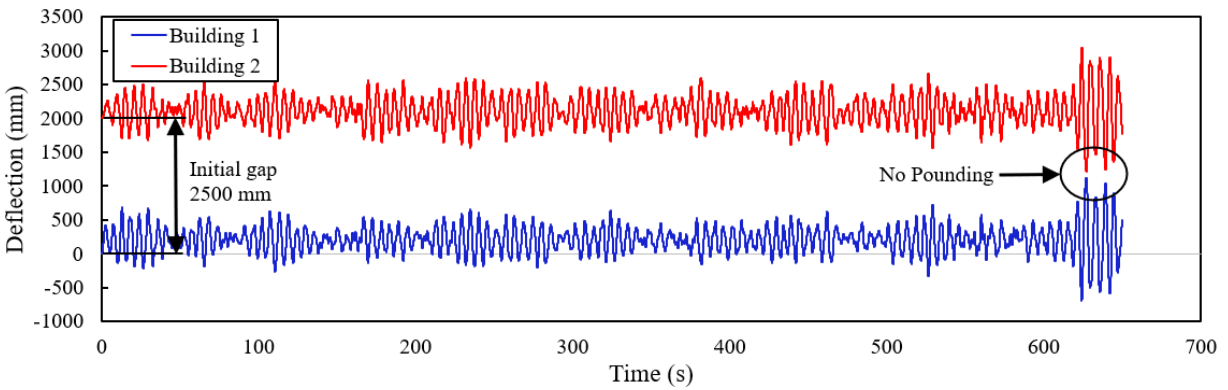
Figure 3.16: Time-history displacement of 180 m structures
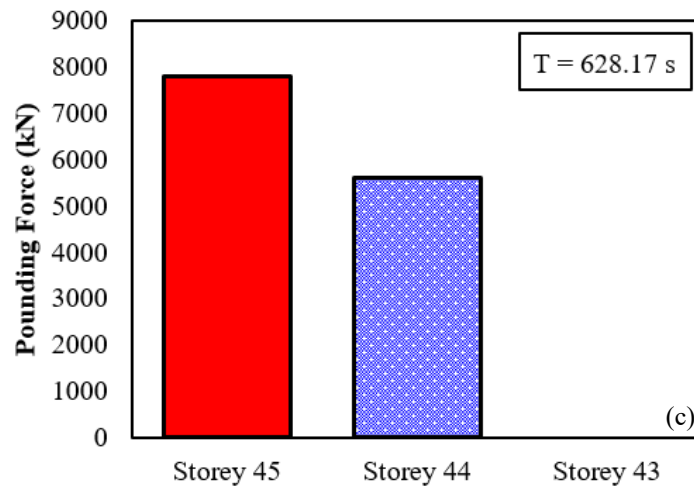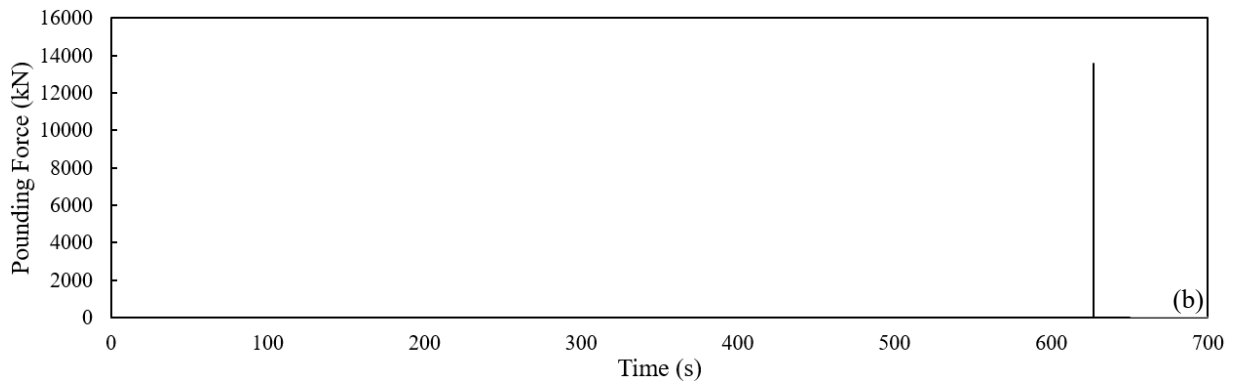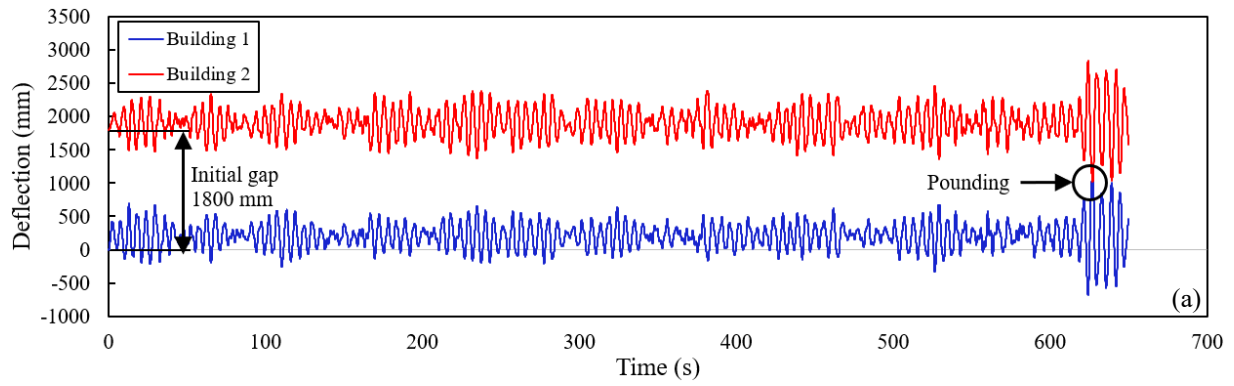
Figure 3.17: Time-history for (a) 45th storey displacement, (b) pounding forces time, and (c) pounding forces on 45th, 44th, and 43rd storey
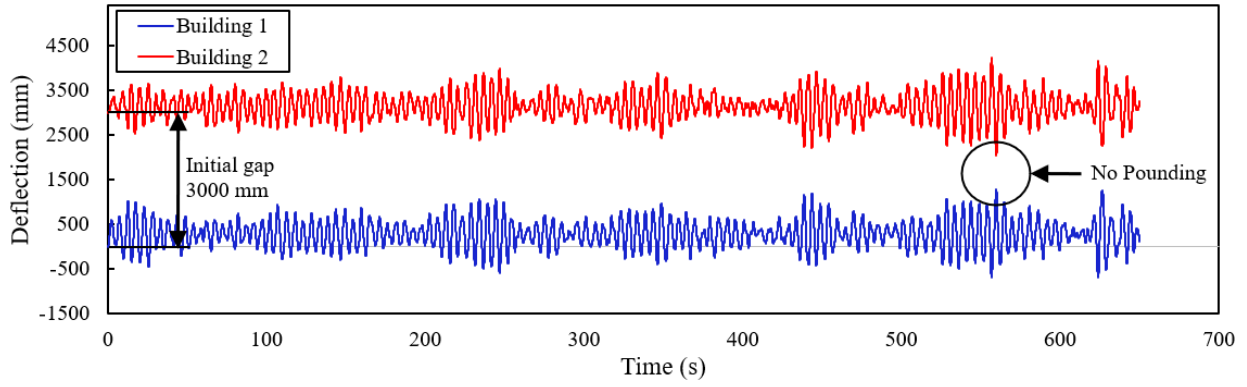
Figure 3.18: Time-history displacement of 180 m structures
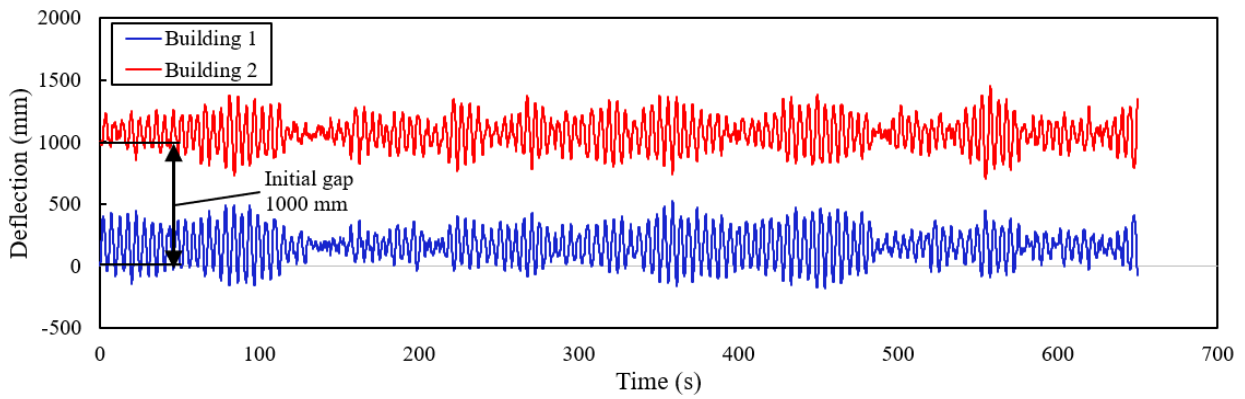
Figure 3.19: Time-history displacement of 140 m structures
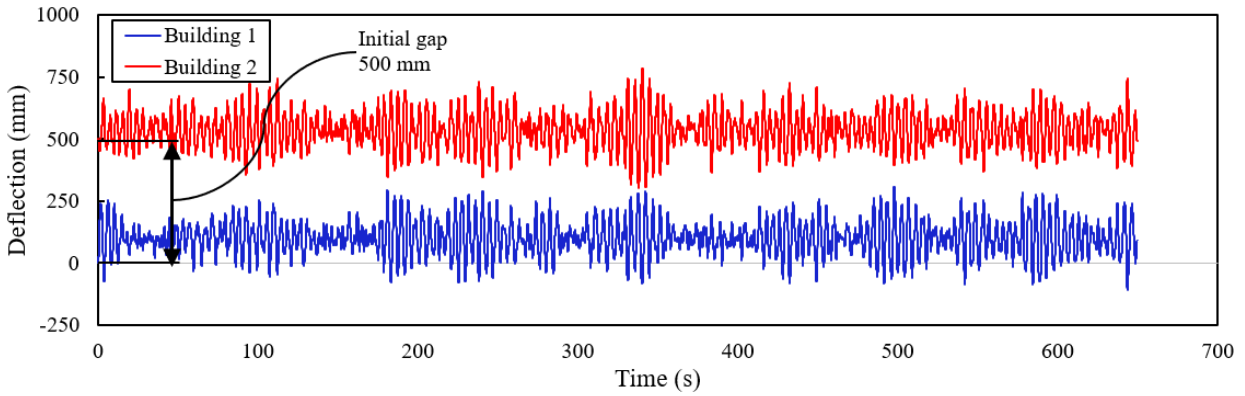
Figure 3.20: Time-history displacement of 100 m structures
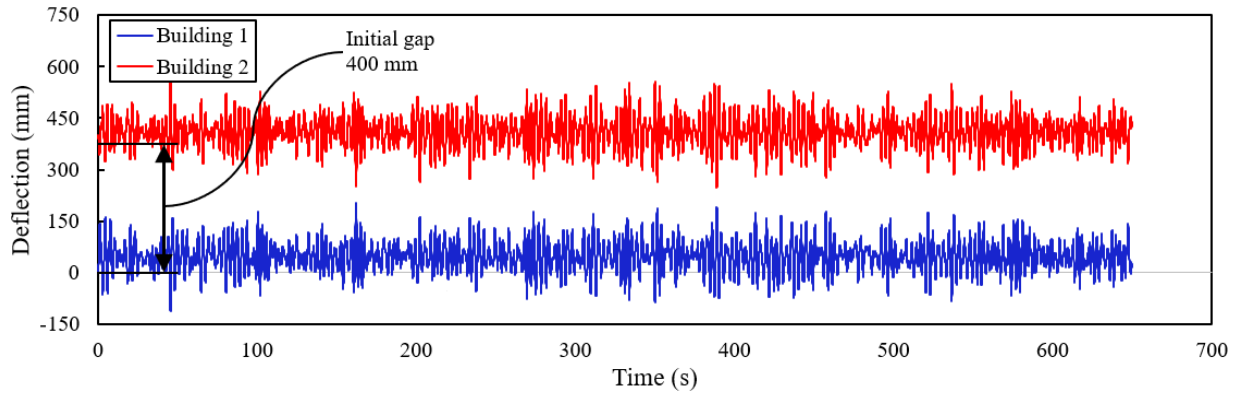
Figure 3.21: Time-history displacement of 60 m structures
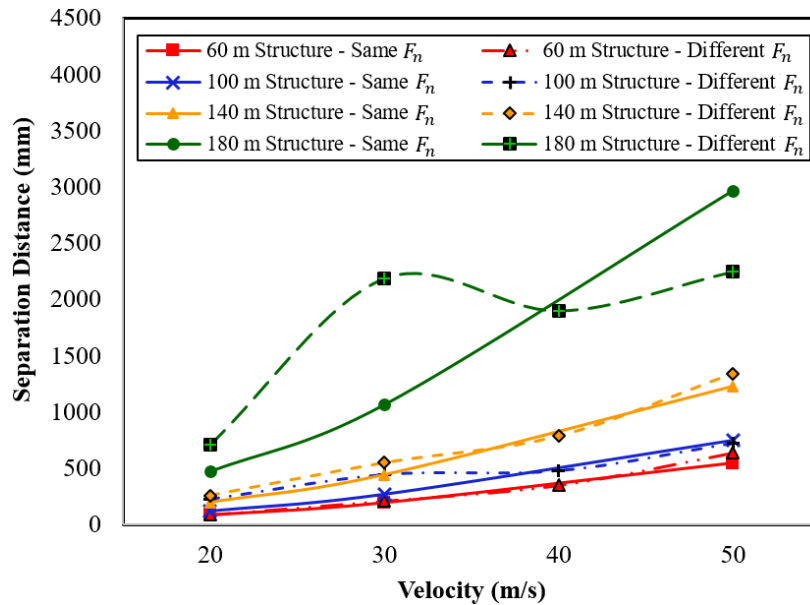
Figure 3.22: $d_{g,min}$ required to mitigate structural pounding

It can be noticed in Figure 3.22 that dependent on the two adjacent structure's heights, an increase in separation distance is required under the applied mean wind velocity to achieve a $d_{g,min}$ to mitigate a pounding event. However, a drastic increase in the required $d_{g,min}$ for the 180 m structures at an applied mean wind velocity of 30 m/s is recorded. This can be due to the structure's natural sway frequency having a similar natural frequency of the vortex shedding on the specific structure from the applied wind force at an instant of time. A more significant lateral deflection can then occur to the structure subjected to wind. This can also be seen on the 100 m tall structure

for the applied 30 m/s mean wind velocity but for a smaller lateral deflection. As can see in Figure 3.22, comparing the $d_{g,min}$ required for all structures subjected to the applied mean wind velocity from 40 m/s to 50 m/s, the smallest change increases by 15% for the 180 m tall structures; however, it decreases from the 30 m/s to 40 m/s at -15%. For comparing the applied mean wind velocity from 20 m/s to 30 m/s on the height of each structure, the smallest change for the required $d_{g,min}$ increases by 49% on the 100 m tall structures. Thus, the $d_{g,min}$ required for the 100 m tall structures subjected to a mean wind velocity of 20 m/s is 229 mm compared to a $d_{g,min}$ required for a similar structure's height subjected to a mean wind velocity of 30 m/s is 446 mm. The most remarkable change in required $d_{g,min}$ appeared at the 180 m structures from 20 m/s to 30 m/s with a change of 68%.
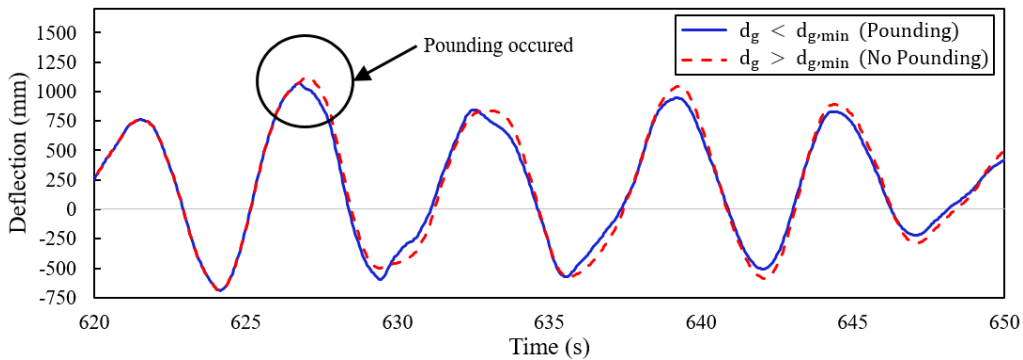
Figure 3.23: Building 1 deflection during pounding versus non-pounding

Figure 3.23 shows a comparison between the deflection time history of the upstream structure (building 1) when adequate gap distance is provided ($dg = 2000\ mm$) to a similar structure with insufficient gap distance ($dg = 1800\ mm$). It can be noted that a drop in deflection happens at the instant when pounding occurs ($t = 628.17\ seconds$). However, the deflection of building 1 alters after pounding happens not substantially. After numerically analyzing the required $d_{g,min}$ to mitigate structural pounding, results indicated that the most critical pounding occurrence (and deflection) occurs at the tallest point of the structure due to the most considerable lateral deflection

(i.e., 45th storey for the 180 m tall structure), and decreases when analyzing lower stories of the structure. From the parametric examination of an adequate $d_{g,min}$ from wind-induced structural pounding, outcomes can conclude that a $d_{g,min}$ will vary depending on the structure's height, modal period, and the applied wind forces. For all structures, the $d_{g,min}$ will increase when the natural frequency decreases, mean wind velocity increases, and structural height increases. This correlation will be discussed in the next section of the manuscript (Section 3.4).

3.4   Formulated Minimum Separation Gap Distance ($d_{g,min}$)

This section aims at developing mathematical formulas to determine the required minimum separation gap distance ($d_{g,min}$) to avoid structural pounding based on the building height, natural frequency, and the applied wind. To select the best model that provides the most reliable evaluation for the objective function, a variety of mathematical models need to be examined (i.e., polynomial, trigonometric, exponential, and logarithmic functions). As mentioned in Section 3.2.3, the GA used different combinations of geometric parameters (i.e., building height, natural frequency, and mean wind velocity) with twenty-eight samples to determine the required $d_{g,min}$. More than $2.1 * 10^{12}$ formulas were evaluated and then ranked based on their correlation coefficient. The most applicable analytical models and their formulas for evaluating the objective function can be seen in Table 3.5. The highest correlation coefficient obtained is 0.9987 and a mean absolute error of 22.34 mm. Figure 3.24 shows the regression plot for different trained GA models dependent on their generated ranking.

Table 3.5: Ranked correlation coefficient GA formula for the analytical models

Rank	Correlation Coefficient	Mean Absolute Error (mm)	Mathematical formula*
Eq 1	0.9987	22.34	$d_{g,min}\,(mm) = (48280 - 3378*v)/(H - 149.49 - 393.25*F_n) + 0.8274/\cos((48280 - 3378*v)/(H - 149.49 - 393.25*F_n)) + (149.49 - 2226*F_n{}^2)/(149.49*F_n + 0.1956*H - v - H*F_n) + \cos((48280 - 3378*v)/(H - 149.49 - 393.26*F_n))$
Eq 2	0.9956	41.16	$d_{g,min}\,(mm) = 84.7/(35.6 - v - 215.2*F_n) + (48383 - 3358*v)/(H - 146.92 - 404.3*F_n)$
Eq 3	0.9806	73.25	$d_{g,min}\,(mm) = 0.022*v{}^2 + (45127 - 3137*v)/(H - 144.4 - 408.75*F_n)$
Eq 4	0.9798	74.58	$d_{g,min}\,(mm) = (47476 - 3323*v)/(H - 147.67 - 399.64*Fn)$

*v, H, and F_n are in m/s, m, and Hz, respectively
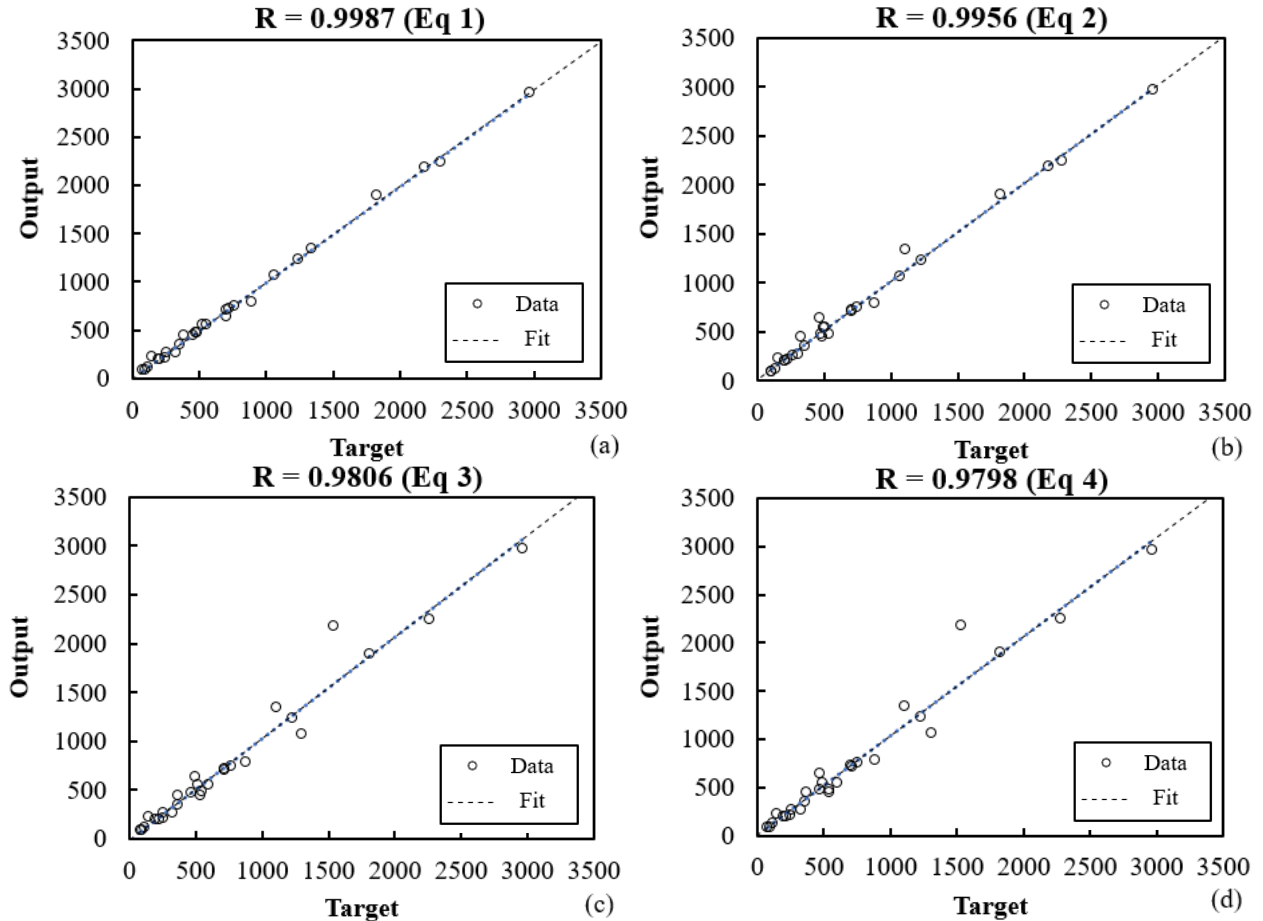
Figure 3.24: Regression plot (a) Eq 1, (b) Eq 2, (c) Eq 3, and (d) Eq 4

The optimized GA procedure is conducted to determine the $d_{g,min}$ between two adjacent structures until the optimal solutions are obtained after 154 generations, in a total of 24 hours on an 11th Gen

Intel(R) i7-11700K, 32 GB RAM, GeForce RTX 3070. Figure 3.25 shows the fitness curve for the optimal GA formula where the objective function (required $d_{g,min}$) of the best fitness candidate accuracy is plotted versus the generation number. The plotted illustration displays the improvement of the objective function ($d_{g,min}$ required) over the optimized GA formula. As mentioned previously, the maximum error recorded is 22.34.
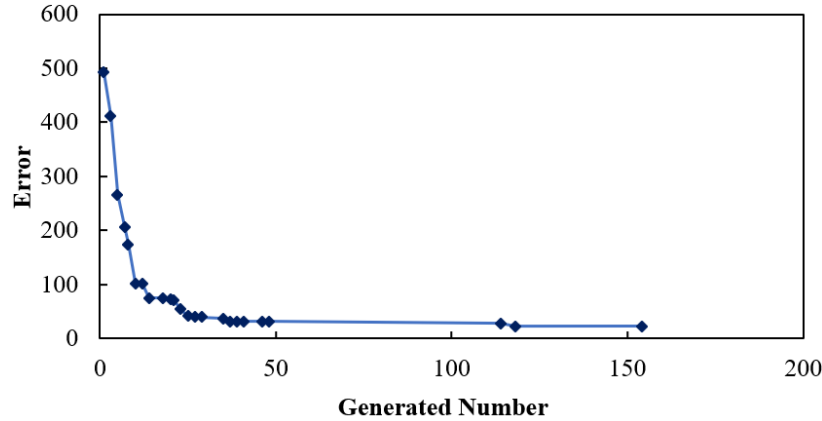
Figure 3.25: Fitness curve for optimal GA formula

After the best candidates were generated and a GA formula was conducted and identified to determine the required $d_{g,min}$, a FEM analysis was produced with modifications toward all the geometric parameters. This is to verify the GA formulation to confirm the $d_{g,min}$ to be acceptable for preventing a wind-induced pounding event. Since all twenty-eight examined samples took into consideration the limits of the preliminary strength check according to the AISC steel code (2001), therefore, the F_n ultimately reached the smallest threshold based on the applied mean wind velocity. Namely, each structure with the most considerable lateral deflection is concluded based on its building heights and applied wind forces. All FEM simulations with altered geometric parameters compared to the highest rank GA formula concluded to have a lower required $d_{g,min}$ since the considered GA formulation for the $d_{g,min}$ reflected on having the maximum lateral deflection on both structures, based on the applied mean wind velocities, structural heights, and

the governing natural frequencies. Therefore, to adequately design for tall structures in proximity in extremely high wind locations, the GA formulation for designing a sufficient $d_{g,min}$ overestimates the required $d_{g,min}$, eliminating any possible wind-induced structural pounding.

3.5   Summary

This chapter conducted a parametric analysis to develop a mathematical formulation for estimating the required separation distance between two adjacent structures in proximity of equal heights subjected to wind. The analysis used LES models to determine the applied time-history wind forces acting on the two adjacent structures. The forces were then applied to a non-linear FEM simulation to predict the structure's response. Twenty-eight modelled buildings were considered as inelastic multi-degree-of-freedom skeletal steel structures. Once developed, a genetic algorithm is then developed to optimize a mathematical formula to determine the required separation distance between the two adjacent structures in proximity, based on the building height and natural frequency along with the applied wind. The developed mathematical formula is then compared to altering geometric parameters through the FEM numerical analysis. The determined separation gap distance during the time history analysis are used as initial parameters of the specified structures for chapter 4.

4 Chapter 4 – Pounding Force Formulation for Tall Structures in Proximity Subjected to Wind

4.1 Background

The new generation of high-rise structures is becoming more flexible due to the buildings becoming increasingly taller and slender (Elshaer et al., 2017). Such structures are ultimately more sensitive to lateral loads, such as wind (Bobby et al., 2014; Ding et al., 2019; Elshaer and Bitsuamlak, 2018; Huang et al., 2012; Irwin et al., 2008; Irwin, 2009; Lam et al., 2009). Additionally, to control the inertial forces developed by earthquakes, a need to lower the structure's weight to gravity loads is required (Rahman et al., 2012). This will further contribute to an increase in the wind-induced forces and motions, leading to the wind being the ultimate governing load for the design of the structure and its lateral load resisting system (Elshaer et al., 2017). A study by (Cui and Caracoglia, 2018) found on the studied 180 m tall structure using their proposed formulation, high wind loads at a certain angle on the structure (i.e., $55°$) can lead to extreme lateral displacements of the structure (i.e., up to 1370 mm). If not correctly acquired in the preliminary design phases, lateral deflection and inter-storey drifts of the structure can reach their limits when unexpected wind events occur. An intensive study from (Aly and Abburu, 2015) examined two high-rise structures under similar natural multi-hazard events (i.e., earthquakes and wind) to compare the dynamic responses of the structures (i.e., acceleration, lateral drift and inter-storey drift). Results concluded that under extreme wind loading events, a considerable overall lateral deflection and inter-storey drift within similar geological locations would be produced compared to earthquake phenomena (i.e., upwards of eight times more significant in lateral deflection and two times more prominent in inter-storey drifts). (Elshaer and Bitsuamlak, 2018) found that over time, maintaining an adequate lateral deflection or controlling the extensive vibration on a tall structure will become more challenging to meet design requirements compared

to the strength and capacity requirements within such structure. Additionally, the lateral deflection in a tall building during its structural sway motion can damage non-structural components (i.e., cladding and partition) and primary structural components (i.e., beams and columns) to the extent of damaging possible adjacent structures if the separation gap distance between structures is lesser than the lateral displacement of the adjacent structures (Chenna and Ramancharla, 2018; Rahman et al., 2012; Wolfgang, 1977). Appropriate measures must be addressed to lower large deflections on tall structures within proximity to neighbouring buildings.

When large deflections of a tall structure are produced within densely populated locations (i.e., adjacent structures), a separation distance between the structures becomes a vulnerable circumstance. The effects (i.e., interference) from wind-induced loading of tall structures within close proximity rows have been investigated in the past (Lam et al., 2011, 2008). Dynamic response, wind pressures, and deflections on all structures were evaluated by alternating the gap distance between the proximate structures. If the gap distance between tall adjacent structures is lesser than the lateral deflection produced from each tall structure, possible collisions (interaction between structures) will arise. Therefore, the term pounding of structures has become a vital definition when building structures in proximity in the past and is continuing to evolve in the newer generation of tall buildings.

The pounding of structures is defined when two or more adjacent structures within proximity are subjected to a great lateral force, making the structures collide from exceeding the adequate separation distance (Anagnostopoulos and Spiliopoulos, 1992a; Efraimiadou et al., 2013; Kasai and Maison, 1997; Maison and Kasai, 1990, 1992). The term pounding was further examined by (Jankowski, 2009) and concluded that an increase in a pounding phenomenon could occur when the structures at proximity produce an out-of-phase vibration due to the structural differences in

their dynamic properties (i.e., stiffness, mass and lateral loading) (Jankowski, 2008a; Mahmoud et al., 2013). These out-of-phase vibrations can also occur in tall structures subjected to extensive wind forces (Abdullah et al., 2001a). (Zhu et al., 2020) studied the use of tuned mass-damper-inerter on two closely linked tall adjacent structures to mitigate wind-induced responses of the linked structures. They determined that out-of-phase vibrations may be induced due to the aerodynamic interference of the two linked structures. The linked structures may lead to structural pounding through the construction and expansion joints within the link connections. Studies have also investigated super-tall twin towers' aerodynamic and structural dynamic characteristics (Qin et al., 2022). (Qin et al., 2022) found that large proportions of out-of-phase components (i.e., the two tall structures in opposite directions) will be conducted from the applied wind forces. The structural response can be controlled by structural links between the two tall structures; however, the structural links must be evaluated to alleviate a possible structural pounding due to the connection joints. Pounding can also be produced when the involved buildings are subjected to an intensive lateral wind load (Brown and Elshaer, 2022; Huang et al., 2012). Such extensive literature reviews on structural pounding phenomena have recently been reviewed and published (Brown and Elshaer, 2022; Miari et al., 2021).

Mitigation measures must be implemented in design when constructing such structures to mitigate arising wind-induced structural pounding. Namely, precautions from past investigations have been conducted to improve the safety and possible avoidance of hazardous pounding events. Past research (Jankowski, 2005; Jankowski and Mahmoud, 2015; Penzien, 1997) has evaluated the required separation distance needed to avoid the potential pounding of structures during possible excessive lateral loading events. An issue that arises for pounding is when existing structures are already building within proximity and were designed before the new building codes and provisions

to determine a minimum required separation distance, leading to possible pre-existing structural pounding events (Rezavandi and Moghadam, 2007). If an adequate separation distance cannot be provided, alternative measures may be considered (e.g., tuned dampers, shock absorbers, etc.). Without such mitigation measures, the pounding of structures can occur if adequate applied wind loads are subjected to adjacent tall structures, leading to possible damages (i.e., minor or major) to the extent of possible total collapse of structures.

As many studies have conducted structural pounding analysis (i.e., experimental and numerical) from earthquake-induced phenomena, wind-induced structural pounding can transpire when one's structure exceeds the separation distance between its other adjacent structure due to lateral deflection produced by wind, similarly to earthquake-induced structural pounding. Therefore, an out-of-phase vibration is more likely to arise in such wind events, having a higher probability of collisions. Out-of-phase vibrations will depend on the applied lateral forces (i.e., wind velocity), structures modal period and its dynamic properties (i.e., materials, height, and frame). For example, (Brown et al., 2022) study conducted the required separation distance to mitigate wind-induced structural pounding. However, the study gap to this date is when a required separation distance cannot be achieved, what possible pounding forces will be produced when a wind-induced structural pounding event arises. Accordingly, the objective of this investigation is to determine the maximum pounding force from two adjacent structures in proximity from wind loading. This will be correlated depending on the applied wind velocity, structure height and dynamic properties, and separation distance. The analysis initializes the research with a numerical wind analysis to determine and capture the applied wind forces over a period of time acting on the two adjacent structures in proximity. The analysis then inputted the captured time-history wind forces into an alternate numerical analysis to define each structure's dynamic responses. The dynamic responses

of each structure throughout the applied wind forces can establish the lateral deflection of each structure, which can correlate with the required separation distance required to mitigate wind-induced structural pounding. Once established, the separation distance is minimized from the required separation distance to configure larger pounding forces. A mathematical equation is then recognized with all the monitored input properties (i.e., applied wind forces, structures height, modal period, and minimum required separation distance) from the studied adjacent structures to determine the pounding forces when a collision occurs if the required gap (separation) distance cannot be achieved.

The present work includes the following major contents (eight sections) to conduct the required study gap: **Section 4.1** (current section) introduces the reader to the research problem and study gap evidence. **Section 4.2** presents the framework of the numerical modelled procedure for this study. **Section 4.3** illustrated the overall geometrical details of the examined structure used throughout the numerical study. **Section 4.4** conducts a Computational Fluid Dynamics (CFD) (numerical wind analysis) with the aid of Large Eddy Simulations (LES) to establish the wind phenomena acting on the adjacent structures in proximity. Once established, **Section 4.5** is then generated to determine the studied structural integrity through a numerical Finite Element Method (FEM) analysis. **Section 4.6** then introduces the Genetic Algorithm (GA) conducted for the study. Results and discussion are presented in **Section 4.7** and will assemble the mathematical formulation for wind-induced pounding.

4.2   Framework of the Numerical Model Procedure

To establish a pounding force acting on two similar adjacent structures during a wind-induced pounding event, variables must be considered for solving such pounding forces in a suitable numerical analysis technique. Such variables can be the height of the structure (H), natural modal frequency (F_n), applied wind velocity (v) and initial Separation Gap Distance (d_g). The method for

solving the pounding forces (F_l) by altering parameters is based on a Genetic Algorithm (GA), mentioned in Section 4.6. GA's are effective optimization techniques that ultimately lead to efficiently identifying the optimal solution, which has the best performance of the objective function (e.g., highest regression) (Pourzeynali et al., 2013). GA are originally created based on the mechanics of natural selection and population genetics (DE Goldberg, 2013; Mettler and Gregg, 1969). The GA used in this analysis is a directed random search technique, and it has been widely used in many optimization problems (Elshaer and Bitsuamlak, 2018; Holland, 1992; Leung et al., 2003; Michalewicz, 1994; Pham and Karaboga, 2012). The use of the GA can be demonstrated for efficient parallelism, multi-point search and global search (Li et al., 2020). The numerical GA can help determine an optimal global solution over a given domain (Holland, 1992; Leung et al., 2003; Pham and Karaboga, 2012), as it mimics the process of natural selection in evolution (Liu et al., 2003). GA is especially valuable for complex and challenging optimization problems with many parameters, and it is challenging to achieve the analytical solution (Leung et al., 2003; Pourzeynali et al., 2013). GA works with a set of points or populations within a particular moment, which means that the GAs are processed at one time as many schemes (more in Section 4.6). The overall procedure of the numerical pounding force, followed by a GA process for determining a pounding force with altering variables, is outlined and presented in a flowchart shown in the following Figure 4.1.

1. For designed structures, numerical LES models are conducted to analyze the uncertain high-intensity wind forces on each structure examined over a given period (i.e., $F_x = (F_{x1}, F_{x2}, \ldots , F_{xn})^T$, $F_y = (F_{y1}, F_{y2}, \ldots , F_{yn})^T$, and $F_z = (F_{z1}, F_{z2}, \ldots , F_{zn})^T$.

2. The time-history wind forces are then applied through the FEM modelled structural analysis to determine the time-dependent dynamic response of each structure (i.e.,

structural lateral deflection and required minimum separation gap distance ($d_{g,\text{min}}$) to alleviate structural pounding).

3. Pounding forces will be monitored and recorded over the applied time-history analysis when the d_g between structures is lowered than the determined $d_{g,\text{min}}$.

4. The maximum F_I is then determined based on the geometrical parameters (i.e., H, F_n, v, initial d_g).

5. A GA will be used to correlate a generic mathematical formulation from optimization cycles for determining the maximum F_I by using the geometrical parameters as input values.
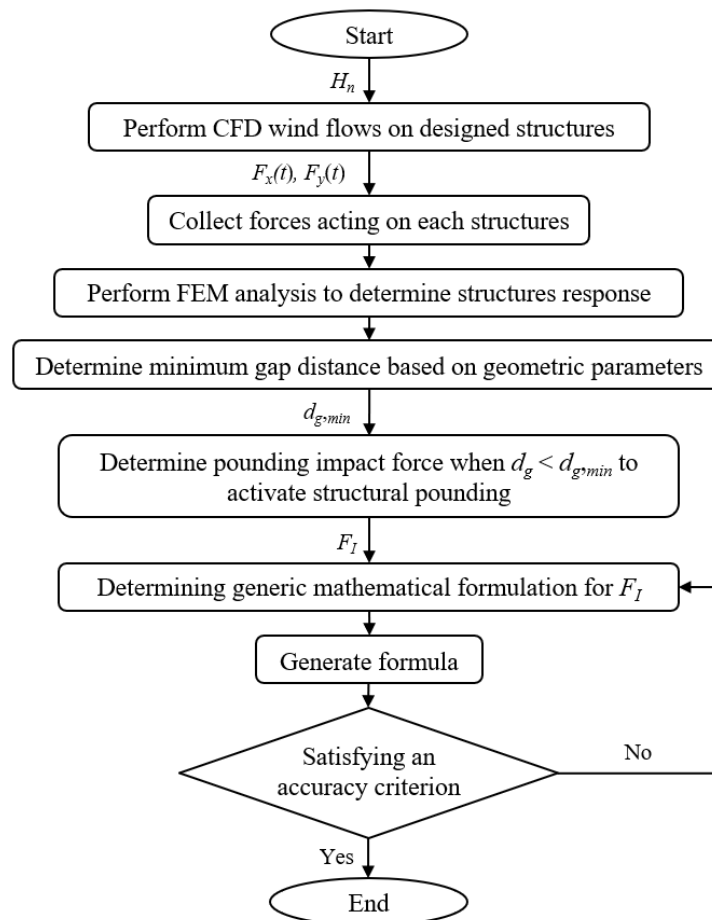
Figure 4.1: Flowchart of the required pounding force (F_I) procedure

4.3   Geometrical Details of the CAARC Building

An illustration example is conducted to examine the developed procedure for determining the wind-induced pounding forces between two adjacent tall structures in proximity. An initial structure will be first validated with a similar FEM model from the literature. A full-scaled 45-storey (180 m) tall steel skeletal structure with a fifteen bay (45 m wide) by ten bay (30 m long) parameter is numerically modelled. The storey height is 4 m, with each bay being 3 m long, as shown in Figure 4.2. The structure observed has the same geometric form as the Commonwealth Advisory Aeronautical Research Council (CAARC) standard building, which has extensively been used and examined for standardization in many experimental wind tunnel laboratories (Melbourne, 1980) and numerical wind analysis (Dragoiescu et al., 2006; Elshaer et al., 2016; Elshaer and Bitsuamlak, 2018). The modelled structure is in a 1:400 modelled scale during the CFD analysis, having a time scale of 1:100. Where the structure in the FEM analysis is considered full-scale. Validated procedures are completed once both numerical simulations are in good agreeance with the validation model. Similar modelled steel structures with alternate properties (i.e., H and F_n) are then produced in both numerical analyses. The separation distance is first determined once the dynamic responses of the two adjacent tall structures in proximity with equal height are measured from the applied wind forces. The separation distance between both structures is lowered to determine the forces when structural pounding arises (more information in Section 4.5.1).
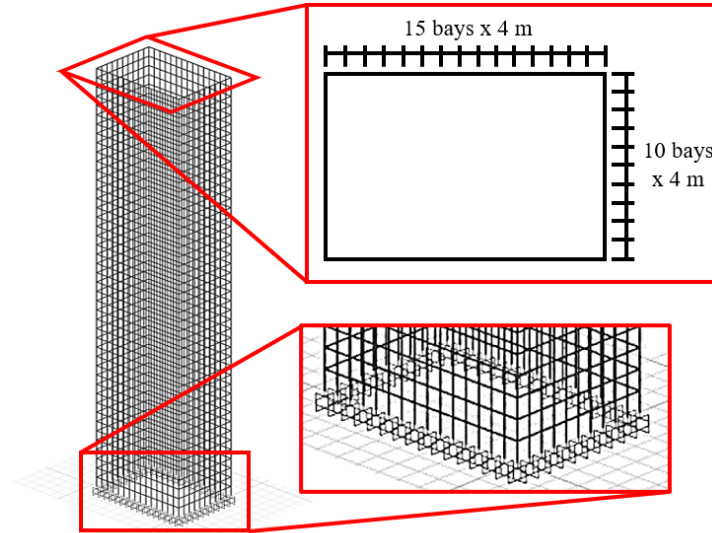
Figure 4.2: Geometric parameters for the selected study structure

4.4   CFD Detail for Wind Load Evaluation

The current study conducts three-dimensional LES models to evaluate the applied wind forces

acting on two adjacent tall structures. All dimensions for the Computational Domain (CD) and

mesh discretization are conducted based on recommendations from previous studies (Brown et al.,

2022; Dagnew and Bitsuamlak, 2013; Elshaer et al., 2016; Franke, 2006; Franke et al., 2011).

Once the initial structure is properly modelled and validated, the following structures are

considered with alteration in H (e.g., 180 m, 140 m, 100 m, and 60 m, in full-scale) and materials,

concerning the sizes of the required materials (more details in Section 4.5) to maintain an accurate

preliminary strength check (in according to the AISC steel code ("American Institute of Steel

Construction, Manual of Steel Construction," 2005; Huang, 2017; Huang et al., 2012)). The inlet

previously shown in Figure 3.2 (a) of the CD is assigned as the inflow boundary condition, which

generates a wind flow field from a Consistent Discrete Random Flow Generator (CDRFG)

technique (Aboshosha et al., 2015; Elshaer et al., 2016). The CDRFG technique utilizes a database

for each wind velocity component depending on its location and time (e.g., u_x (x, y, z, and t)). The

top and sides of the CD represent symmetry plane boundary conditions, whereas the building's

surfaces and the bottom of the CD are non-slip walls. As previously mentioned in Section 3.2.1.1, Figure 3.2 (b) shows the adopted inflow mean wind profile acting on the validated CAARC structure, which is adapted from a wind tunnel simulation (Dragoiescu et al., 2006) and numerical wind simulation from (Elshaer et al., 2016). The exposure factor of the structures is located in an open terrain environment. To conduct the LES simulation, a dynamic sub-grid scale with a commercial CFD package (STAR-CCM+ v.15.04.008) is used (Germano et al., 1991; Smagorinsky, 1963). Each simulation represented a total time of 7.0 seconds in the modelled scale (i.e., 11.5 minutes for full-scale), having a total of 14000 time steps with a single time step equal to 5 milli-seconds. This allows for the Courant Friedrichs-Lewy (CFL) number to be maintained less than 1.0 for wind solutions to be accurate and allow for convergence (i.e., maximum $CFL =$ 0.5 at the top of the CAARC structure). ("SharcNet," 2022) is a High-Performance Computer (HPC) facility, which was used to conduct the CFD numerical simulations. The computational time required for each simulation took 60 hours on 96 processors.

Hexahedral control volumes are used in the CD, where the mesh sizes are divided into four zones for the complexity of the wind flow on the structures to be captured, as previously mentioned in Section 3.2.1.2 and shown in Figure 3.3. A total of 1.75 million mesh cells are used within the CD. Parallel to the examined structure, fifteen prism layers (i.e., surface-following grids) are used with a stretching factor of 1.05 to satisfy the recommendations (Elshaer and Bitsuamlak, 2018; Franke, 2006; Murakami, 1998; Tominaga et al., 2008)

The referenced length scale at the top of the modelled structure in the *x*, *y*, and *z*-directions are 0.563 m, 0.147 m, and 0.186 m, respectively. The turbulence intensity at the modelled scale reference height is 0.197, 0.167, and 0.145 in the *u*, *v*, and *w*-directions, respectively. A mean pressure coefficient (C_p mean) and root mean square pressure coefficient (C_p RMS) are compared,

acting on 2/3 of the height of the CAARC structure to validate the LES model, as can be shown in Figure 4.3 (a) and (b).

Individual time-history wind forces in the x and y direction must be captured to perform the structure's dynamic responses on two adjacent tall structures in proximity. Wind forces are monitored individually per storey, per structure as a summed force from all surfaces on each storey. The applied time-history wind force will act as a singular force located at each structure's center diaphragm of each storey to be applied to the FEM model (more details in Section 4.5). The structures are split into two equal-sized buildings to represent two modelled buildings, having no separation distance between the buildings to fulfill any convergent issues over the simulated time, as shown in Figure 4.4. Each structure is then divided into 45 equal stories to represent each floor. The yellow highlighted surface area shown in Figure 4.4 replicates the 25th storey for the upstream structure (Building 1), where the applied wind forces are captured. To allow for initial converging of the wind velocity flows, the first 50 seconds (in full-scale) are not considered in the monitored CFD results. Time-history wind forces are then conducted for other examined structures with altering heights, in addition to varying the applied mean wind velocities ranging from 20 m/s to 50 m/s, further discussed in Section 4.5.

141
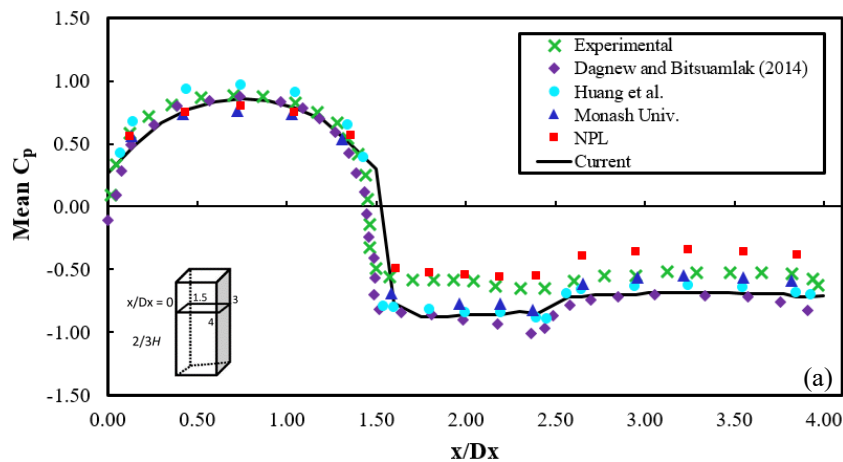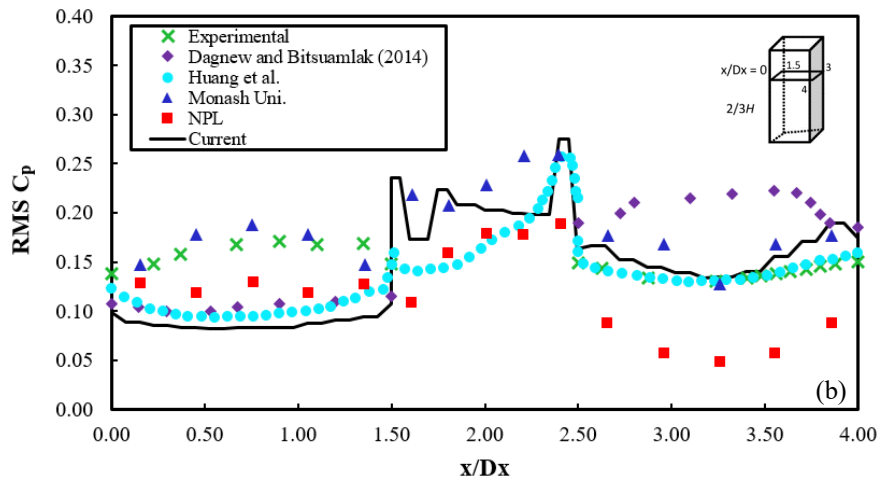
Figure 4.3: (a) Mean and (b) RMS Pressure Coefficient at 2/3 reference height, adapted from (Brown et al., 2022)
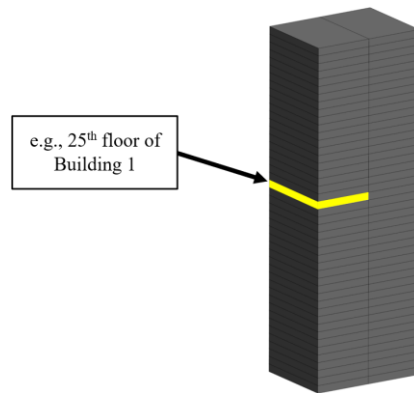
Figure 4.4: Derived surfaces for both structures with the 25th storey of the first structure as highlighted

4.5 Adopted Structural Details in the FEM Model

A 180 m, 45-storey tall steel rectangular skeletal structure with a 10-bay by 15-bay long structure (i.e., 30 m by 45 m long, respectively) is used as the initial validated structure for the FEM analysis, as previously mentioned in Section 4.3 (i.e., CAARC structure). The initial structure is designed initially based on a preliminary strength check according to the AISC steel code (2001) from (Chan et al., 2009a; Huang, 2017) analysis. All beam and column members are made from steel (i.e., W14 and W30 sizes, respectively) on the initial CAARC structure and can be noted in Table 4.1. Structures steel columns will vary with the applied mean wind velocity. The computer program used in this work is the program package ("ETABS," 2018). The skeletal steel structure has a Young's Modulus of 200,000 MPa with a Poison's ratio of 0.25. The steel density is 7850 kg/m^3 and a model damping ratio of 2%. The fixity of the structure located at the ground surface is considered fixed, allowing the overall structure to have a rigid floor connection.

Additionally, the structure acted as a moment-resisting frame, allowing forces from the beams and columns to transfer to the connections and down to the fixed ground surface. The structures first, second and third natural frequency (F_n) is equal to 0.198 Hz, 0.281 Hz, and 0.361 Hz, respectively, which are in similar agreement with (Chan et al., 2009a; Huang, 2017). For validation purposes, the structure is considered in a dense, metropolitan location, having many tall structures in proximity. The applied wind on the structure is applied as a static wind analysis with a mean wind velocity at the top of the structure equal to 41 m/s per the NBCC (2020). This is compared to a dynamic wind analysis with the same mean wind velocity of 41 m/s, assuming a 50-year return period of wind located at the top of the building. The dynamic wind loads from (Huang, 2017) are calculated based on the wind tunnel data derived from the aerodynamic load database of the NatHaz Modeling Laboratory (Zhou et al., 2003). As previously mentioned in Section 3.2.2.1, Figure 3.7 shows the structures lateral deflection and inter-storey drift in comparison to (Huang,

2017) numerical FEM study, considering the longer side of the examined structure perpendicular to the applied wind (i.e., 0° wind angle of attack), shown in Figure 3.7 (c), is found to have the most significant lateral and inter-storey drift, respectively (Huang, 2017). Generally, the allowable drift ratio is typically 1/400 but can appear to be within the range of 1/750 to 1/250 (Ellingwood, 1986). For validation purposes, the initial chosen steel member has exceeded both the maximum deflection of H/400 and inter-storey drift limit ratio of 1/400, respectively (Chan et al., 2009a; Huang, 2017), since the structures system is initially intended for optimization purposes to evaluate its drift and deflection strains.

Table 4.1: Steel member sizes for the 180 m tall structures framework

Storey level	Beam size	Column size			
		$v = 20\,m/s$	$v = 30\,m/s$	$v = 40\,m/s$	$v = 50\,m/s$
1 - 9	W30 x 357	W14 x 342	W14 x 398	W14 x 550	W14 x 730
10 - 18	W30 x 326	W14 x 283	W14 x 342	W14 x 500	W14 x 550
19 - 27	W30 x 292	W14 x 193	W14 x 233	W14 x 370	W14 x 398
28 - 36	W30 x 261	W14 x 132	W14 x 159	W14 x 257	W14 x 283
37 - 45	W30 x 211	W14 x 82	W14 x 99	W14 x 159	W14 x 176

(Table header: 180 m tall CAARC structure)

Once the validated steel skeletal structure is in good agreeance for its design, the remaining examined structures (e.g., 140 m, 100 m, and 60 m tall buildings) are then calculated per the preliminary strength check for the AISC (2001) to accurately replicate the validated model; selected steel members are shown in Table 4.2. Sixteen additional structures, corresponding to the same structure's height, used the same steel and columns selected as the structure subjected to an applied mean wind velocity of 40 m/s are also considered, making a total of 28 structures examined. As stated in Section 4.2 and Section 4.4, the gathered time-history wind loads from the numerical LES modelled analysis are then scaled to full-scale and applied to the two adjacent steel structures in proximity in the FEM model. Table 4.3 presents the along-wind and across-wind base shear forces, the torsional base torque from the wind-induced structural loads at a velocity of 40

m/s acting on a singular 180 m CAARC structure, 140 m, 100 m, and 60 m tall structure, respectively, before applying two structures at proximity. In accordance, applied mean wind velocities vary from 20 m/s to 50 m/s at the height of 180 m with increments of 10 m/s. The wind forces acting on the structure act as a singular wind force, located at the center of each floor's diaphragm in the x, y, and z-directions. The two adjacent CAARC structures in proximity subjected to a mean wind velocity of 40 m/s can be see Figure 4.5 for three dimensional view.

Table 4.2: Steel member sizes for alternate examined structures

Storey level	Beam size	Column size			
		$v = 20\,m/s$	$v = 30\,m/s$	$v = 40\,m/s$	$v = 50\,m/s$
140 m tall structure					
1 - 9	W30 x 235	W14 x 233	W14 x 311	W14 x 398	W14 x 500
10 - 18	W30 x 211	W14 x 159	W14 x 211	W14 x 283	W14 x 370
19 - 27	W30 x 191	W14 x 109	W14 x 145	W14 x 193	W14 x 257
28 - 35	W30 x 148	W14 x 68	W14 x 90	W14 x 120	W14 x 159
100 m tall structure					
1 - 9	W30 x 132	W14 x 159	W14 x 193	W14 x 257	W14 x 311
10 - 18	W30 x 124	W14 x 109	W14 x 132	W14 x 176	W14 x 211
19 - 25	W30 x 116	W14 x 74	W14 x 90	W14 x 120	W14 x 145
60 m tall structure					
1 - 9	W30 x 99	W14 x 99	W14 x 120	W14 x 145	W14 x 176
10 - 15	W30 x 90	W14 x 68	W14 x 82	W14 x 99	W14 x 120

Table 4.3: Structural wind loads for all structures framework

Structure height (m)	Along wind base shear (kN)	Across wind base shear (kN)	Torsional base torque (kN.m)
180 (CAARC)	18826	28238	688307
140	13569	20354	496129
100	8752	13128	319986
60	4495	6742	164333
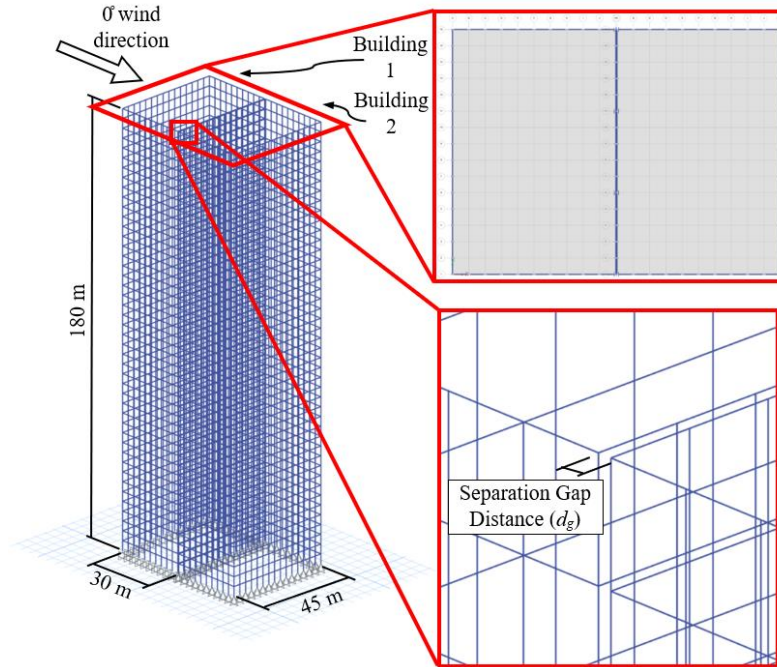
Figure 4.5: 3-dimensional and plan view of the two CAARC structures with a d_g

4.5.1 Modelling of Structural Pounding

Two identical tall structures in proximity are considered to determine a possible pounding force when wind-induced structural pounding occurs. Structures are altered through the numerical FEM analysis with specific monitored input properties (i.e., H, F_n, v, d_g). Results can then determine the maximum F_I the pounding of tall structures may correlate. In Section 4.7.3, a GA will orient the monitored inputs with the recorded pounding forces to determine a mathematical equation for the pounding force based on the monitored input properties. Each structure is modelled independently with its own dynamic responses and vibrations as it is an inelastic, multi-degree-of-freedom system with moment-resisting frames. A gap element is used and discussed in the following Section 4.5.2 to record the pounding interaction. The pounding location considered in this analysis is located as floor-to-floor pounding (floor diaphragms among the storey's masses) because the structures examined have identical overall heights and storey level heights. The numerical time-history analysis captures the pounding forces in the longitudinal and transverse directions. To mitigate

146

structural pounding, the d_g influences the pounding force when the d_g is less than the minimum separation gap distance ($d_{g,min}$). Therefore, it will be altered and monitored throughout the numerical FEM analysis and later used in the GA.

4.5.2   Pounding Contact Link Elements

In practice, when two structures in proximity reach a separation gap distance, d_g, of zero, a structural pounding will occur, and therefore, the colliding structures will experience a pounding impact force, F_I. Thus, a compression-only gap element is used in the FEM modelling to accurately capture forces from a pounding event. The compression gap element uses a specified "gap distance" which replicated the d_g between the two proximate structures. The gap element will only start recording axial F_I over the period when pounding takes place as the specified gap distance in the gap element is less than zero. No axial compression forces will be recorded when the dg is greater than zero (i.e., no structural interaction is achieved). Therefore, F_I only arises when both the adjacent structures laterally deflect towards each other, having a d_g less than zero. Figure 4.6 (a) and (b) replicate the mechanism of how the gap element will capture F_I concerning the d_g. The F_I can only be monitored where the gap elements are located to record the structural interaction, ideally located at the beams, columns or slabs (Karayannis and Favvata, 2005a). Since the structures examined are of the same structural heights, the gap elements will only be located along the beam-to-column connections (i.e., located on each storey level). Four gap elements per floor are determined to achieve a more accurate analysis as a compared evaluation of 1, 4, 9, and 16 compression gap elements were studied. A total of 16 gap elements per storey could only be considered in the longitudinal direction of the structure (e.g., 45 m long side) since there are a total of 15 bays. Figure 4.7 shows the number of gap elements used compared to the total F_I captured

when pounding arises. The most significant difference in the captured total F_l is between 9 and 1 gap elements per storey, only having a difference of 2.4%.
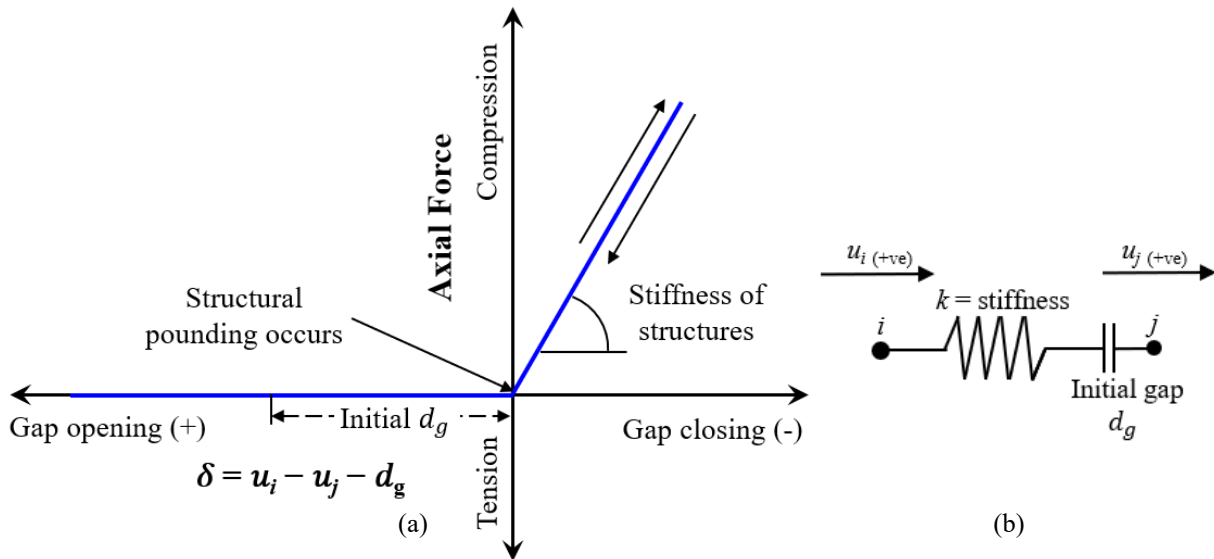
Figure 4.6: (a) Response of gap element for pounding forces and (b) replicated gap element
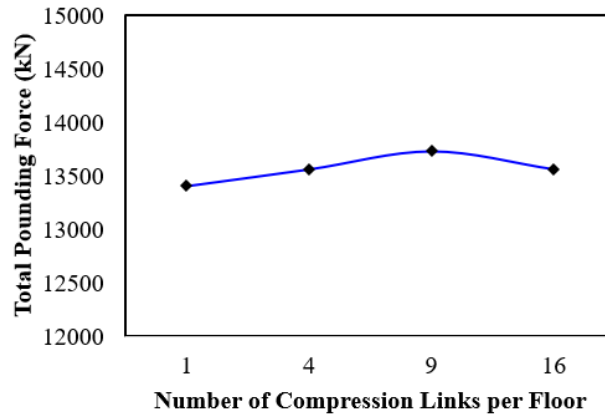
Figure 4.7: Pounding force with alteration of the number of gap elements

The compression gap element implemented in this study is a linear elastic compression model (Jankowski, 2005, 2006b, 2008b; Miari et al., 2019). Two scenarios for the contact gap elements comply when examining the adjacent structures at proximity subjected to a time-history wind analysis. The first scenario consists of the first structure (i.e., upstream structure) either being stationary (laterally stable), laterally deflecting in a negative x-direction away from the other proximate structure, or laterally deflecting in a positive x-direction towards the other proximate

structure but lesser than the subtraction of the d_g and the second structure (downstream structure). Concurrently, the downstream structure is either stationary (laterally stable), laterally deflecting in a positive x-direction (opposite of the upstream structure), or laterally deflecting in a negative x-direction that is lesser than the d_g and the upstream structures lateral deflection combined. Therefore, no structural interaction between the two tall proximate structures will arise. The first scenario can be seen in Figure 4.8 (a). The gap element, in this sense, will act as a non-active component. They will not register to monitor any axial pounding force impact ($F_I(t)$) at the location of impact where the gap elements are located, see Equation (6(a)). The second scenario consists of the summation of the structure's lateral deflection to be greater than the d_g. Therefore, the upstream structure will laterally deflect in a positive x-direction while the downstream structures laterally deflecting in a negative x-direction, having the summation of the two structures' lateral deflections greater than the designated d_g. Nevertheless, the upstream structure can laterally deflect in a negative x-direction. However, the downstream structure has to laterally deflect significantly more in a negative x-direction to have the summation of the two structures' lateral deflection greater than the designated d_g (e.g., this can also be opposite for the upstream and downstream structures, respectively). Scenario two is shown in Figure 4.8 (b). The gap element will then be produced as an active compression spring element, allowing the gap element to monitor the $F_I(t)$ where the location of impact transpires (e.g., the gap elements must be in that specified location to capture $F_I(t)$) over the allocated pounding period. The second scenario is expressed in Equation (6(b)), which is expressed as:

$$F_I(t) = 0 \qquad \text{for } \delta(t) < u_i(t) - u_j(t) - d_g \qquad \text{(a)}$$
$$F_I(t) = k\delta(t) \qquad \text{for } \delta(t) \geq u_i(t) - u_j(t) - d_g \qquad \text{(b)} \qquad \text{Equation (6)}$$

where $\delta(t)$ is defined as the relative displacement between the interactive structure's elements. $u_i(t)$ and $u_j(t)$ are the displacement of the element nodes i and j, respectively. k is defined as the

spring stiffness, which is only activated when pounding of adjacent structures occurs in the second scenario shown in Figure 4.8 (b).
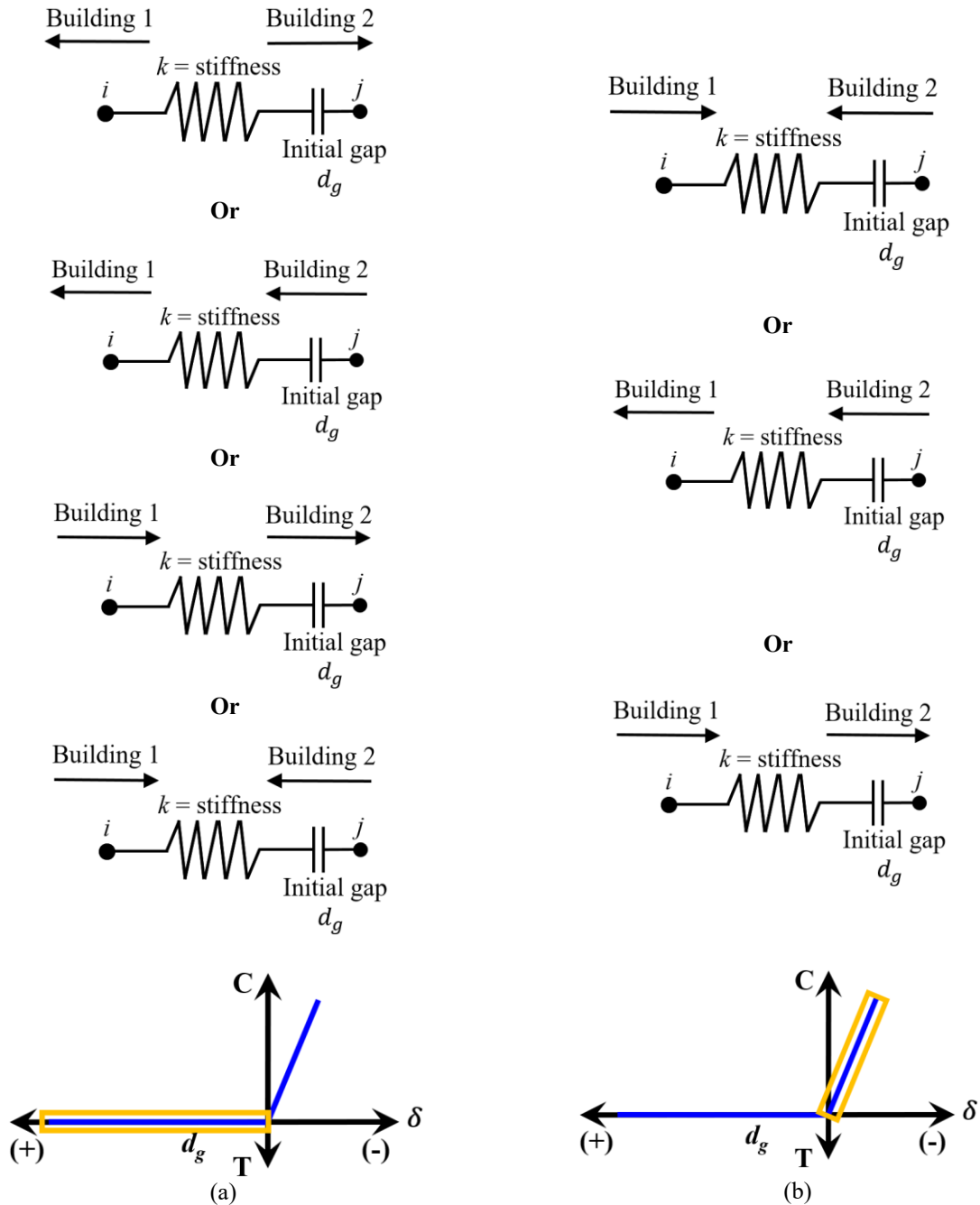
Figure 4.8: Response of compression link in deflection scenarios; (a) Scenario 1 ($\Delta_1 + \Delta_2 < d_g$), and (b) Scenario 2 ($\Delta_1 + \Delta_2 \geq d_g$)

To determine k for the gap element, the examined models' structural stiffness must be considered (Naserkhaki et al., 2012). No exact formulation or value for determining k has been recognized for the gap element (Karayannis and Naoum, 2018b; Miari et al., 2019). However, past studies have stated that the k is relatively large when a pounding event arises (Anagnostopoulos, 1988; Karayannis and Naoum, 2018b; Mahmoud et al., 2013). (Ghandil and Aldaikh, 2017b) determined that when pounding stiffness is greater than 10^{10} N/mm, the response of the structures during pounding interaction is insensitive to the actual impact stiffness. Past literature mentioned that the alteration of the k does not affect the structural response sensitivity when considering at relatively high stiffnesses (i.e., amplification factor upwards of 100 times larger). Ideally, the impact stiffness coefficient should be 50-100 times larger than the lateral stiffness of the interactive structures (Naserkhaki et al., 2012). Therefore, to determine a relative k for the gap element, the modelled structural stiffness (k_T) can be factored by 100 (Naserkhaki et al., 2012). The shear force (V) of the structure can be rearranged to determine the structure's stiffness (k_T) from the applied loading acting on the examined structure from the following equation:

$$V = k_T * \Delta u \hspace{5cm} \text{Equation (7)}$$

where k_T is defined as the overall structural stiffness and Δu is the lateral displacement of the examined skeletal frame structure, which can also be seen in Figure 4.9. A single applied force of 10^7 N is applied to the top-storey diaphragm perpendicular to the longest side of the building (i.e., 45 m long side) of the validated steel CAARC structure to achieve a lateral displacement (Δu) of 826.4 mm. An overall structural stiffness (k_T) is determined to be $12.1 * 10^6 \ N/m$. Therefore, the spring stiffness (k) per storey of the steel structure is determined to be equal to $12 * 10^8 \ N/m$ (i.e., $kT * 100$) (Naserkhaki et al., 2012). Since four gap elements are determined on each floor, each gap element k is $3 * 10^8 \ N/m$. A comparison of k is examined to assure the acquired k is sufficient for the interactive structures (i.e., 20/3k, 5k, 3k, 2k, 5/3k, 4/3k, k, 2/3k, and k/3). It is concluded to

have an average $F_I(t)$ equal to $1.28 * 10^7$ N, shown in Figure 4.10, and therefore, the acquired k is adequate to capture the $F_I(t)$ for all other examined models. The pounding model at specified d_g showed a variation in pounding floor interactions, therefore altering the total number of gap elements required per pounding model examined.
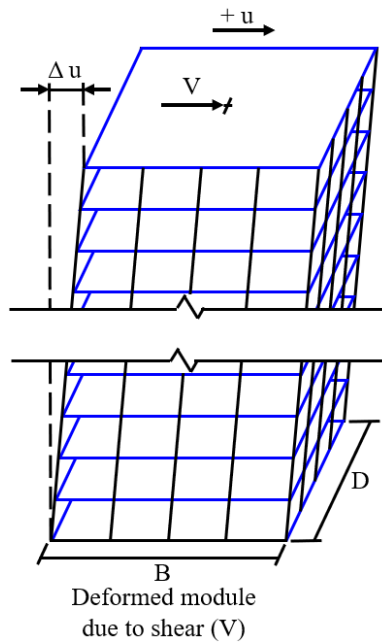
Figure 4.9: Deflection of structure from applied force (V)
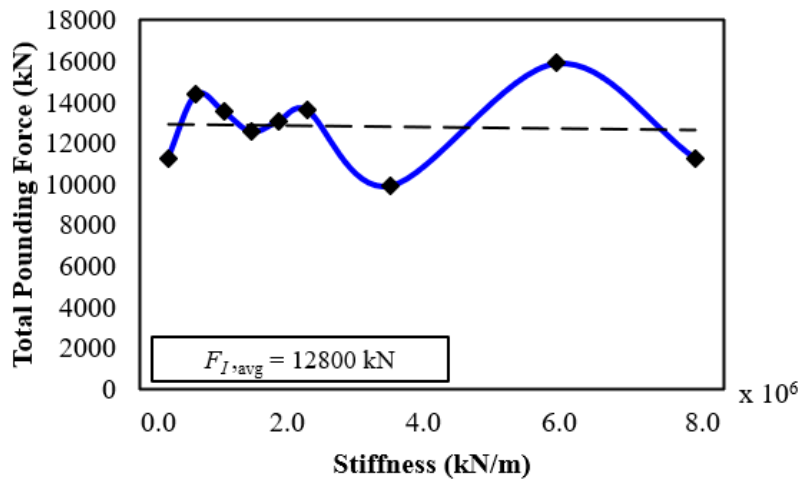
Figure 4.10: Variation of pounding force with the change in the compression link stiffness (k)

4.6 Procedure of Developing the Mathematical Formulas for Pounding Force Determination

A GA is adopted to optimize a general numerical formulas for determining the design pounding force. The formulated mathematical equation will be formulated through a GA by examining a quantified amount of input parameters from the structures being examined. Such input parameters include H, the building's dynamic properties (i.e., F_n), structures' dynamic responses (i.e., lateral deflection), v, and d_g between structures. The formulated equation will be generated from the GA to determine the maximum F_I of the two adjacent tall structures in proximity when a d_g is insufficient to mitigate structural pounding from wind-induced lateral deflections of the structures. This algorithm will use the design GA to optimize the numerical function. The numerical software (Euraqa) is used as the GA method (Edwards, n.d.; Keim, n.d.) and was first developed at the Computational Synthesis Lab at Cornell University (Schmidt and Lipson, 2009). The application of GA has increased significantly in speed, capability and flexibility in recent years (Pourzeynali et al., 2013). To achieve the maximum pounding forces with alternate input parameters, a single-objective optimization is performed using GA. The primary purpose of using the single-objective optimization procedure using GA is to find a specific value of the design variables. This is to find the optimum value of a single objective function (i.e., maximum F_I).

In general, GA's have been applied in many civil engineering structural vibration control designs as effective optimization search techniques (Pourzeynali and Zarif, 2008). GAs are stochastic search techniques based on natural genetics and the mechanism of natural selection. The GA uses design variables (i.e., coded as real numbers) and is adopted through optimization formulations. To detect equations and hidden mathematical relations through raw input data, the GA uses symbolic regression (Dubčáková, 2011). The advantage of using a GA is not being confined to local extreme values while finding possible extreme global values (i.e., maximum or minimum

extreme values). Additionally, GA's will include mutation operations that will generate search points away from the hit fitness regions, which will help avoid any search points being trapped within local extreme values, as previously mentioned (Elshaer et al., 2017). The GA process will also initiate from a search process, including the multiple raw data points within the search space. The GA's technique contains multiple numerical simulations of the objective function associated with the numerous preliminary entries (i.e., a combination of different variables over multiple generations) (Elshaer et al., 2017). The GA process has been a very effective optimization approach in determining the optimal solution in comparable complex engineering optimization problems (Ansary et al., 2011; Elshaer et al., 2017; Pourzeynali et al., 2013; Pourzeynali and Zarif, 2008; Zhou and Haghighat, 2009). If the objective function (i.e., maximum F_I) is to be evaluated directly using the CFD and FEM analysis, the process for the computational simulation costs will become extremely costly. More information regarding the GA process can be available in the following scholars (Davis, 1991; DE Goldberg, 2013).

In this research study, applied time-history wind forces acting on both adjacent tall structures will be determined. This will depend on the overall building's height and the applied mean wind velocities. The collected wind forces will then be applied to the two adjacent structures in the FEM analysis. This will determine the structure's dynamic response characteristics. The d_g is then altered to where structural pounding takes place. The structural F_I (i.e., known as the objective function) will then be recorded and determined based on the initial design variables (i.e., H, F_n, v, and d_g), the size of the population search points, the number of required generations and lastly, the upper/lower bound for each design variable. The GA will first require an initial set of random selections (initial population). The GA starts its optimization by initiating the search using the initial population. Within the initial population, the objective function is evaluating each initial

individual design parameter (candidate), which represents a solution to the problem at hand. The initial candidates will evolve through successive iterations (generations). During each generation, the candidates are evaluated using some measure of fitness (Pourzeynali and Zarif, 2008). The GA uses each candidate from the different design combinations and represents other dynamic variables. By doing so, the GA can sort the candidates according to their fitness (i.e., the objective function can be lowered in value). In GA optimization, three main operators are used (i.e., selection, crossover, and mutation). Commonly, initialization is to be assumed as random (Pourzeynali and Zarif, 2008). The crossover and mutation operators are applied to the current population through generations. This will produce better candidates (offspring's). In every generation, the crossover operator (parents) will be applied to candidates with higher fitness to produce offspring's, while the mutation operators are applied to the parents with lower fitness. This will allow the mutation operator to explore the search space for more possibilities of different regions to help avoid additional stagnation of any extreme local values (Elshaer et al., 2017; Mengistu and Ghaly, 2008). The GA will maintain optimization by applying the operators and producing new generations until there are no significant progressions from the formed GA. This will determine the optimized GA solution from the final generation (i.e., the highest fitting candidate).

In conclusion, an optimal GA aims at optimizing the maximum F_I during structural pounding if a determined $d_{g,min}$ is insufficient between two tall structures in proximity. The objective function in the GA is determined as the F_I. For each candidate in the design variables, the objective function evaluates the applied mean wind velocity (v) in four increments (i.e., 20, 30, 40, and 50 m/s, respectively), the H as four designated sizes (i.e., 60, 100, 140, and 180 m, respectively), the F_n is altered, dependent on the structural properties (i.e., representing the overall mass and stiffness),

and the varying d_g (e.g., if d_g is less than $d_{g,min}$). In this research study, a total of 112 pounding models are examined. Table 4.4 summarizes all the studied design variables. The minimum separation gap distance ($d_{g,min}$) was determined by (Brown et al., 2022) of similar structures. Therefore, the examined separation gap distances (d_g) are determined based on d_g being less than $d_{g,min}$. The upper and lower bounds for H are determined as 180 m and 60 m, respectively, v is set at 50 m/s and 20 m/s, respectively, d_g will vary based on the design parameters, and lastly, F_n is set at 0.416 Hz and 0.148 Hz, respectively. F_n can be defined as follows:

$$F_n = \frac{1}{2\pi}\sqrt{\frac{k}{m}} \text{ (Hz)} \hspace{4cm} \text{Equation (8)}$$

where m is the mass (kg) and k is the stiffness (N/m) of the structure, based on the storey properties. These parameters are all applied throughout the numerical FEM analysis.

Table 4.4: Values of the input parameters for GA training

Building Height (H) (m)	Applied Mean Wind Velocity (v) (m/s)	Natural Modal Frequency (F_n) (Hz)	Minimum Gap Distance ($d_{g,min}$) (mm)	Examined Gap Distance (d_g) (mm)
	50	0.211	2246	2200, 1500, 900, 300
	50[a]	0.198	2408	2400, 1700, 1000, 300
	40	0.198	1899	1800, 1300, 800, 300
180	30	0.166	2185	2100, 1500, 900, 300
	30[a]	0.198	861	800, 600, 400, 200
	20	0.148	708	700, 550, 400, 250
	20[a]	0.198	383	350, 300, 250, 200
	50	0.249	1344	1300, 1000, 600, 300
	50[b]	0.222	903	900, 700, 500, 300
	40	0.222	788	700, 550, 400, 250
140	30	0.197	550	500, 400, 300, 200
	30[b]	0.222	324	300, 250, 200, 150
	20	0.195	260	250, 200, 150, 100
	20[b]	0.222	144	125, 100, 75, 50
	50	0.302	722	700, 550, 400, 250
	50[c]	0.277	567	550, 450, 350, 250
	40	0.277	480	450, 400, 350, 300
100	30	0.239	446	400, 350, 300, 250
	30[c]	0.277	204	200, 175, 150, 125
	20	0.209	229	225, 200, 175, 150
	20[c]	0.277	91	90, 80, 70, 60
	50	0.416	640	600, 500, 400, 300
	50[d]	0.381	437	400, 350, 300, 250
	40	0.381	352	350, 300, 250, 200
60	30	0.308	213	200, 175, 150, 125
	30[d]	0.381	157	150, 125, 100, 75
	20	0.281	91	90, 80, 70, 60
	20[d]	0.381	70	65, 55, 45, 35

[a] F_n same as 180 m structure for $v = 40\ m/s$
[b] F_n same as 140 m structure for $v = 40\ m/s$
[c] F_n same as 100 m structure for $v = 40\ m/s$
[d] F_n same as 60 m structure for $v = 40\ m/s$

4.7   Results and Discussion

4.7.1   Examined Cases

The parametric study uses FEM analysis to simulate the dynamic responses of two adjacent structures in proximity. The numerical analysis will correlate recorded pounding forces (F_l) based on the inputted initial separation gap distance (d_g). Graphical comparisons are shown in the upcoming figures of the examined pounding structures. A total of 112 pounding cases between structures with equal overall heights based on a preliminary check (AISC 2001) (Huang, 2017) are

examined and discussed. These are the interaction cases between the 45-storey CAARC structure, 35-storey, 25-storey, and 15-storey high structures with varying F_n and applied v as mentioned in the previous sections. The pounding cases of the structures with the same F_n as those applied to a $v = 40\ m/s$ based on the structure's height are also included. Each pair of structure heights is examined with four different applied v's. Out of each applied v; four different d_g are then examined to compare the pounding impact forces (F_I) based on the impact location (i.e., storey height). The examined pounding scenarios are previously presented in Table 4.4.

4.7.2   Numerical Results

Maximum pounding forces (F_I) results of the examined pounding cases between the two adjacent structures of similar height are presented in Table 4.5. The separation gap distances (d_g) were evaluated to be less than the $d_{g,min}$ for pounding to arise. It can be seen in Table 4.5 that when the d_g is closer to the $d_{g,min}$, determined from Table 4.4, a significant decrease in F_I was recorded during pounding. As the pounding structures became closer in proximity, an increase in F_I became larger. However, for the taller structures (e.g., 140 m and 180 m high buildings), as the structures became too close in proximity (i.e., $d_g < 300\ mm$), F_I decreased.

Table 4.5: Maximum pounding force (F_I) on examined structures

Building Height (H) (m)	Applied Mean Wind Velocity (v) (m/s)	Examined Gap Distance (d_g) (mm)	Maximum Pounding Force (kN)	Building Height (H) (m)	Applied Mean Wind Velocity (v) (m/s)	Examined Gap Distance (d_g) (mm)	Maximum Pounding Force (kN)
180	50	2200	4253	140	50	1300	6126
		1500	35666			1000	27860
		900	60757			600	19369
		300	37133			300	27501
	50[a]	2400	1478		50[b]	900	301
		1700	30314			700	17044
		1000	51957			500	15358
		300	51957			300	15286
	40	1800	7883		40	700	8767
		1300	19265			550	10994
		800	44598			400	16751
		300	27193			250	16063
	30	2100	12664		30	500	4107
		1500	28385			400	7248
		900	25234			300	11455
		300	27081			200	9728
	30[a]	800	4253		30[b]	300	1432
		600	11265			250	5484
		400	16772			200	7538
		200	15160			150	4325
	20	700	757		20	250	1870
		550	7386			200	3519
		400	11312			150	4118
		250	9901			100	5516
	20[a]	350	3350		20[b]	125	1369
		300	4340			100	3552
		250	4569			75	2473
		200	5708			50	2442

Building Height (H) (m)	Applied Mean Wind Velocity (v) (m/s)	Examined Gap Distance (d_g) (mm)	Maximum Pounding Force (kN)	Building Height (H) (m)	Applied Mean Wind Velocity (v) (m/s)	Examined Gap Distance (d_g) (mm)	Maximum Pounding Force (kN)
100	50	700	4795	60	50	600	11905
		550	19928			500	18803
		400	23460			400	34634
		250	28725			300	37662
	50[c]	550	1845		50[d]	400	7615
		450	10486			350	12239
		350	14707			300	16473
		250	19542			250	20225
	40	450	3200		40	350	1215
		400	6610			300	8403
		350	11836			250	20708

v	d_g	F_I	v	d_g	F_I
	300	13593		200	21576
	400	5790		200	771
	350	6610		175	5297
30	300	8930	30	150	4087
	250	11701		125	9724
	200	1281		150	2104
30[c]	175	2953	30[d]	125	4746
	150	4488		100	7496
	125	5174		75	6906
	225	452		90	353
	200	3623		80	1579
20	175	4747	20	70	2503
	150	3783		60	2908
	90	329		65	743
	80	1532		55	2423
20[c]	70	1656	20[d]	45	3673
	60	1945		35	3520

[a] F_n same as 180 m structure for $v = 40\ m/s$
[b] F_n same as 140 m structure for $v = 40\ m/s$
[c] F_n same as 100 m structure for $v = 40\ m/s$
[d] F_n same as 60 m structure for $v = 40\ m/s$

A graphical comparison of the maximum F_I can be seen in Figure 4.11 based on the height of the structure (*H*), varying applied mean wind velocity (*v*), and examined separation gap distance (d_g), similarly to Table 4.5. In Figure 4.11 (a), the d_g for the 60 m tall structure varies between 35 mm and 600 mm, based on the applied *v*, which compares the maximum F_I when pounding is evident. In Figure 4.11 (b), similar d_g for the 100 m tall structure is examined, ranging from 60 mm to 700 mm. A substantial increase in the larger examined d_g was determined and can be seen in Figure 4.11 (c) and (d) for structures 140 m and 180 m tall, respectively. This is due to the lateral deflection of taller structures (i.e., 140 m and 180 m tall buildings) becoming increasingly more significant compared to the smaller structures, requiring larger $d_{g,min}$ for mitigating pounding.

Figure 4.11 (a) and (b) show that for most of the examined pounding structures, the FI increases as the dg decreases in size. However, for the lower applied *v*, F_I is slightly lowered for the structures in proximity are at their closest (i.e., $v = 20\ m/s$ and $30\ m/s$). Similar observations can be confirmed for the lower applied *v* for structure heights of 140 m and 180 m, as shown in Figure 4.11 (c) and (d). Moreover, for the taller structures (i.e., 140m and 180 m tall buildings), at

higher applied v, the F_I lowers when the pounding structures are at their closest (i.e., $d_g <$ 300 mm). A maximum F_I (60,757 kN) arises at the 180 m tall structure applied to a v equal to 50 m/s with an evaluated d_g of 900 mm, where the smallest F_I is ultimately zero if the d_g is equal to $d_{g,min}$.

When comparing the overall maximum F_I with all structures, the 45-storey pounding structure has the most significant maximum F_I for an applied v equal to 50 m/s compared to the other examined pounding models. However, when comparing the other structures' heights, the 15-storey pounding structure has a noticeable significant maximum F_I when subjected to high applied mean wind velocities (i.e., 50 m/s) when comparing the maximum F_I to the 25-storey and 35-storey structures (i.e., 23.5% and 26.0% difference for the 25-storey and 35-storey structure, respectively).
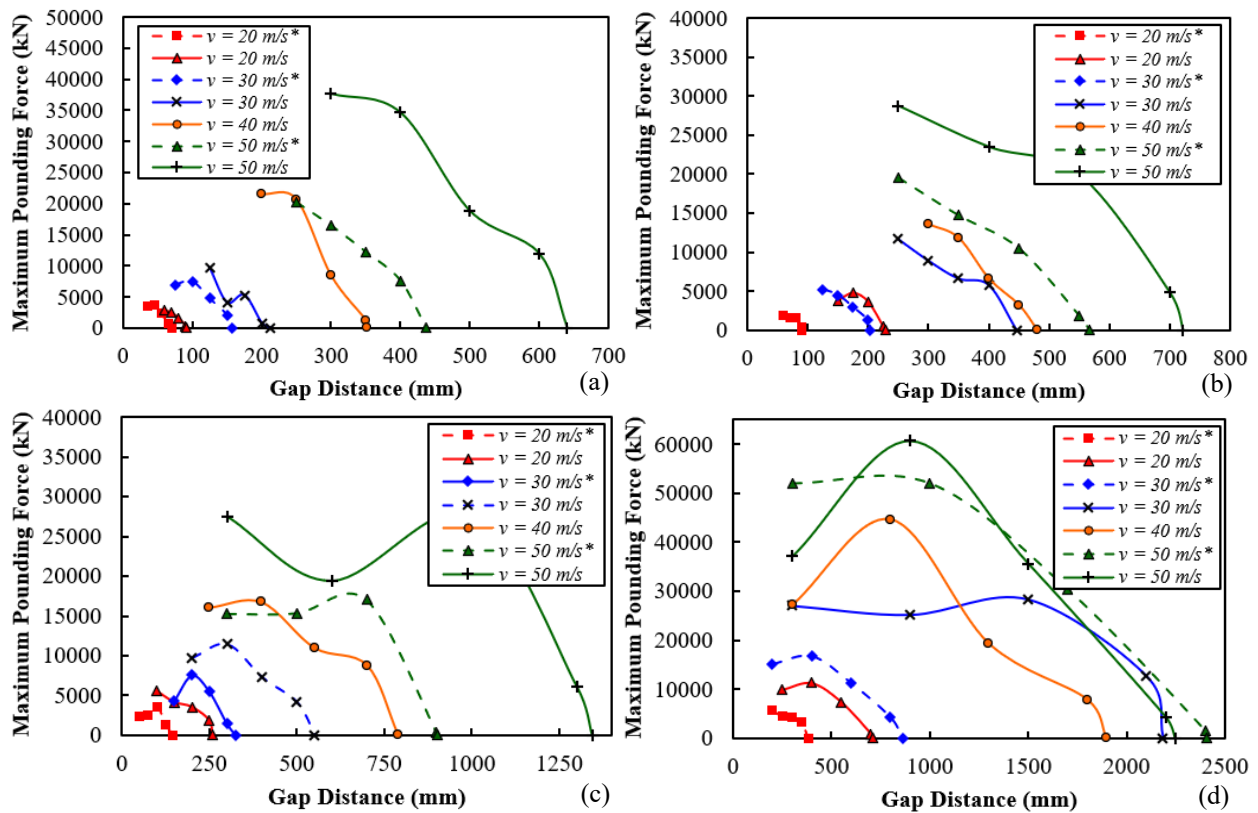
Figure 4.11: Maximum pounding force from colliding buildings; (a) 60 m, (b) 100 m, (c) 140 m, and (d) 180 m tall structures (*same F_n as the structure design for $v = 40$ m/s)

4.7.3 Mathematical Formulas to Determine the Pounding Impact Force (F_I)

To determine a suitable mathematical equation for predicting the maximum impact force (F_I) when two adjacent structures in proximity come into collision based on their preliminary factors (i.e., H, v, F_n, and $d_{g,min}$), a reliable evaluation for the objective function must be achieved from large quantities of analytical models (i.e., polynomials, trigonometric, exponential, and logarithmic functions). 112 testing samples are produced in the GA with observed outcomes for the maximum F_I. Over $2.9 * 10^{12}$ formulations are evaluated through the GA analysis, which is then ranked based on their correlation coefficient and complexity. Table 4.6 shows that a set of mathematical formulations have been collected based on their rank and correlation coefficient. These formulations are chosen since the highest rank gave the highest correlation coefficient, leading to the lowest mean absolute error. However, the lowest rank mathematical formulation was based on the least complex, including all variables (i.e., H, v, F_n, and d_g). The highest ranked (i.e., Eq. 1) had the highest correlation coefficient possible, obtaining a value of 0.9344 with a mean absolute error of 2387.89 kN. Regression plots for the targeted versus the output maximum pounding force (F_I) are presented in Figure 4.12. Figure 4.12 (a-d) vary depending on the different ranked mathematical formulations.

Table 4.6: Top Ranked mathematical formulas for maximum pounding force determination

Rank	Correlation Coefficient	Mean Absolute Error (kN)	Mathematical formula*
Eq 1	0.9344	2387.89	$F_I(kN) = ((16.5 * v^2 + 1.21 * v * d_g * \sin(2.38 * H) + 1.21 * v^2 - d_g - 2.38 * H \,/ \sin(197 * F_n)\,\hat{}\, \cos(0.304 + 21.6 * d_g)) * \cos(\cos(d_g))$
Eq 2	0.9061	3068.05	$F_I(kN) = (13.1 * v^2 + 1.02 * 10^3 / \sin(14 * F_n * v) + v * d_g * \sin(2.18 * H^2))\,\hat{}\, \cos(323 * d_g)$
Eq 3	0.8679	3775.43	$F_I(kN) = 793 * v + 1.95 * 10^3 * \sin(793 * v) + 0.00637 * v^2 * \exp(0.0455 * H) + 2.63 * d_g * \mathrm{sqrt}(v) * \cos(2.84 * 10^3 * F_n) - 1.39 * 10^4 - 17.3 * d_g$
Eq 4	0.8190	4480.73	$F_I(kN) = 0.00218 * d_g * H^2 + 0.451 * H * F_n * v^2 - 2.54 * 10^{-6} * d_g^3 - 2.03 * H * F_n * d_g$

* v, d_g, H, and F_n are in m/s, mm, m, and Hz, respectively
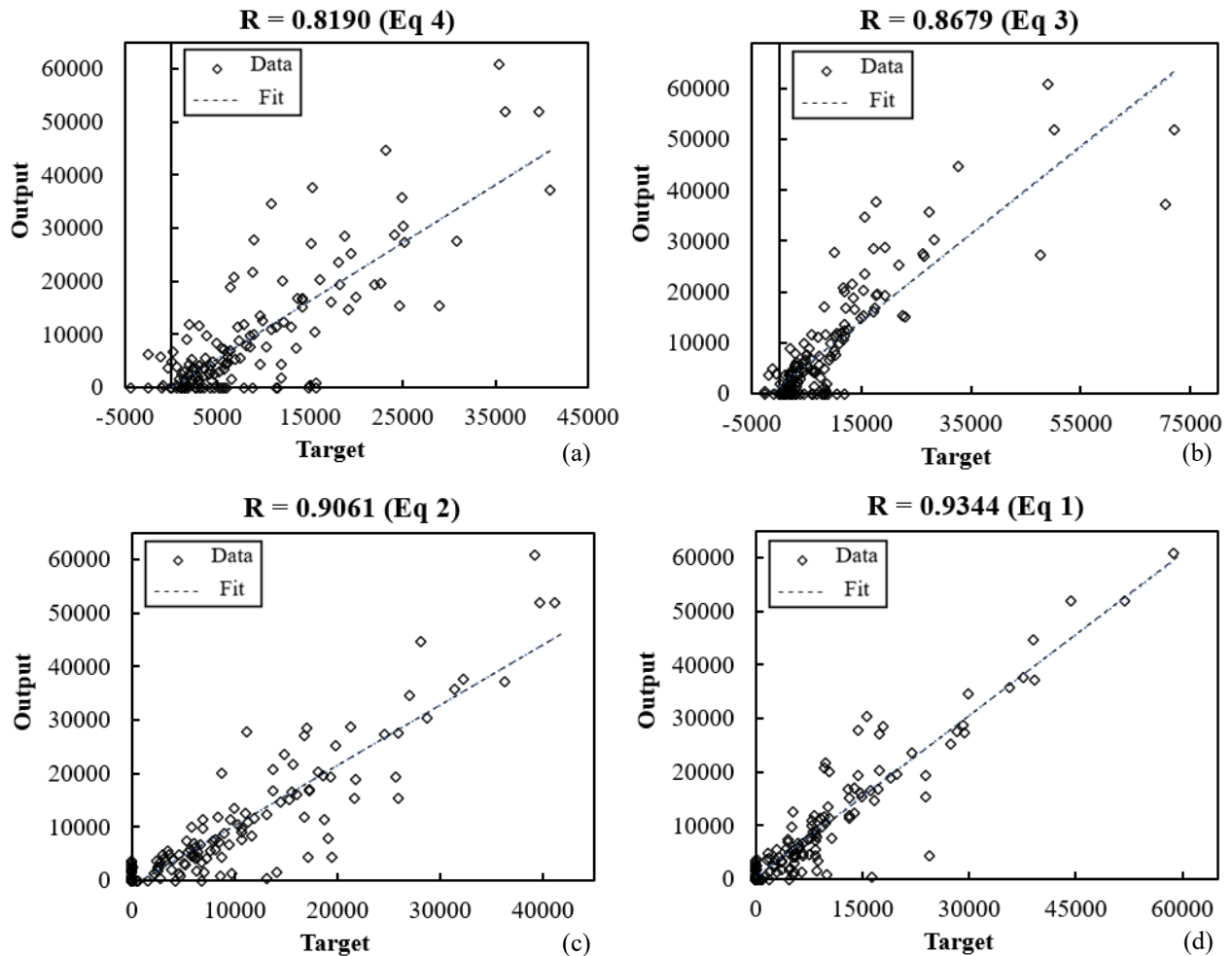
Figure 4.12: Regression plot for ranked sampled; (a) Eq 1, (b) Eq 2, (c) Eq 3, and (d) Eq 4

An optimal mathematical solution was obtained after 120 generations within 24 hours of running on a high-performance computer (Brown et al., 2022). The mathematical formulation was

optimized through the GA process to conduct equations for determining the maximum F_I when two adjacent structures in proximity collide with each other. A fitness curve is shown in Figure 4.13, achieving the mean absolute error for the maximum pounding force (F_I) over 24 hours.

The maximum F_I is initially determined through a FEM analysis with specified altering parameters, which is then collected and produced through a GA formulation to conduct a best-fitted mathematical equation to estimate the maximum F_I, dependent on the applied input parameters. A comparison of the highest ranked mathematical formulation with a mean absolute error of 2387 kN was assessed through the FEM simulations and concluded to have similar maximum F_I values for the taller structures. The shorter neighbouring structures (i.e., 60 m and 100 m) had higher maximum F_I from the highest ranked mathematical formulation. Therefore, the formulation overestimated the possible maximum F_I compared to the applied FEM model.
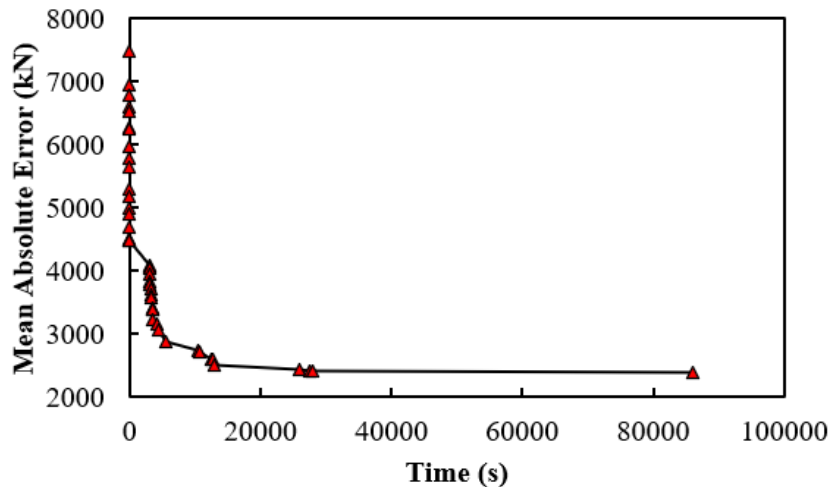
Figure 4.13: Fitness curve for the GA procedure in identifying the optimal mathematical formulas

4.7.4 Time-History Pounding Response

The top storey displacement time-history of the examined pounding cases for the 60 m, 100 m, 140 m, and 180 m tall buildings subjected to an applied $v = 40\ m/s$ are presented in Figure 4.14. Additionally, a time history recorded for the maximum F_I of the examined structures is shown in

Figure 4.15 for the same time histories as Figure 4.14 (a-d). The results in all four time-history scenarios indicate that the downstream structure (building 2) subjected to the applied v has a relatively similar lateral displacement at the upstream structure (building 1) if no pounding incidents occur.

In Figure 4.14 (a), two identical structures, 60 m tall, are initially separated with a d_g of 350 mm. It can be seen in Figure 4.14 (a) that the pounding occurs only once at a time instant of 162.2 seconds. Table 4.5 recorded that a maximum F_I for this instant was 1215 kN, as shown in Figure 4.15 (a). An initial d_g of 450 mm for the examined time-history pounding for the 100 m tall structures is shown in Figure 4.14 (b). The first instant of pounding arises at a time of 333.05 seconds with a minor F_I equal to 483 kN, shown in Figure 4.15 (b). Two additional pounding forces occur shortly after at 337.6 and 342.2 seconds, equal to 1150 and 3200 kN, respectively. The maximum F_I can also be seen in Table 4.5. Figure 4.14 (c) has three separate occurrences of pounding for the neighbouring building of 140 m tall with an initial d_g of 700 mm. The three separate pounding events appeared at 83.9, 358.5, and 554.4 seconds with a maximum F_I on the top storey being 3148, 8767, and 5439 kN, respectively. The pounding occurrences can also be seen in Figure 4.15 (c), and the maximum F_I of 8767 kN can be noted in Table 4.5. For the examined 180 m structure with an initial d_g of 1800 mm, the pounding occurred at the end of the observed time history at 626.8 seconds, shown in Figure 4.14 (d) and Figure 4.15 (d). The maximum F_I was to be 7883 kN, which was recorded in Table 4.5.
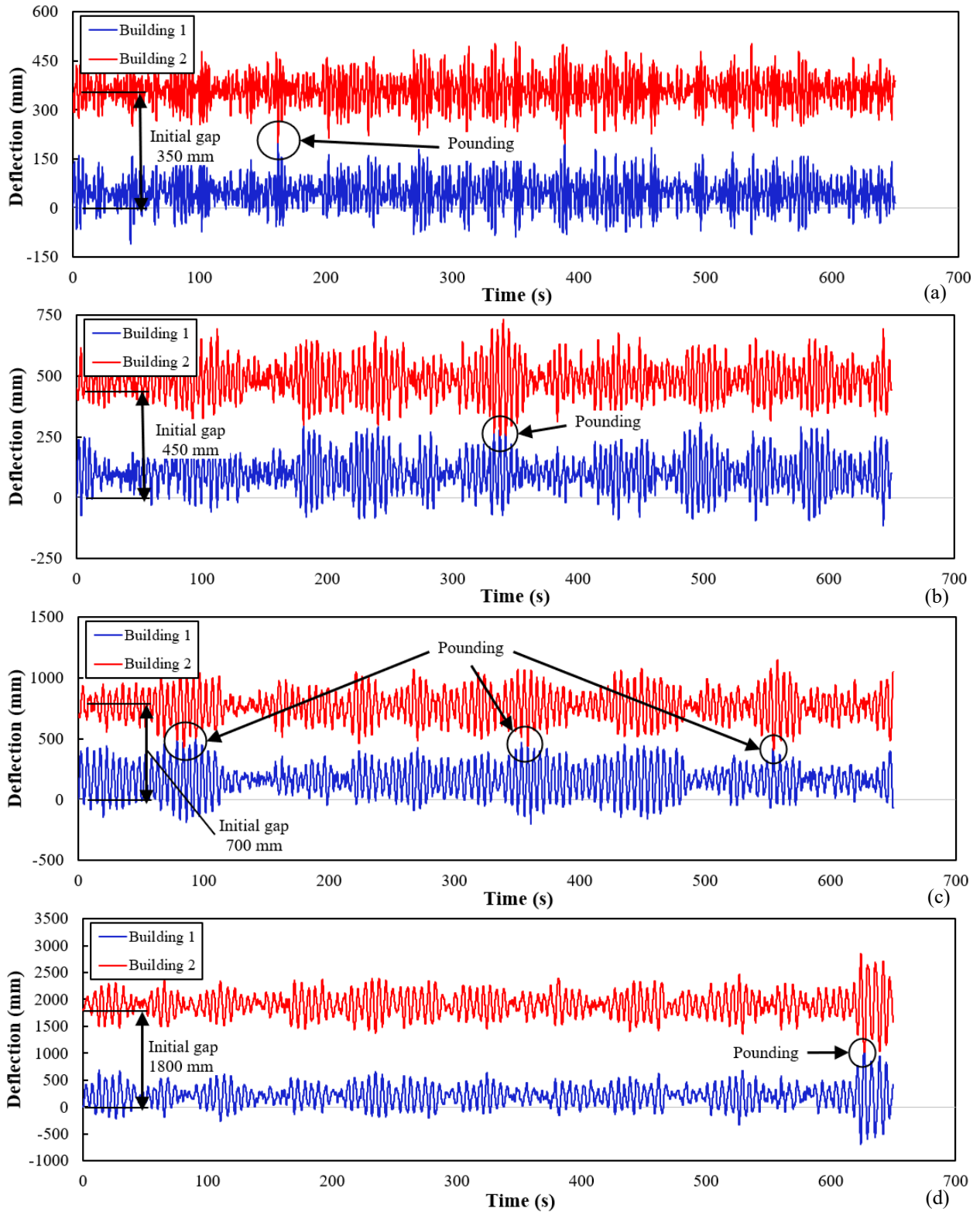
Figure 4.14: Time-history pounding cases; (a) 60 m, (b) 100 m, (c) 140 m, and (d) 180 m height (v = 40 m/s)
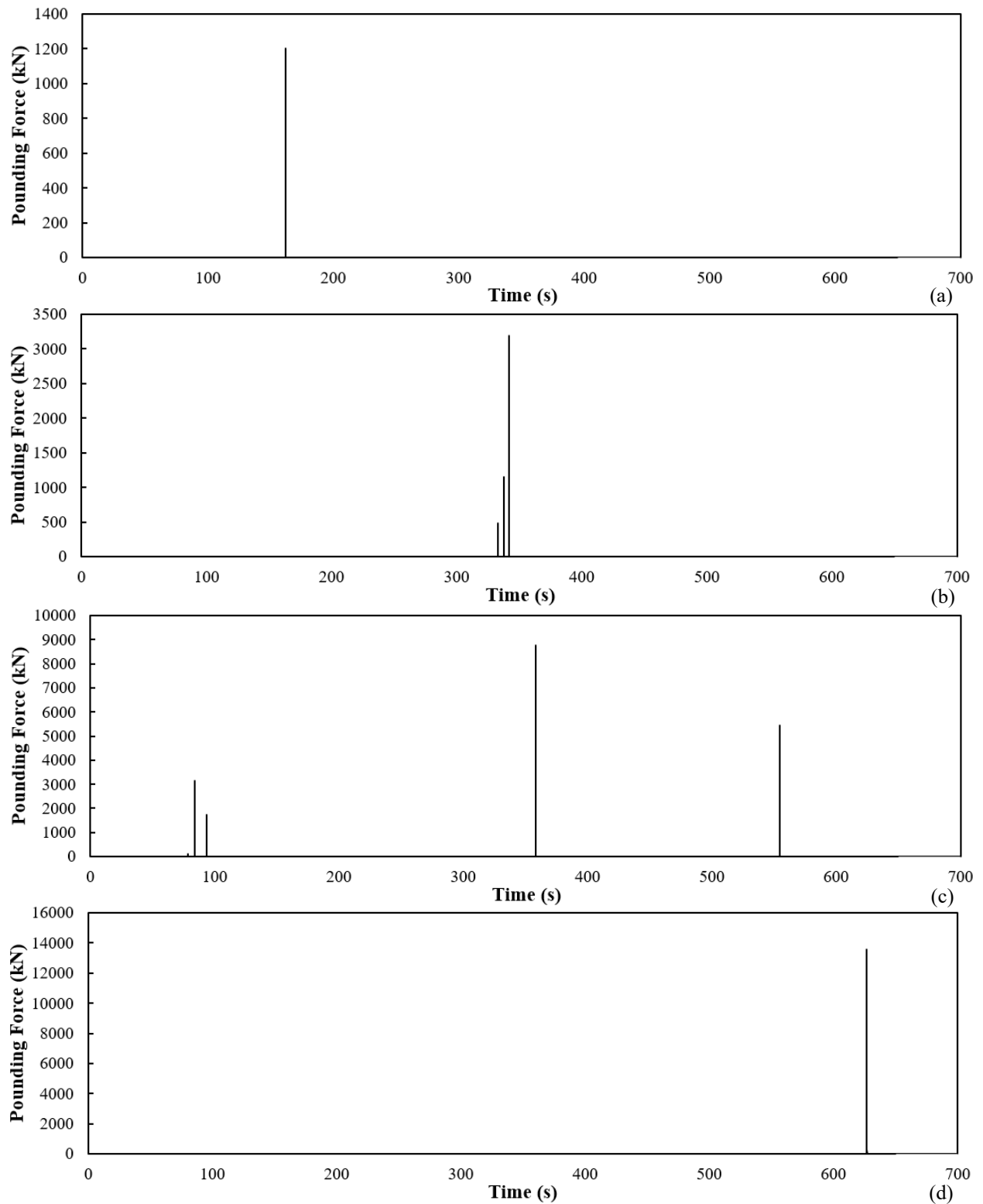
Figure 4.15: Maximum pounding force time-history; (a) 60 m, (b) 100 m, (c) 140 m, and (d) 180 m tall structures ($v = 40 \, m/s$)

Four time-history pounding scenarios for two adjacent structures of 180 m tall subjected to an applied v of 50 m/s with various initial d_g are shown in Figure 4.16 and Figure 4.17. The lateral deflection and F_I for an initial d_g of 2200 mm are shown in Figure 4.16 (a) and Figure 4.17 (a). As can be seen, pounding only transpired once in this scenario at a time instant of 559.7 seconds with a maximum F_I of 4253 kN, see Table 4.5. Five separate pounding events came into contact for an initial dg equal to 1500 mm; see Figure 4.16 (b) and Figure 4.17 (b). The first pounding instant occurred at 228.7 seconds, with a maximum F_I equal to 7910 kN. The second pounding instant was relatively small, with a maximum $F_I = 4671\ kN$ at a time of 348.6 seconds. The third and fifth pounding occurrences had the largest maximum F_I, equal to 35666 kN and 32087 kN at 443 and 625.6 seconds, respectively (see Table 4.5 for maximum F_I). The fourth instant of pounding took place at 528.4 seconds with a maximum F_I of 8072 kN. It can also be seen in Figure 4.16 (b) that the lateral deflection of both structures drastically changes after the events of pounding.

The maximum F_I was determined to take place with an initial d_g of 900 mm for the 180 m tall structures subjected to a $v = 50\ m/s$, see Figure 4.16 (c) and Figure 4.17 (c). The maximum F_I occurred at the end of the evaluated time history at 638.3 seconds. The recorded maximum F_I was determined to be 60757 kN, as recorded in Table 4.5. The following maximum F_I for this scenario took place at 451.1 seconds with a F_I of 43752 kN. At the two maximum F_I and one at the time of 527.8 seconds, the lateral deflection of the upstream structure (building 1) can be seen to have substantial lateral deflections away from the downstream structure (building 2). Such occurrences can arise due to the pounding force acting as an extreme lateral load on the structure. Figure 4.16 (d) and Figure 4.17 (d) show the last set of the examined time-history pounding scenario for the 180 m tall structure subjected to a v of 50 m/s. The initial d_g was set to be 300 mm (ideally touching). Throughout the examined scenario, the structures came into contact multiple times.

Only in a few time instances do the structures avoid pounding. At the time instant of 231.2 and 619.9 seconds, the maximum F_I was recorded as 31104 kN and 37133 kN, also shown in Figure 4.17 and Table 4.5 for the maximum F_I.

As previously mentioned in Section 4.7.2, taller structures (i.e., 140 m and 180 m) have lower F_I when the initial d_g is ultimately low (e.g., $d_g < 300\ mm$). This can be due to the structures being limited to excessive lateral sway, causing larger pounding forces when the proximate structures arise. When the structures have a relatively close d_g but are large enough for the structures to excessively deflect laterally, then the F_I will be substantially large.
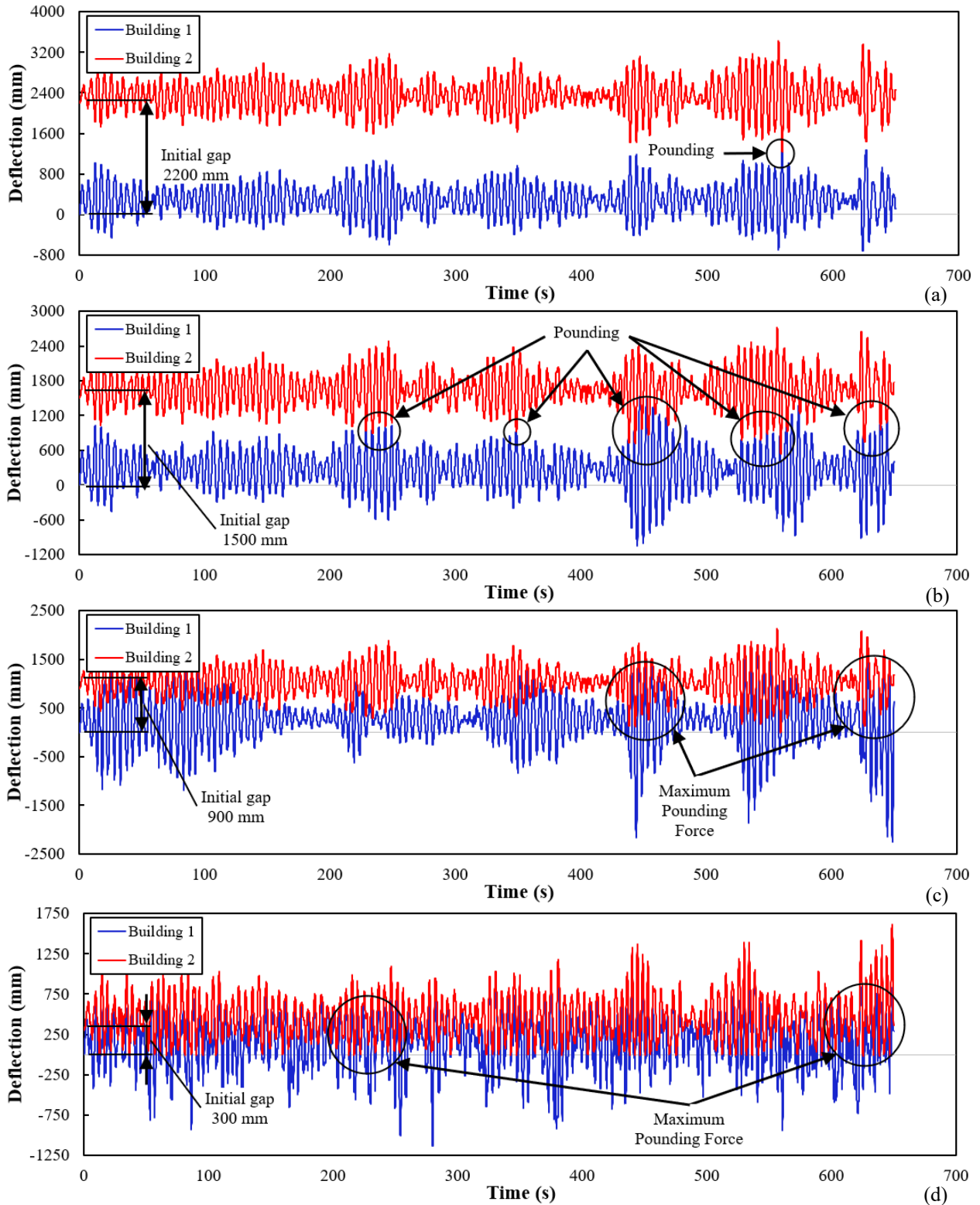
Figure 4.16: Time-history deflection for 180 m structure with varying d_g; (a) 2200 mm, (b) 1500 mm, (c) 900 mm, and (d) 300 mm ($v = 50\ m/s$)
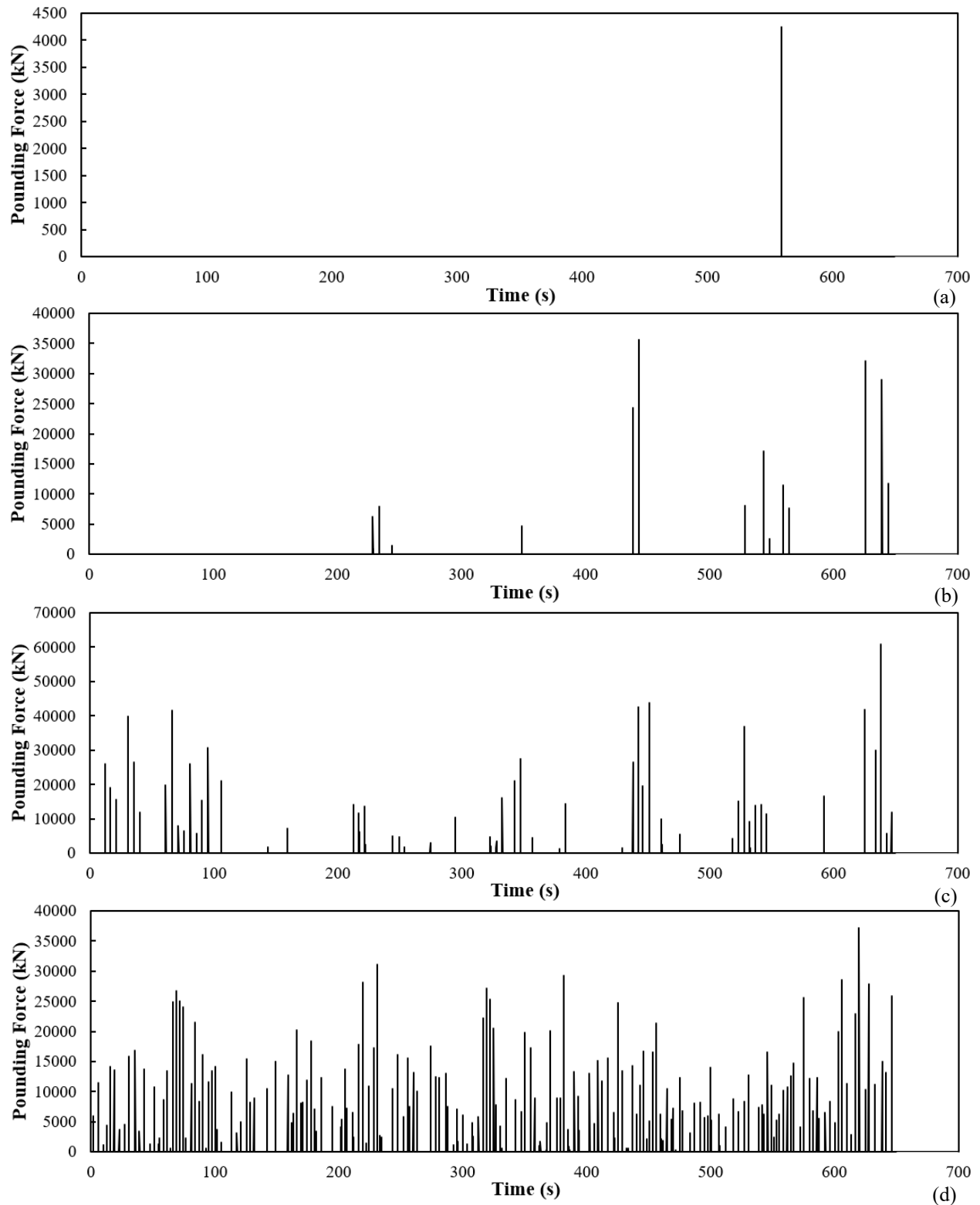
Figure 4.17: Maximum pounding force time-history for 180 m structure with varying d_g; (a) 2200 mm, (b) 1500 mm, (c) 900 mm, and (d) 300 mm ($v = 50 \ m/s$)

4.7.5   Maximum Pounding Force (F_I) with Various Separation Gap Distances (d_g)

The results of the pounding numerical analysis for two structures with varying heights (i.e., 180 m, 140 m, 100 m, and 60 m tall) with an applied v of 50 m/s show the maximum F_I at the top storey of the examined structure with various d_g are presented in Figure 4.18. Maximum F_I for the adjacent 180 m tall structures with varying d_g is presented in Figure 4.18 (a). As previously examined and discussed in Section 4.7.4, the maximum F_I for the pounding structures occurred at a d_g equal to 900 mm. When the d_g either increased or decreased in size, the F_I decreased in pounding. When comparing the d_g of 300 mm with 900 mm, a difference in the maximum F_I was determined to be 38.9%. A similar trend can also be seen in Figure 4.18 (b) for the 140 m tall structures in proximity with a d_g equal to 1000 mm. Although a d_g of 300 mm is relatively close to a d_g of 1000 mm with having similar F_I, the F_I is still more significant at further d_g for taller structures. When comparing the d_g of 600 mm with 1000 mm, a difference in the maximum F_I was determined to be 30.5%. A comparison of the maximum F_I at varying d_g for the 100 m and 60 m tall structures is shown in Figure 4.18 (c) and (d), respectively. For Figure 4.18 (c) and (d), the maximum F_I has an increasing linear trend when the d_g decreases. This can be due to the structure's heights being relatively shorter than taller structures (i.e., 140 m and 180 m) and ultimately having lower lateral displacements. As previously mentioned in Section 4.7.4, it can be seen in Figure 4.18 (a) and (b) for taller structures that as the structures become relatively closer to each other (d_g lowers), the maximum F_I tends to decrease. Maximum F_I for Figure 4.18 (c) and (d) both occurred at the lowest d_g of 250 and 300 mm, respectively.
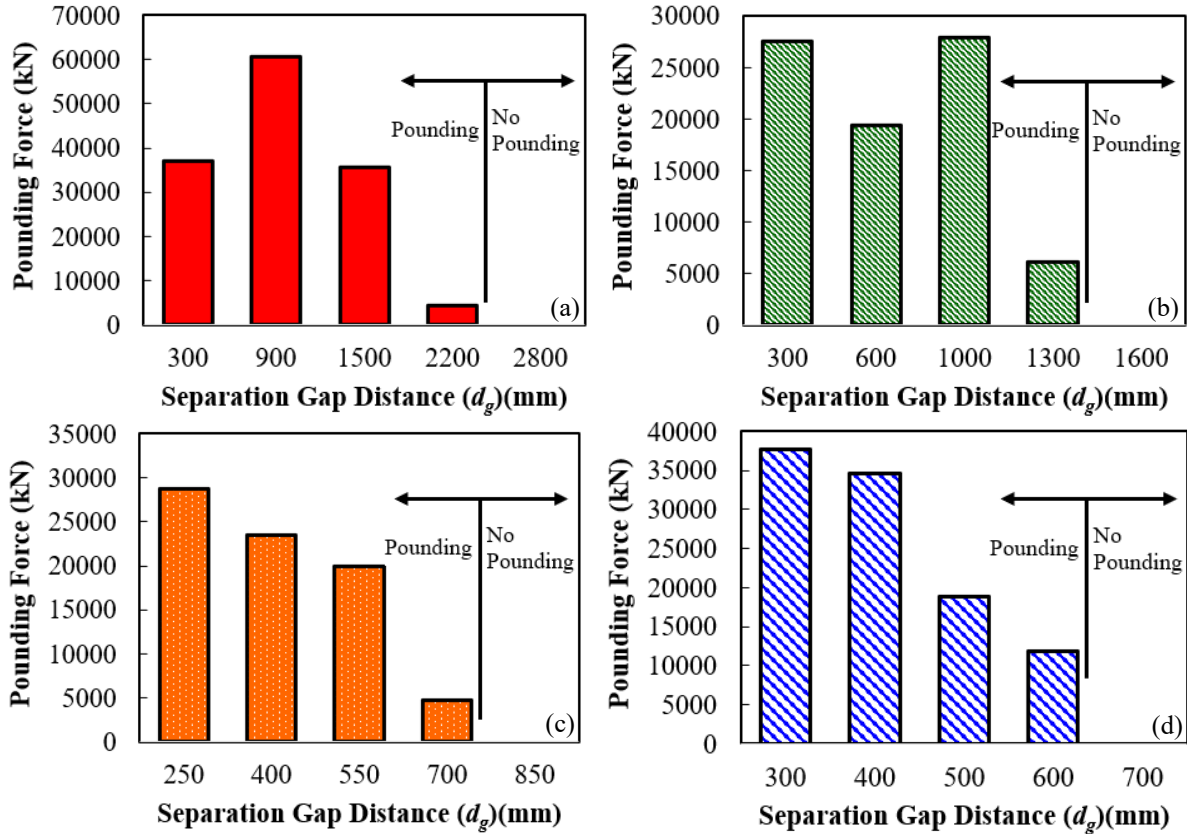
Figure 4.18: Maximum pounding force (F_I) at applied mean wind velocity (v) of 50 m/s with varying separation gap distances (d_g); (a) 180 m, (b) 140 m, (c) 100 m, and (d) 60 m height

4.7.6   Peak Pounding Force (F_I) at Different Storey Levels

A comparison of the maximum F_I per storey height is determined and presented in Figure 4.19-Figure 4.22 for the 180 m, 140 m, 100 m, and 60 m tall pounding structures, respectively. Additionally, maximum F_I for similar story heights at other time instances are also examined and compared in Figure 4.20 (b), Figure 4.21 (b), and Figure 4.22 (b). Figure 4.19 presents the 180 m tall structure with an applied v of 30 m/s at an initial d_g of 200 mm and compares the maximum F_I based on the top six storey levels. It can be seen that at a pounding instant at $T = 625.3\ seconds$, the maximum F_I decreases at higher structural heights. The maximum F_I occurs on the 40th storey structure equalling 15160 kN, compared to the 45-storey structure, which is equal to 12485 kN. A maximum F_I difference of 17.65% between the 40th and 45th levels was determined.

173

Figure 4.20 (a) and (b) compare the maximum F_I at different top storey levels for the 140 m tall structure when applied to a v of 50 m/s with the initial d_g equal to 300 mm. The highest max F_I at a time instant of 553.4 seconds occurred at the top storey height of 35th storey, equalling 23537 kN, where the lowest compared maximum F_I was on the 31st storey height being 3949 kN, as presented in Figure 4.20 (a). An 83.2% difference for the maximum F_I was achieved in comparison with the 35th storey level and the 31st storey level. However, a few seconds later ($T = 555.9\ seconds$), the largest maximum FI was at the 31st storey height equalling 27501 kN. The maximum F_I difference comparing the 35th storey level with the 31st storey level was determined to be 14.4%.

Similar results have occurred for the 25 and 15-storey structures, as presented in Figure 4.21 and Figure 4.22, respectively. Comparable results of the maximum F_I at varying top storey levels for the 100 m tall structure when subjected to an applied v of 50 m/s with the initial d_g equal to 250 mm are presented in Figure 4.21 (a) and (b). Accordingly, Figure 4.22 (a) and (b) present the 60 m tall structures' maximum F_I at various top storey levels with the initial d_g equal to 100 mm when subjected to an applied v of 30 m/s. For the 100 m tall structure shown in Figure 4.21 (a), the maximum F_I was determined to be equal to 19542 kN located on the 24th storey level at the time of impact, being 334.7 seconds. The maximum F_I difference comparing the 25th and 22nd storey levels was 80.1%. However, at a time instant of 555.8 seconds for the 22nd storey level displayed in Figure 4.21 (b), a maximum F_I was equal to 12855 kN, only having a maximum F_I difference of 33.6%. The maximum F_I for the 60 m tall structure shown in Figure 4.22 (a) was determined to be 7496 kN located on the 10th storey level at the time of impact, equalling 584.8 seconds. A difference of only 2.69% was determined when comparing the maximum F_I for the 15th storey level with the 10th storey level. However, a difference of 72.9% for the maximum F_I was

determined when comparing the 10th storey level with the 12th storey level. Storey level 12 increased in the maximum F_I equaling 5599 kN at 355.7 seconds. Having only a maximum F_I difference being 25.3% when compared to the 10th storey maximum F_I.
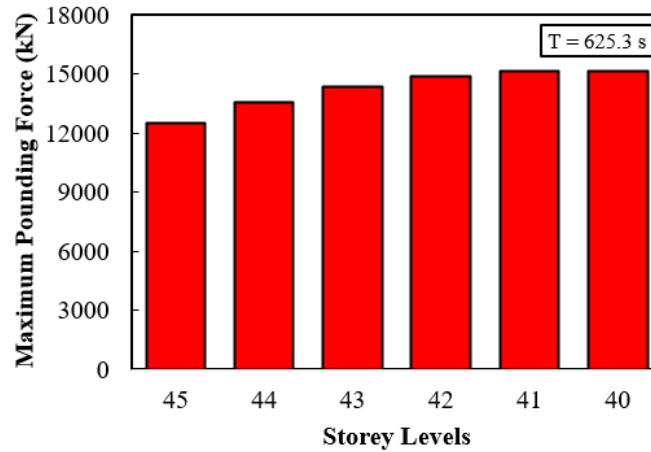
Figure 4.19: Pounding force (F_I) at the top six storey levels ($H = 180\ m, v = 30\ m/s, d_g = 200\ mm, F_n = 0.198$)
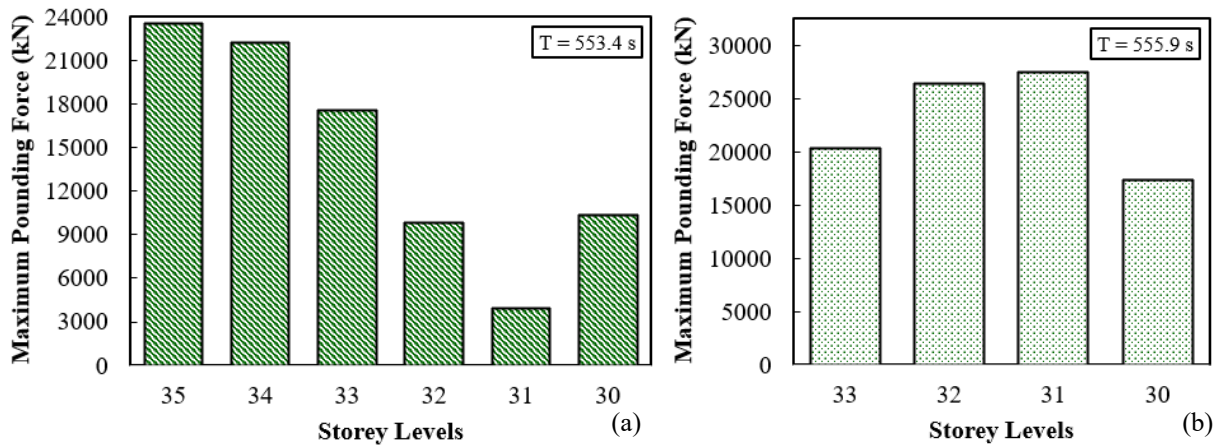
Figure 4.20: Pounding force (F_I) at storey levels ($H = 140\ m, v = 50\ m/s, d_g = 300\ mm, F_n = 0.249\ Hz$); (a) $T = 553.4\ seconds$, and (b) $T = 555.9\ seconds$
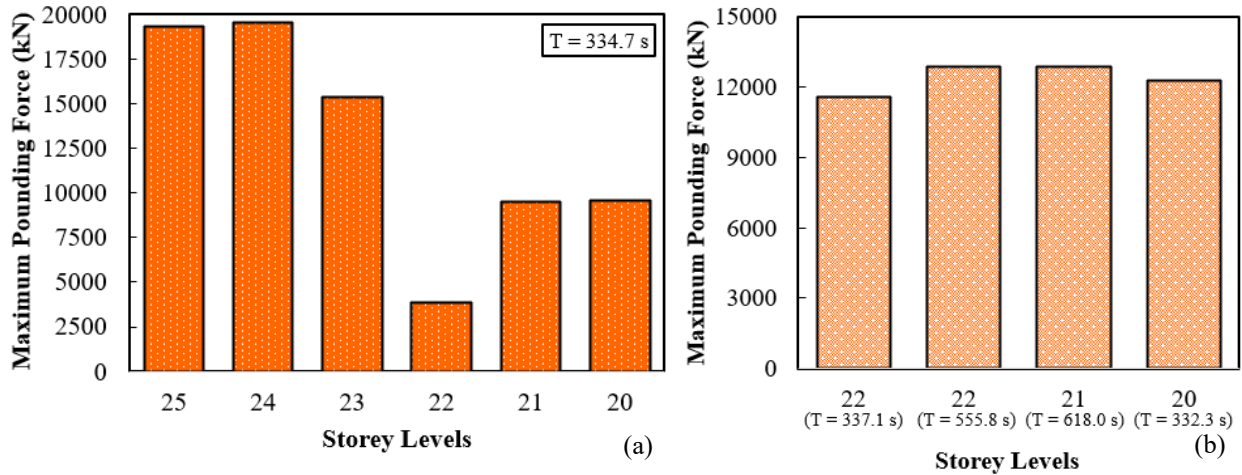
Figure 4.21: Pounding force (F_I) at storey levels ($H = 100\ m$, $v = 50\ m/s$, $d_g = 250\ mm$, $F_n = 0.277\ Hz$); (a) $T = 334.7\ seconds$, and (b) varying impact times
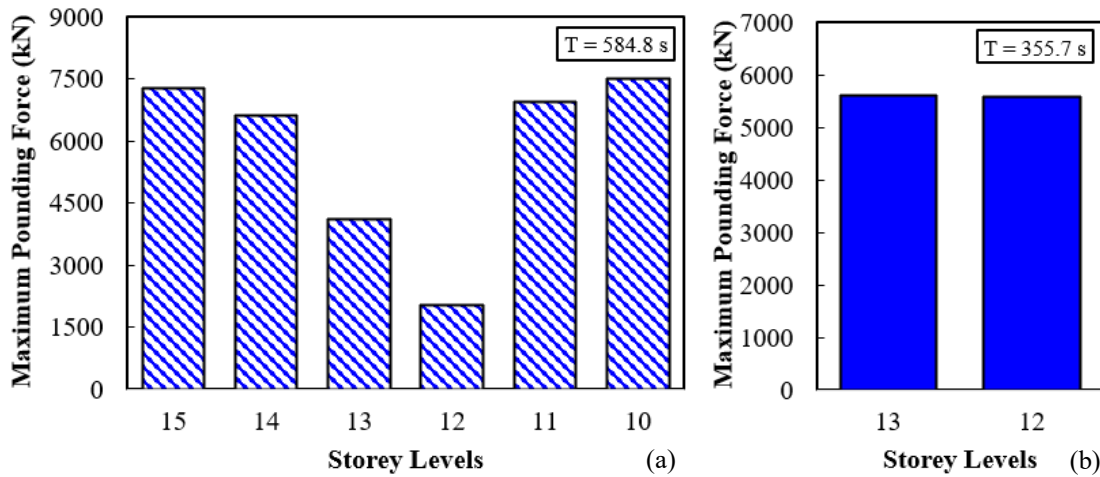
Figure 4.22: Pounding force (F_I) at storey levels ($H = 60\ m$, $v = 30\ m/s$, $d_g = 100\ mm$, $F_n = 0.381\ Hz$); (a) $T = 584.8\ seconds$, and (b) $T = 355.7\ seconds$

4.8   Summary

This chapter presents a developed mathematical formulas for determining the maximum design pounding forces between two tall buildings in proximity based on the applied mean wind velocity, building height, building natural frequency, and initial separation gap distance. CFD and FEM numerical simulations have been performed to model wind-induced pounding of structures for buildings of equal heights and dynamic properties. The maximum pounding force is recorded by extracting the pounding force time history at each story. This chapter then conducts a parametric examination to develop a database of design pounding forces corresponding to various building

configurations, which is used to formulate mathematical equations for estimating the maximum pounding force between two adjacent structures when the separation distance is lowered than the required minimum separation distance to prevent pounding. Overall, the developed mathematical formulations can be compared to the numerical FEM models for evaluating the overall differences in the maximum pounding forces of the two adjacent structures in proximity.

5 Chapter 5 – Conclusion and Future Work

5.1 General

In order to address the arising phenomena of wind-induced pounding of tall structures, a greater understanding through extensive literature review, analytical modelling, and mathematical formulations needs to be developed for mitigations and determinations towards pounding interactions. The study gap to this date is identifying possible mitigation measures towards avoiding a wind-induced pounding of tall structures. Pounding mitigation should be considered either by providing safe separation distances between structures or by designing for the additional lateral loads resulting from pounding.

In order to bridge this aforementioned knowledge gap, the current thesis presented a summary of numerical modelling examining a wide range of structures at proximity with altering applied winds based on a numerical simulation. A detailed literature review was produced from a state-of-the-art review for current problems and mitigation measures for the pounding of structures. The thesis initializes the research with a numerical wind analysis to determine and capture the applied wind forces over a period of time acting on the two adjacent structures in proximity. Computational Fluid Dynamic models were then developed and validated for capturing applied wind analysis. The analysis then inputted the captured time-history wind forces into Finite Element models to define each structure's dynamic responses. The dynamic responses of each structure throughout the applied wind forces can establish the lateral deflection of each structure, which can correlate with the required separation distance required to mitigate wind-induced structural pounding. Once established, the separation distance is minimized from the required separation distance to configure larger pounding forces.

This thesis develops mathematical formulas from an optimization process through Genetic Algorithm to determine the minimum separation gap distance required to mitigate structural

pounding and alternatively, the possible maximum pounding forces when a collision occurs if the required gap (separation) distance cannot be achieved.

5.2   Research Contributions

The outcome of this research work is to expand the understanding of the phenomena of wind-induced pounding of structures in proximity. This is expected to open more possibilities for future comings concerning the planning and designing of tall structures in dense metropolitan locations subjected to high-intensity wind flows. The core contributions of this thesis are as follows:

- Development of numerical LES models to analyze the uncertain high-intensity wind forces on each structure examined over a given period

- Development of a FEM modelled structural analysis from the captured time-history wind forces to determine the time-dependent dynamic response of each structure

- Identifying a minimum separation gap distance where no structural pounding occurs during the FEM modelled simulation

- Identifying the maximum pounding force applied in the FEM model over the applied time-history analysis when the minimum separation gap distances between structures are not provided.

- A GA used to optimize and formulate a reliable mathematical formula for determining an adequate minimum separation gap distance between two structures at proximity to prevent pounding.

- A GA used to correlate a generic mathematical formulation from optimization cycles for determining the maximum pounding force, F_I, by using the geometrical parameters as input values.

5.3 Conclusion

5.3.1 State-of-the-Art towards Pounding of Structures

The risk of pounding is expected to be magnified when the adjacent buildings are placed with a separation distance that is less than the suitable gap space or the structural system can not withstand the additional colliding load. Pounding events have occurred in many different hazardous events while subjected to lateral motion, specifically during earthquake excitations (e.g., 1940 El Centro earthquake, 1985 Mexico City earthquake, 1989 Loma Prieta earthquake, and 2011 Christchurch earthquake). Pounding due to earthquake excitation can occur to tall, mid-rise, or relatively low structures such as one or two stories, in addition to bridges. However, unreinforced masonry buildings and buildings with large windows and doors were the most vulnerable to damage from pounding phenomena. Floor-to-column pounding can lead to more risk for structural failures compared to structures with similar floor elevations. During these natural hazard events, pounding between such structures can lead to undesirable damages even if these structures are adequately designed to resist these natural hazards without the occurrence of pounding.

Pounding incidents have been reported in many cases, such as large city-scale earthquake occurrences (e.g., 40% of severely damaged structures in the Mexico City earthquake were involved in pounding), out-of-phase vibrations leading to the pounding of adjacent structures (e.g., Olive View Hospital), and within the same structure that has expansion joints (e.g., Shipshaw Bridge located outside of Jonquiere, Quebec). Different arrangements for a two-building pounding event (e.g., stiff-flexible) can change the amplification factor up to 200%. However, more flexible structures can significantly reduce the pounding of structures by increasing effective damping by utilizing structural motion control techniques (e.g., dampers and base isolation). Motivated by the

numerous pounding incidents, several studies have adopted experimental and numerical approaches to model structural pounding behaviours and possible damages during past earthquake phenomena, such as models conducted through shaking tables, single-degree-of-freedom, multiple-degrees-of-freedom, finite element method or applied element method analyses. Studying structural pounding through the utilization of multi-degree-of-freedom models provided a more reliable result for pounding behaviour due to the accuracy of the higher-order vibration modes, which are sometimes harder to capture even using experimental modelling. Extrapolation through numerical analysis may be used to assist in the building design process if the physical problem characteristics are similar to those employed. In addition to earthquake excitations, tall structures may also be subjected to strong wind loads; as a result, they may experience out-of-phase vibrations despite similarities towards their dynamic structural properties. Such vibrations can be allocated to the differences in the wind load distribution resulting from the building shapes and their surrounding structures.

5.3.2   Determined Minimum Separation Distance to Mitigate Structural Pounding

In this thesis, a parametric study has been conducted to develop a mathematical formulation for estimating the required separation distance between two adjacent structures in proximity of equal heights subjected to wind. Throughout the process of the study, various detailed conclusions are deduced as follows:

- Introducing a required separation gap distance between two adjacent structures in proximity from a wind-induced can ultimately mitigate any additional lateral forces from a collision.

- The majority of the upstream structure subjected to wind in proximity based on their height, dynamic responses, and applied mean wind velocities have a more significant peak lateral deflection than the following adjacent structure.

- A similar trend in the required separation distance is noticed compared to structures of similar height with altering natural frequencies and applied mean wind velocities. The lowest change in the required separation distance is at the 180 m structure from an applied mean wind velocity of 40 m/s to 50 m/s having a change of 15.46%. The most significant change in required separation distance is at the 180 m structure from an applied mean wind velocity of 20 m/s to 30 m/s having a change of 67.61%.

- Determined mathematical formulas for the required separation distance can become complex. Nevertheless, the developed mathematical formulas accurately captured the expected required separation distance. Including all parameters in the genetic algorithm is the most consistent when such parameters are altered (i.e., building height, natural frequency, applied mean wind velocity).

- The best-fitted genetic algorithm determined can acquire complex variations in the objective function and fitting the trained database with a correlation coefficient of 0.9987. This has accelerated the mathematical optimization process substantially.

5.3.3 Wind-Induced Pounding of Tall Structures in Determination of Pounding Forces

This part of the thesis highlights the developed mathematical formulas for determining the maximum design pounding forces between two tall buildings in proximity based on the applied mean wind velocity, building height, building natural frequency, and initial separation gap distance. The following conclusion can be drawn from this study:

- The results of the pounding of structures during wind events collected from the numerical analysis show that when the proximate structures are very close to their neighbouring buildings, an increase in the maximum pounding force was captured. This was proven for structures lower than 140 m tall (i.e., 60 m and 100 m). On the other hand, for the taller structures (i.e., 140 m and 180 m tall), when the structures become significantly closer, lower maximum pounding forces were collected. This can be due to the taller structures being limited to excessive lateral sway, leading to larger lateral pounding forces. As all examined structures became closer in proximity, multiple pounding instances transpired.

- The results of the parametric investigation of wind-induced pounding show a substantial increase in the maximum pounding force when the applied mean wind velocity increases. This can be compared to any of the studied models (i.e., height, applied mean velocity, or natural frequencies). A noticeable difference in the maximum recorded pounding forces mainly occurs during the 40 m/s and 50 m/s applied mean wind velocities on every examined structure. For the tallest examined structures (i.e., 180 m tall), a constant maximum pounding force for the applied mean wind velocity of 30 m/s for a more flexible structure was noted. For the 15-storey pounding structure, a significant maximum pounding force was determined when subjected to high applied mean wind velocities (i.e., 50 m/s) compared to the maximum pounding force for the 25 and 35-storey structures (i.e., 23.5% and 26.0% difference for the 25-storey and 35-storey structure, respectively).

- The numerical analysis results show that pounding during wind events significantly influences the storey levels of the pounding structures when the initial separation distance is significantly small. Results show that when the examined structures is just insufficient of the minimum separation gap distance to prevent pounding, pounding mostly only occurs

183

once, and the majority of the pounding locations arise at the highest part of the structures. This is primarily because the largest lateral sway occurs at the top of the building. However, when the structures become ultimately very close in proximity, the maximum pounding forces captured can be triggered at lower locations of the interactive buildings. An upwards of 14.4% difference in the maximum pounding forces transpired on the 31st storey of the 140 m tall structure in very close proximity.

- The complexity can become challenging for defining a best-fitted mathematical formulation for determining the maximum pounding force for two adjacent structures. By including all the required parametric data points in the genetic algorithm, the best-suited parameters being altered should consist of the building's height, applied mean wind velocity, the initial separation gap distance, and the natural frequency of the structures examined. The developed mathematical formulas can accurately capture the maximum pounding force using a more complex equation. The GA determined the best fitting formula with a correlation coefficient of ~ 0.93.

5.4   Recommendations for Future Works

This thesis aims to study wind-induced pounding of tall structures in proximity by determining the possible separation gap distance to mitigate pounding and the pounding force when the structures collide if such mitigated separation gap distance cannot be achieved. Different approach methods can be used to achieve such phenomena, such as experimental tests towards tall structures pounding, wind tunnel testing towards load evaluation, numerical analysis with alteration in such structural parameters. The thesis used a numerical Large Eddy Simulation model to determine the applied time-history wind forces acting on the two adjacent structures. Wind forces were then applied to a non-linear Finite Element Method modelled simulation to predict the structure's response. A Genetic Algorithm was then used to optimize a generic mathematical formulation for

184

determining certain parameters (i.e., minimum separation gap distance and maximum pounding force). The thesis results indicate that special attention should be addressed to upcoming research on the wind-induced pounding of structures. Thus, the following recommendations are proposed for future work:

- Wind-induced torsional pounding of structures and altering wind directions.

- Alterations for the pounding gap element can be further investigated to record energy dissipation from wind-induced pounding.

- Pounding from wind events can be examined in structures with unequal heights to determine the required minimum separation distance to mitigate pounding.

- Examination of structures with unequal heights to determine possible damages and recording or progressive collapse if structural failures arise.

- The use of composite structures from wind-induced pounding and additional parameters such as soil-structure interaction.

Reference

2, E., 1991. Design of Concrete Structures—Part 1. General Rules and Rules for Building. , ENV 1992-1-1, 1991.8, in: CEN, Technical Committee 250/SG2 ENV 1992-1-1.

8, E., n.d. Structures in Seismic Regions, Design—Part 1. General and Building, in: CEC, Report EUR 12266EN.

A. Hameed, M. Saleem, A.U. Qazi, S.S. and M.A.B., 2012. Mitigation Of Seismic Pounding Between Adjacent Buildings. Pak. J. Sci. **64**, pp-326-333.

Abdeddaim, M, Ounis, A., Djedoui, N., Shrimali, M.K., 2016. Reduction of pounding beuildings using fuzzy controller 985–1005.

Abdeddaim, M., Ounis, A., Djedoui, N., Shrimali, M.K., 2016. Pounding hazard mitigation between adjacent planar buildings using coupling strategy. J. Civ. Struct. Heal. Monit. **6**, 603–617. https://doi.org/10.1007/s13349-016-0177-4

Abdeddaim, M., Ounis, A., Shrimali, M.K., 2017. Pounding Hazard Reduction Using a Coupling Strategy for Adjacent Buildings. 16th World Conf. Earthq. Eng. Santiago, Chile, 9-13 January. **3541**.

Abdel Raheem, S.E., 2013. Evaluation of Egyptian code provisions for seismic design of moment-resisting-frame multi-story buildings. Int. J. Adv. Struct. Eng. **5**, 1–18. https://doi.org/10.1186/2008-6695-5-20

Abdullah, M.M., Hanif, J.H., Richardson, A., Sobanjo, J., 2001a. Use of a shared tuned mass damper (STMD) to reduce vibration and pounding in adjacent structures. Earthq. Eng. Struct. Dyn. **30**, 1185–1201. https://doi.org/10.1002/eqe.58

Abdullah, M.M., Hanif, J.H., Richardson, A., Sobanjo, J., 2001b. Use of a shared tuned mass damper (STMD) to reduce vibration and pounding in adjacent structures. Earthq. Eng. Struct. Dyn. **30**, 1185–1201. https://doi.org/10.1002/eqe.58

Aboshosha, H., Elshaer, A., Bitsuamlak, G.T., El Damatty, A., 2015. Consistent inflow turbulence generator for LES evaluation of wind-induced responses for tall buildings. J. Wind Eng. Ind. Aerodyn. **142**, 198–216. https://doi.org/10.1016/j.jweia.2015.04.004

ACI Committee, 1995. Building code requirements for structural concrete (ACI 318-95) and Commentary (ACI 318R-95), in: American Concrete Institute. Detroit.

Aldemir, Ü., Aydin, E., 2005. An active control algorithm to prevent the pounding of adjacent structures, in: Vibration Problems ICOVP 2005. Springer Netherlands, Dordrecht, pp. 33–38. https://doi.org/10.1007/978-1-4020-5401-3_7

Aldemir, U., Bakioglu, M., Akhiev, S.S., 2001. Optimal control of linear buildings under seismic excitations. Earthq. Eng. Struct. Dyn. **30**, 835–851. https://doi.org/10.1002/eqe.41

Aldemir, Ü., Güney, D., 2005. Vibration control of non-linear buildings under seismic loads, in: Vibration Problems ICOVP 2005. Springer Netherlands, Dordrecht, pp. 39–44. https://doi.org/10.1007/978-1-4020-5401-3_8

Ali, M.M., Moon, K.S., 2006. Structural developments in tall buildings: Current trends and future prospects. Archit. Sci. Rev. **50**, 37–41. https://doi.org/10.3763/asre.200

Aly, A.M., Abburu, S., 2015. On the design of high-rise buildings for multihazard: Fundamental differences between wind and earthquake demand. Shock Vib. **2015**. https://doi.org/10.1155/2015/148681

American Institute of Steel Construction, Manual of Steel Construction, 2005.

American Society of Civil Engineers, 2006. Minimum Design Loads for Buildings and Other Structures. American Society of Civil Engineers, Reston, VA. https://doi.org/10.1061/9780784408094

Anagnostopoulos, S.A., 2004. Equivalent viscous damping for modeling inelastic impacts in

earthquake pounding problems. Earthq. Eng. Struct. Dyn. **33**, 897–902. https://doi.org/10.1002/eqe.377

Anagnostopoulos, S.A., 1995. Earthquake induced pounding: State of the art, in: In Proceedings of the 10th European Conference on Earthquake Engineering. Balkema: Rotterdam, pp. 897–905.

Anagnostopoulos, S.A., 1988. Pounding of buildings in series during earthquakes. Earthq. Eng. Struct. Dyn. **16**, 443–456. https://doi.org/10.1002/eqe.4290160311

Anagnostopoulos, S.A., Karamaneas, C.E., 2008. Use of collision shear walls to minimize seismic separation and to protect adjacent buildings from collapse due to earthquake-induced pounding. Earthq. Eng. Struct. Dyn. **37**, 1371–1388. https://doi.org/10.1002/eqe

Anagnostopoulos, S.A., Spiliopoulos, K. V., 1992a. An investigation of earthquake induced pounding between adjacent buildings. Earthq. Eng. Struct. Dyn. **21**, 289–302. https://doi.org/10.1002/eqe.4290210402

Anagnostopoulos, S.A., Spiliopoulos, K. V., 1992b. An investigation of earthquake induced pounding between adjacent buildings. Earthq. Eng. Struct. Dyn. **21**, 289–302.

Ansary, A. El, Damatty, A. El, Nassef, A., 2011. Optimum Shape and Design of Cooling Towers. World Acad. Sci. Eng. Technol. **5**, 12–21.

Athanassiadou, C.J., Penelis, G.G., Kappos, A.J., 1994. Seismic Response of Adjacent Buildings with Similar or Different Dynamic Characteristics. Earthq. Spectra **10**, 293–317. https://doi.org/10.1193/1.1585775

Australia Standard, 2007. Structural design actions Part 4: Earthquake actions in Australia, in: AS/NZS 1170.4: 2007.

Badawi, H.S., Mourad, S.A., 1994. Observations from the 12 October 1992 Dahshour earthquake

in Egypt. Nat. Hazards **10**, 261–274. https://doi.org/10.1007/BF00596146

Bamer, F., Markert, B., 2018. A nonlinear visco-elastoplastic model for structural pounding. Earthq. Eng. Struct. Dyn. **47**, 2490–2495. https://doi.org/10.1002/eqe.3095

Barbato, M., Tubaldi, E., 2013. A probabilistic performance-based approach for mitigating the seismic pounding risk between adjacent buildings. Earthq. Eng. Struct. Dyn. **42**, 1203–1219. https://doi.org/10.1002/eqe.2267

Barros, R.C., Khatami, S.M., 2012. Seismic Response Effect of Shear Walls in Reducing Pounding Risk of Reinforced Concrete Buildings Subjected to Near-Fault Ground Motions. 15th World Conf. Earthq. Eng. Lisbon Port.

Beck, H., 1962. Contribution to the analysis of coupled shear walls. Int. Concr. Abstr. Portal **59**, 1055–1070.

Bernardini, E., Spence, S.M.J., Wei, D., Kareem, A., 2015. Aerodynamic shape optimization of civil structures: A CFD-enabled Kriging-based approach. J. Wind Eng. Ind. Aerodyn. **144**, 154–164. https://doi.org/10.1016/j.jweia.2015.03.011

Bhaskararao, A. V., Jangid, R.S., 2006. Seismic analysis of structures connected with friction dampers. Eng. Struct. **28**, 690–703. https://doi.org/10.1016/j.engstruct.2005.09.020

Bi, K., Hao, H., 2013. Numerical simulation of pounding damage to bridge structures under spatially varying ground motions. Eng. Struct. **46**, 62–76. https://doi.org/10.1016/j.engstruct.2012.07.012

Bi, K., Hao, H., Chouw, N., 2009. Required separation distance between decks and at abutments of a bridge crossing a canyon site to avoid seismic pounding. Earthq. Eng. Struct. Dyn. 303–323. https://doi.org/10.1002/eqe.943

Bi, K., Hao, H., Chouw, N., 2008. Stochastic analysis of the required separation distance to avoid

seismic pounding between adjacent bridge decks. 14th World Conf. Earthq. Eng.

Bi, K., Hao, H., Ren, W., 2011. Non-linear 3D FEM Pounding Analysis of a Bridge Structure to Multi-Component Spatially Varying Ground Motions. 15 Wcee 1–10.

Bobby, S., Spence, S.M.J., Bernardini, E., Kareem, A., 2014. Performance-based topology optimization for wind-excited tall buildings: A framework. Eng. Struct. **74**, 242–255. https://doi.org/10.1016/j.engstruct.2014.05.043

Braun, A.L., Awruch, A.M., 2009. Aerodynamic and aeroelastic analyses on the CAARC standard tall building model using numerical simulation. Comput. Struct. **87**, 564–581. https://doi.org/10.1016/j.compstruc.2009.02.002

Brown, T., Alanani, M., Elshaer, A., Issa, A., 2022. Determination of Separation Distance to Mitigate Wind-Induced Pounding of Tall Buildings (under revision). J. Struct. Eng.

Brown, T., Elshaer, A., 2022. Pounding of structures at proximity: A state-of-the-art review. J. Build. Eng. **48**, 103991. https://doi.org/10.1016/j.jobe.2022.103991

Bruneau, M., 1998. Performance of steel bridges during the 1995 Hyogoken-Nanbu (Kobe, Japan) earthquake - A North American perspective. Eng. Struct. **20**, 1063–1078. https://doi.org/10.1016/S0141-0296(97)00203-4

Bruneau, M., Wilson, J.C., Tremblay, R., 1996. Performance of steel bridges during the 1995 Hyogo-ken Nanbu (Kobe, Japan) earthquake. Can. J. Civ. Eng. **23**, 678–713. https://doi.org/10.1139/l96-883

Chan, C.M., 2001. Optimal lateral stiffness design of tall buildings of mixed steel and concrete construction. Struct. Des. Tall Build. **10**, 155–177. https://doi.org/10.1002/tal.170

Chan, C.M., Chui, J.K.L., Huang, M.F., 2009a. Integrated aerodynamic load determination and stiffness design optimization of tall buildings. Struct. Des. Tall Spec. Build. **18**, 59–80.

https://doi.org/10.1002/tal.397

Chan, C.M., Huang, M.F., Kwok, K.C.S., 2009b. Stiffness Optimization for Wind-Induced Dynamic Serviceability Design of Tall Buildings. J. Struct. Eng. **135**, 985–997. https://doi.org/10.1061/(ASCE)ST.1943-541X.0000036

Chan, C.M., Ning, F., Mickleborough, N.C., 2000. Lateral stiffness characteristics of tall reinforced concrete buildings under service loads. Struct. Des. Tall Build. **9**, 365–383. https://doi.org/10.1002/1099-1794(200012)9:5<365::AID-TAL158>3.0.CO;2-B

Chau, K.T., Wei, X.X., 2001. Pounding of structures modelled as non-linear impacts of two oscillators. Earthq. Eng. Struct. Dyn. **30**, 633–651. https://doi.org/10.1002/eqe.27

Chau, K.T., Wei, X.X., Guo, X., Shen, C.Y., 2003. Experimental and theoretical simulations of seismic poundings between two adjacent structures. Earthq. Eng. Struct. Dyn. **32**, 537–554. https://doi.org/10.1002/eqe.231

Chen, G., Wu, J., 2001. Optimal Placement of Multiple Tune Mass Dampers for Seismic Structures. J. Struct. Eng. **127**, 1054–1062. https://doi.org/10.1061/(ASCE)0733-9445(2001)127:9(1054)

Chenna, R., Ramancharla, P.K., 2018. Damage assessment due to pounding between adjacent structures with equal and unequal heights. J. Civ. Struct. Heal. Monit. **8**, 635–648. https://doi.org/10.1007/s13349-018-0296-1

Chouw, N., Hao, H., 2012. Pounding damage to buildings and bridges in the 22 February 2011 Christchurch earthquake. Int. J. Prot. Struct. **3**, 123–140. https://doi.org/10.1260/2041-4196.3.2.123

Chouw, N., Hao, H., 2008. Significance of SSI and nonuniform near-fault ground motions in bridge response I: Effect on response with conventional expansion joint. Eng. Struct. **30**, 141–

153. https://doi.org/10.1016/j.engstruct.2007.03.002

Chung, H.S., Moon, B.W., Lee, S.K., Park, J.H., Min, K.W., 2009. Seismic performance of friction dampers using flexure of RC shear wall system. Struct. Des. Tall Spec. Build. **18**, 807–822. https://doi.org/10.1002/tal.524

Colajanni, P., Papia, M., 1995. Seismic response of braced frames with and without friction dampers. Eng. Struct. **17**, 129–140. https://doi.org/10.1016/0141-0296(95)92644-N

Cole, G.L., Dhakal, R.P., Turner, F.M., 2012. Building pounding damage observed in the 2011 Christchurch earthquake. Earthq. Eng. Struct. Dyn. **41**, 893–913. https://doi.org/10.1002/eqe

Comartin, C.D., Greene, M., Tubbesing, S.K., 1995. The Hyogo-ken Nanbu (Kobe) earthquake, January 17,1995: Preliminary reconnaissance report, in: Earthquake Engineering Research Institute. p. 116.

Conoscente, J.P., Hamburger, R.O., Johnson, J.J., 1992. Dynamic analysis of impacting structual systems, in: Earthquake Engineering, Tenth World Conference at 1992 Balkema, Rotterdam. pp. 3899–3903.

Coull, A., Choudhury, J.R., 1967. Stresses and deflections in coupled shear walls. Int. Concr. Abstr. Portal **64**, 65–72.

Coull, A., Wahab, A.A.F., 1993. Lateral load distribution in asymmetrical tall building structures **119**, 1032–1047.

Cui, W., Caracoglia, L., 2018. A fully-coupled generalized model for multi-directional wind loads on tall buildings: A development of the quasi-steady theory. J. Fluids Struct. **78**, 52–68. https://doi.org/10.1016/j.jfluidstructs.2017.12.008

Dagnew, A.K., Bitsuamlak, G.T., 2013. Computational evaluation of wind loads on buildings: A review. Wind Struct. An Int. J. **16**, 629–660. https://doi.org/10.12989/was.2013.16.6.629

Davis, L., 1991. Handbook of genetic algorithms.

Davis, R.O., 1992. Pounding of buildings modelled by an impact oscillator. Earthq. Eng. Struct. Dyn. **21**, 253–274.

DE Goldberg, 2013. Genetic algorithms. Pearson Educ. India.

Ding, F., Kareem, A., Wan, J., 2019. Aerodynamic Tailoring of Structures Using Computational Fluid Dynamics. Struct. Eng. Int. **29**, 26–39. https://doi.org/10.1080/10168664.2018.1522936

Doğan, M., Günaydın, A., 2009. Pounding of Adjacent RC Buildings During Seismic Loads. J. Eng. Archit. Fac. Eskişehir Osmangazi Univ. **22**, 129–145.

Dragoiescu, C., Garber, J., Kumar, K.S., 2006. A comparison of force balance and pressure integration techniques for predicting wind-induced responses of tall buildings. Proc. Struct. Congr. Expo. **2006**, 14. https://doi.org/10.1061/40889(201)14

Dubčáková, R., 2011. Eureqa: software review. Genet. Program. Evolvable Mach. **12**, 173–178. https://doi.org/10.1007/s10710-010-9124-z

Edwards, L., n.d. Eureqa, the Robot Scientist.

Efraimiadou, S., Hatzigeorgiou, G.D., Beskos, D.E., 2013. Structural pounding between adjacent buildings subjected to strong ground motions. Part I: The effect of different structures arrangement. Earthq. Eng. Struct. Dyn. **42**, 1509–1528. https://doi.org/10.1002/eqe

Ehab, Mariam, Salem, H., Mostafa, H., 2014. Earthquake pounding effect on adjacent reinforced concrete buildings. Int. J. Comput. Appl. **106**, 27–34.

Ehab, Mariem, Salem, H., Mostafa, H., Yehia, N., 2014. Earthquake Pounding Effect on Adjacent Reinforced Concrete Buildings Blast Resistant Building Design View project reinforced concrete structures View project Earthquake Pounding Effect on Adjacent Reinforced

Concrete Buildings. Artic. Int. J. Comput. Appl. **106**, 975–8887.

Ellingwood, B., 1986. Structural Serviceability: A Critical Appraisal and Research Needs. J. Struct. Eng. **112**, 2646–2664. https://doi.org/10.1061/(ASCE)0733-9445(1986)112:12(2646)

Elnashai, A.S., Gencturk, B., Kwon, O.S.O.-S., Al-Qadi, I.L., Hashash, Y., Roesler, J.R., Kim, S.J.S.J., Jeong, S.-H., Dukes, J., Valdivia, A., 2010. The Maule (Chile) earthquake of February 27, 2010: Consequence assessment and case studies. MAE Cent. Rep. No. 10-04 208.

Elnashai, A.S., Kim, S.J., Yun, G.J., Sidarta, D., 2007. The Yogyakarta Earthquake of May 27, 2006. MAE Cent. CD Release 1–57.

Elshaer, A., Aboshosha, H., Bitsuamlak, G., El Damatty, A., Dagnew, A., 2016. LES evaluation of wind-induced responses for an isolated and a surrounded tall building. Eng. Struct. **115**, 179–195. https://doi.org/10.1016/j.engstruct.2016.02.026

Elshaer, A., Bitsuamlak, G., 2018. Multiobjective aerodynamic optimization of tall building openings for wind-induced load reduction. J. Struct. Eng. (United States) **144**, 1–11. https://doi.org/10.1061/(ASCE)ST.1943-541X.0002199

Elshaer, A., Bitsuamlak, G., Damatty, A. El, 2017. Enhancing wind performance of tall buildings using corner aerodynamic optimization. Eng. Struct. **136**, 133–148. https://doi.org/10.1016/j.engstruct.2017.01.019

Elwardany, H., Seleemah, A., Jankowski, R., 2017. Seismic pounding behavior of multi-story buildings in series considering the effect of infill panels. Eng. Struct. **144**, 139–150. https://doi.org/10.1016/j.engstruct.2017.01.078

ETABS, 2018.

Favvata, M.J., 2017. Minimum required separation gap for adjacent RC frames with potential

inter-story seismic pounding. Eng. Struct. **152**, 643–659. https://doi.org/10.1016/j.engstruct.2017.09.025

Favvata, M.J., Karayannis, C.G., 2013. The inter-storey pounding effect on the seismic behaviour of infilled and pilotis RC structures, in: Geotechnical, Geological and Earthquake Engineering. pp. 81–101. https://doi.org/10.1007/978-94-007-5377-8

Favvata, M.J., Karayannis, C.G., 2009. Influence of exterior joint effect on the inter-story pounding interaction of structures. Struct. Eng. Mech. **33**, 113–136.

Favvata, M.J., Karayannis, C.G., Anagnostopoulou, V., 2012. Influence of infill panels with and without openings on the pounding effect of RC structures. Proc. 15th world Conf. Earthq. Eng. Lisbon, Port. **2**, 24–28.

Favvata, M.J., Naoum, M.C., Karayannis, C.G., 2013. Earthquake induced interaction between RC frame and steel frame structures. WIT Trans. Built Environ. **134**, 839–851. https://doi.org/10.2495/SAFE130741

Filiatrault, A., Cervantes, M., Folz, B., Prion, H., 1994. Pounding of buildings during earthquakes: a Canadian perspective. Can. J. Civ. Eng. **21**, 251–265. https://doi.org/10.1139/l94-028

Filiatrault, A., Tinawi, R., Massicotte, B., 1993. Damage to cable-stayed bridge during 1988 Saguenay earthquake. I: Pseudostatic analysis. J. Struct. Eng. **119**, 1432–1449.

Filiatrault, A., Wagner, P., Cherry, S., 1995. Analytical prediction of experimental building pounding. Earthq. Eng. Struct. Dyn. **24**, 1131–1154.

Flenga, M.G., Favvata, M.J., 2021. Probabilistic seismic assessment of the pounding risk based on the local demands of a multistory RC frame structure. Eng. Struct. **245**, 112789. https://doi.org/10.1016/j.engstruct.2021.112789

Franke, J., 2006. Recommendations of the COST action C14 on the use of CFD in predicting

pedestrian wind environment. Recomm. COST action C14 use CFD Predict. Pedestr. Wind Environ. 529–532.

Franke, J., Hellsten, A., Schlunzen, K.H., Carissimo, B., 2011. The COST 732 Best Practice Guideline for CFD simulation of flows in the urban environment: a summary. Int. J. Environ. Pollut. **44**, 419–427.

Galal, K., El-Sawy, T., 2010. Effect of retrofit strategies on mitigating progressive collapse of steel frame structures. J. Constr. Steel Res. **66**, 520–531. https://doi.org/10.1016/j.jcsr.2009.12.003

Gazetas, G., 2006. Seismic design of foundations and soil-structure interaction, in: First European Conference on Earthquake Engineering and Seismology, Geneva, Switzerland. pp. 3–8.

Germano, M., Piomelli, U., Moin, P., Cabot, W.H., 1991. A dynamic subgrid-scale eddy viscosity model. Phys. Fluids A **3**, 1760–1765. https://doi.org/10.1063/1.857955

Ghandil, M., Aldaikh, H., 2017a. Damage-based seismic planar pounding analysis of adjacent symmetric buildings considering inelastic structure-soil-structure interaction. Earthq. Eng. Struct. Dyn. **46**, 1141–1159. https://doi.org/10.1002/eqe.2848

Ghandil, M., Aldaikh, H., 2017b. Damage-based seismic planar pounding analysis of adjacent symmetric buildings considering inelastic structure-soil-structure interaction. Earthq. Eng. Struct. Dyn. **46**, 1141–1159. https://doi.org/10.1002/eqe.2848

Godínez-Domínguez, E.A., Tena-Colunga, A., 2010. Nonlinear behavior of code-designed reinforced concrete concentric braced frames under lateral loading. Eng. Struct. **32**, 944–963. https://doi.org/10.1016/j.engstruct.2009.12.020

Goldsmith, W., 1960. Impact: The theory and physical behavior of colliding solids. E. Arnold.

Grigoriu, M., 1981. Mean-square structural response to stationary ground acceleration. J. Eng. Mech. Div. **105**, 969–986.

Guo, A., Li, Z., Li, H., 2011. Point-to-surface pounding of highway bridges with deck rotation subjected to bi-directional earthquake excitations. J. Earthq. Eng. **15**, 274–302. https://doi.org/10.1080/13632461003739730

Gurley, K., Kareem, A., Bergman, L.A., Johnson, E.A., Klein, R.E., 1994. Coupling tall buildings for control of response to wind. Struct. Saf. Reliab. **1553**.

Halabian, A.M., El Naggar, M.H., Vickery, B.J., 2003. Reliability analysis of wind response of flexibly supported tall structures. Struct. Des. Tall Build. **12**, 1–20. https://doi.org/10.1002/tal.207

Halis Gunel, M., Emre Ilgin, H., 2007. A proposal for the classification of structural systems of tall buildings. Build. Environ. **42**, 2667–2675. https://doi.org/10.1016/j.buildenv.2006.07.007

Hao, H., 2015. Analysis of seismic pounding between adjacent buildings. Aust. J. Struct. Eng. **16**, 208–225. https://doi.org/10.1080/13287982.2015.1092684

Hao, H., 1998. A parametric study of the required seating length for bridge decks during earthquake. Earthq. Eng. Struct. Dyn. **27**, 91–103. https://doi.org/10.1002/(SICI)1096-9845(199801)27:1<91::AID-EQE722>3.0.CO;2-I

Hartmann, D., Breidt, M., Nguyen, van V., Stangenberg, F., Höhler, S., Schweizerhof, K., Mattern, S., Blankenhorn, G., Möller, B., Liebscher, M., 2008. Structural collapse simulation under consideration of uncertainty - Fundamental concept and results. Comput. Struct. **86**, 2064–2078. https://doi.org/10.1016/j.compstruc.2008.03.004

Holland, J.H., 1992. Adaptation in Natural and Artificial Systems: An Introductory Analysis with Applications to Biology, Control, and Artificial Intelligence.

Huang, M., 2017. High-Rise Buildings under Multi-Hazard Environment, High-Rise Buildings

under Multi-Hazard Environment: Assessment and Design for Optimal Performance. Springer Singapore, Singapore. https://doi.org/10.1007/978-981-10-1744-5

Huang, M.F., Chan, C.M., Lou, W.J., 2012. Optimal performance-based design of wind sensitive tall buildings considering uncertainties. Comput. Struct. **98**–**99**, 7–16. https://doi.org/10.1016/j.compstruc.2012.01.012

Irwin, P., Kilpatrick, J., Robinson, J., Frisque, A., 2008. Wind and tall buildings: negatives and positives. Struct. Des. Tall Spec. Build. **17**, 915–928. https://doi.org/10.1002/tal.482

Irwin, P.A., 2009. Wind engineering challenges of the new generation of super-tall buildings. J. Wind Eng. Ind. Aerodyn. **97**, 328–334. https://doi.org/10.1016/j.jweia.2009.05.001

Ismail, M., 2015a. Inner pounding control of the RNC isolator and its impact on seismic isolation efficiency under near-fault earthquakes. Eng. Struct. **86**, 99–121. https://doi.org/10.1016/j.engstruct.2014.12.041

Ismail, M., 2015b. Elimination of torsion and pounding of isolated asymmetric structures under near-fault ground motions. Struct. Control Heal. Monit. **22**, 1295–1324. https://doi.org/10.1002/stc.1746

Ismail, M., 2015c. An isolation system for limited seismic gaps in near-fault zones. Earthq. Eng. Struct. Dyn. **44**, 1115–1137. https://doi.org/10.1002/eqe.2504

Ismail, M., López-Almansa, F., Benavent-Climent, A., Pujades-Beneit, L.G., 2014. Finite element code-based modeling of a multi-feature isolation system and passive alleviation of possible inner pounding. Int. J. Adv. Struct. Eng. **6**. https://doi.org/10.1007/s40091-014-0069-y

Ismail, M., Rodellar, J., Pozo, F., 2015. Passive and hybrid mitigation of potential near-fault inner pounding of a self-braking seismic isolator. Soil Dyn. Earthq. Eng. **69**, 233–250. https://doi.org/10.1016/j.soildyn.2014.10.019

Ismail, R., Hasnan, M.H., Shamsudin, N., 2017. Structural pounding of concrete frame structure with masonry infill wall under seismic loading. AIP Conf. Proc. **1892**, 1200011.

Jamal, K.A., Vidyadhara, H.S., 2013. Seismic Pounding of Multistoreyed Buildings. Int. J. Res. Eng. Technol. **15**, 12–17. https://doi.org/10.15623/ijret.2013.0213003

Jameel, M., Saiful Islam, A.B.M., Hussain, R.R., Hasan, S.D., Khaleel, M., 2013. Non-linear FEM analysis of seismic induced pounding between neighbouring Multi-storey Structures. Lat. Am. J. Solids Struct. **10**, 921–939. https://doi.org/10.1590/S1679-78252013000500004

Jankowski, R., 2012. Non-linear FEM analysis of pounding-involved response of buildings under non-uniform earthquake excitation. Eng. Struct. **37**, 99–105. https://doi.org/10.1016/j.engstruct.2011.12.035

Jankowski, R., 2010. Experimental study on earthquake-induced pounding between structural elements made of different building materials. Earthq. Eng. Struct. Dyn. **39**, 343–354. https://doi.org/10.1002/eqe

Jankowski, R., 2009. Non-linear FEM analysis of earthquake-induced pounding between the main building and the stairway tower of the Olive View Hospital. Eng. Struct. **31**, 1851–1864. https://doi.org/10.1016/j.engstruct.2009.03.024

Jankowski, R., 2008a. Earthquake-induced pounding between equal height buildings with substantially different dynamic properties. Eng. Struct. **30**, 2818–2829. https://doi.org/10.1016/j.engstruct.2008.03.006

Jankowski, R., 2008b. Comparison of Numerical Models of Impact Force for Simulation of Earthquake-Induced Structural Pounding, in: Lecture Notes in Computer Science (Including Subseries Lecture Notes in Artificial Intelligence and Lecture Notes in Bioinformatics). pp. 710–717. https://doi.org/10.1007/978-3-540-69384-0_76

Jankowski, R., 2006a. Analytical expression between the impact damping ratio and the coefficient of restitution in the non-linear viscoelastic model of structural pounding. Earthq. Eng. Struct. Dyn. **35**, 517–524. https://doi.org/10.1002/eqe.537

Jankowski, R., 2006b. Pounding force response spectrum under earthquake excitation. Eng. Struct. **28**, 1149–1161. https://doi.org/10.1016/j.engstruct.2005.12.005

Jankowski, R., 2005. Non-linear viscoelastic modelling of earthquake-induced structural pounding. Earthq. Eng. Struct. Dyn. **34**, 595–611. https://doi.org/10.1002/eqe.434

Jankowski, R., Mahmoud, S., 2016. Linking of adjacent three-storey buildings for mitigation of structural pounding during earthquakes. Bull. Earthq. Eng. **14**, 3075–3097. https://doi.org/10.1007/s10518-016-9946-z

Jankowski, R., Mahmoud, S., 2015. Mitigation of pounding effects. Earthquake-Induced Struct. Pound. 103–132.

Jeng, V., Kasai, K., 1996. Spectral relative motion of two structures due to seismic travel waves. J. Struct. Eng. **122**, 1128–1135. https://doi.org/10.1061/(ASCE)0733-9445(1996)122:10(1128)

Jeng, V., Kasai, K., Maison, B.F., 1992. A Spectral Difference Method to Estimate Building Separations to Avoid Pounding. Sage Journals **8**, 201–223.

Jeng, V., Tzeng, W.., 2000. Assessment of seismic pounding hazard for Taipei City. Eng. Struct. **22**, 459–471. https://doi.org/10.1016/S0141-0296(98)00123-0

Jennings, P.C., 1971. Engineering features of the San Fernando earthquake of February 9, 1971.

Karayannis, C.G., Favvata, M.J., 2005a. Inter-story pounding between multistory reinforced concrete structures. Struct. Eng. Mech. **20**, 505–526.

Karayannis, C.G., Favvata, M.J., 2005b. Earthquake-induced interaction between adjacent

reinforced concrete structures with non-equal heights. Earthq. Eng. Struct. Dyn. **34**, 1–20. https://doi.org/10.1002/eqe.398

Karayannis, C.G., Naoum, M.C., 2018a. Torsional behavior of multistory RC frame structures due to asymmetric seismic interaction. Eng. Struct. **163**, 93–111. https://doi.org/10.1016/j.engstruct.2018.02.038

Karayannis, C.G., Naoum, M.C., 2018b. Torsional behavior of multistory RC frame structures due to asymmetric seismic interaction. Eng. Struct. **163**, 93–111. https://doi.org/10.1016/j.engstruct.2018.02.038

Karayannis, C.G., Naoum, M.C., 2017a. Torsion effect due to asymmetric pounding between multistory RC buildings. COMPDYN 2017 - Proc. 6th Int. Conf. Comput. Methods Struct. Dyn. Earthq. Eng. **2**, 3519–3529. https://doi.org/10.7712/120117.5662.17503

Karayannis, C.G., Naoum, M.C., 2017b. Inter-story pounding and torsional effect due to interaction between adjacent multistory RC buildings. COMPDYN 2017 - Proc. 6th Int. Conf. Comput. Methods Struct. Dyn. Earthq. Eng. **2**, 3556–3567. https://doi.org/10.7712/120117.5665.17929

Kasai, K., Jagiasi, A.R., Jeng, V., 1996. Inelastic vibration phase theory for seismic pounding mitigation. J. Struct. Eng. **122**, 1136–1146.

Kasai, K., Jeng, V., Maison, B.F., 1990. The significant effects of pounding-induced accelerations on building appurtenances. Proc. Semin. Seism. Des. Retrofit, Perform. Nonstructural Components **29**.

Kasai, K., Jeng, V., Patel, P.C., Munshi J A, B F Maison, 1992. Seismic Pounding Effects - Survey and Analysis. Earthq. Eng. 10th World Conf.

Kasai, K., Maison, B.F., 1997. Building pounding damage during the 1989 Loma Prieta

earthquake. Eng. Struct. **19**, 195–207. https://doi.org/10.1016/S0141-0296(96)00082-X

Kaushik, H.B., Dasgupta, K., Sahoo, D.R., Kharel, G., 2006. Performance of structures during the Sikkim earthquake of 14 February 2006. Curr. Sci. **91**, 449–455.

Kawashima, K., Unjoh, S., Hoshikuma, J.I., Kosa, K., 2011. Damage of bridges due to the 2010 Maule, Chile, earthquake. J. Earthq. Eng. **15**, 1036–1068. https://doi.org/10.1080/13632469.2011.575531

Kazemi, F., Mohebi, B., Jankowski, R., 2021. Predicting the seismic collapse capacity of adjacent SMRFs retrofitted with fluid viscous dampers in pounding condition. Mech. Syst. Signal Process. **161**, 107939. https://doi.org/10.1016/j.ymssp.2021.107939

Kazemi, F., Mohebi, B., Yakhchalian, M., 2018. Enhancing the seismic performance of adjacent pounding structures using viscous dampers. 16th Eur. Conf. Earthq. Eng. 18–21.

Keim, B., n.d. Download Your Own Robot Scientist.

Khaled, M.F., Aly, A.M., Elshaer, A., 2021. Computational efficiency of CFD modeling for building engineering: An empty domain study. J. Build. Eng. **42**, 102792. https://doi.org/10.1016/j.jobe.2021.102792

Khatiwada, S., Chouw, N., Butterworth, J.W., 2013. Evaluation of numerical pounding models with experimental validation. Bull. New Zeal. Soc. Earthq. Eng. **46**, 117–130. https://doi.org/10.5459/bnzsee.46.3.117-130

Khatiwada, S., Chouw, N., Butterworth, J.W., 2011. Development of pounding model for adjacent structures in earthquakes. Proc. ninth pacific Conf. Earthq. Eng. **1**, 1–8.

Kim, H.S., 2016. Seismic response control of adjacent buildings coupled by semi-active shared TMD. Int. J. Steel Struct. **16**, 647–656. https://doi.org/10.1007/s13296-016-6030-0

Kiureghian, A. Der, 1980. Structural response to stationary excitation. J. Eng. Mech. Div. **106**,

1195–1213.

Klein, R.E., Stukel, J., 1972. Investigation of a method to stabilize wind induced oscillations in large structures.

Komodromos, P., 2008. Simulation of the earthquake-induced pounding of seismically isolated buildings. Comput. Struct. **86**, 618–626. https://doi.org/10.1016/j.compstruc.2007.08.001

Komodromos, P., Polycarpou, P.C., Papaloizou, L., Phocas, M.C., 2007. Response of seismically isolated buildings considering poundings. Earthq. Eng. Struct. Dyn. **36**, 1605–1622. https://doi.org/10.1002/eqe.692

Kumar, P., Kumar, J.D.C., 2015. Seismic Pounding of the Adjacent Buildings With Different Heights. Int. J. Engg. Res. Sci. Tech **4**.

Kwon, D.K., Kareem, A., 2013. Comparative study of major international wind codes and standards for wind effects on tall buildings. Eng. Struct. **51**, 23–35. https://doi.org/10.1016/j.engstruct.2013.01.008

Lam, K.M., H. Leung, M.Y., Zhao, J.G., 2008. Interference effects on wind loading of a row of closely spaced tall buildings. J. Wind Eng. Ind. Aerodyn. **96**, 562–583. https://doi.org/10.1016/j.jweia.2008.01.010

Lam, K.M., Wong, S.Y., To, A.P., 2009. Dynamic wind loading of H-shaped tall buildings. 7th Asia-Pacific Conf. Wind Eng. APCWE-VII.

Lam, K.M., Zhao, J.G., Leung, M.Y.H., 2011. Wind-induced loading and dynamic responses of a row of tall buildings under strong interference. J. Wind Eng. Ind. Aerodyn. **99**, 573–583. https://doi.org/10.1016/j.jweia.2011.02.006

Langlade, T., Bertrand, D., Grange, S., Candia, G., de la Llera, J.C., 2021. Modelling of earthquake-induced pounding between adjacent structures with a non-smooth contact

dynamics method. Eng. Struct. **241**, 112426. https://doi.org/10.1016/j.engstruct.2021.112426

Lee, G.C., Loh, C.H., 2000. The Chi-Chi, Taiwan, Earthquake of September 21, 1999: Reconnaissance Report, Multidisciplinary Center for Earthquake Engineering Research.

Leung, F.H.F., Lam, H.K., Ling, S.H., Tam, P.K.S., 2003. Tuning of the structure and parameters of a neural network using an improved genetic algorithm. IEEE Trans. Neural Networks **14**, 79–88. https://doi.org/10.1109/TNN.2002.804317

Li, J., Peng, T., Xu, Y., 2008. Damage investigation of girder bridges under the Wenchuan earthquake and corresponding seismic design recommendations. Earthq. Eng. Eng. Vib. **7**, 337–344. https://doi.org/10.1007/s11803-008-1005-6

Li, P., Liu, S., Lu, Z., 2017. Studies on pounding response considering structure-soil-structure interaction under seismic loads. Sustain. **9**. https://doi.org/10.3390/su9122219

Li, Y., Duan, R.B., Li, Q.S., Li, Y.G., Huang, X., 2020. Wind-resistant optimal design of tall buildings based on improved genetic algorithm. Structures **27**, 2182–2191. https://doi.org/10.1016/j.istruc.2020.08.036

Lin, J.H., 2005. Evaluation of seismic pounding risk of buildings in Taiwan. J. Chinese Inst. Eng. Trans. Chinese Inst. Eng. A/Chung-kuo K. Ch'eng Hsuch K'an **28**, 867–872. https://doi.org/10.1080/02533839.2005.9671057

Lin, J.H., 1997. Separation distance to avoid seismic pounding of adjacent buildings. Earthq. Eng. Struct. Dyn. **26**, 395–403. https://doi.org/10.1002/(SICI)1096-9845(199703)26:3<395::AID-EQE655>3.0.CO;2-F

Lin, J.H., Weng, C.C., 2002. A study on Seismic pounding probability of buildings in Taipei metropolitan area. J. Chinese Inst. Eng. Trans. Chinese Inst. Eng. Ser. A/Chung-kuo K. Ch'eng Hsuch K'an **25**, 123–135. https://doi.org/10.1080/02533839.2002.9670687

Lin, J.H., Weng, C.C., 2001. Spectral analysis on pounding probability of adjacent buildings. Eng. Struct. **23**, 768–778. https://doi.org/10.1016/S0141-0296(00)00098-5

Liu, D.K., Yang, Y.L., Li, Q.S., 2003. Optimum positioning of actuators in tall buildings using genetic algorithm. Comput. Struct. **81**, 2823–2827. https://doi.org/10.1016/j.compstruc.2003.07.002

Liu, Y., Liu, W.G., Wang, X., He, W.F., Yang, Q.R., 2014. New equivalent linear impact model for simulation of seismic isolated structure pounding against moat wall. Shock Vib. **2014**. https://doi.org/10.1155/2014/151237

Lopez-Garcia, D., Soong, T.T., 2009. Assessment of the separation necessary to prevent seismic pounding between linear structural systems. Probabilistic Eng. Mech. **24**, 210–223. https://doi.org/10.1016/j.probengmech.2008.06.002

Mahin, S.A., Bertero, V. V., Chopra, A.K., Collins, R.G., 1976. Response of the Olive view hospital main building during the San Fernando earthquake. Rep. No. EERC 76-22 320.

Mahmoud, S., Abd-Elhamed, A., Jankowski, R., 2013. Earthquake-induced pounding between equal height multi-storey buildings considering soil-structure interaction. Bull. Earthq. Eng. **11**, 1021–1048. https://doi.org/10.1007/s10518-012-9411-6

Mahmoud, S., Jankowski, R., 2011. Modified linear viscoelastic model of earthquake-induced structural pounding 51–62. https://doi.org/https://www.sid.ir/en/journal/ViewPaper.aspx?ID=197021

Maison, B.F., Kasai, K., 1992. Dynamics of pounding when two buildings collide. Earthq. Eng. Struct. Dyn. **21**, 771–786.

Maison, B.F., Kasai, K., 1990. Analysis for a Type of Structural Pounding. J. Struct. Eng. **116**, 957–977. https://doi.org/10.1061/(ASCE)0733-9445(1990)116:4(957)

Maison, B.F., Neuss, C.F., Kasai, K., 1983. The comparative performance of seismic response spectrum combination rules in building analysis. Earthq. Eng. Struct. Dyn. **11**, 623–647.

Malhotra, A., Roy, T., Matsagar, V., 2020. Effectiveness of Friction Dampers in Seismic and Wind Response Control of Connected Adjacent Steel Buildings. Shock Vib. **2020**. https://doi.org/10.1155/2020/8304359

Mavronicola, E.A., Polycarpou, P.C., Komodromos, P., 2016. Effect of planar impact modeling on the pounding response of base-isolated buildings. Front. Built Environ. **2**, 1–16. https://doi.org/10.3389/fbuil.2016.00011

Mavronicola, E.A., Polycarpou, P.C., Komodromos, P., 2015. The effect of modified linear viscoelastic impact models on the pounding response of a base-isolated building with adjacent structures. COMPDYN 2015 - 5th ECCOMAS Themat. Conf. Comput. Methods Struct. Dyn. Earthq. Eng. https://doi.org/10.7712/120115.3676.992

Meguro, K., Tagel-Din, H., 2003. AEM used for large displacement structure analysis. J. Nat. Disaster Sci. **24**, 25–34.

Meguro, K., Tagel-Din, H., 2001. Applied element simulation of RC structures under cyclic loading. J. Struct. Eng. **127**, 1295–1305.

Meguro, K., Tagel-Din, H., 2000. Applied element method for structural analysis: Theory and application for linear materials. Struct. Eng. Eng. **17**, 31–45. https://doi.org/10.2208/jscej.2000.647_31

Melbourne, W.H., 1980. Comparison of measurements on the CAARC standard tall building model in simulated model wind flows. J. Wind Eng. Ind. Aerodyn. **6**, 73–88. https://doi.org/https://doi.org/10.1016/0167-6105(80)90023-9

Mengistu, T., Ghaly, W., 2008. Aerodynamic optimization of turbomachinery blades using

evolutionary methods and ANN-based surrogate models. Optim. Eng. **9**, 239–255. https://doi.org/10.1007/s11081-007-9031-1

Mettler, L.E., Gregg, T.G., 1969. Population genetics and evolution. New Jers.: Prentice-Hall, Inc.

Miari, M., Choong, K.K., Jankowski, R., 2021. Seismic Pounding Between Bridge Segments: A State-of-the-Art Review. Arch. Comput. Methods Eng. **28**, 495–504. https://doi.org/10.1007/s11831-019-09389-x

Miari, M., Choong, K.K., Jankowski, R., 2019. Seismic pounding between adjacent buildings: Identification of parameters, soil interaction issues and mitigation measures. Soil Dyn. Earthq. Eng. **121**, 135–150. https://doi.org/https://doi.org/10.1016/j.soildyn.2019.02.024

Michalewicz, Z., 1994. GAs: Why Do They Work?, in: Genetic Algorithms + Data Structures = Evolution Programs. Springer Berlin Heidelberg, Berlin, Heidelberg, pp. 43–53. https://doi.org/10.1007/978-3-662-07418-3_4

Moehle, J.P., 1995. Northridge earthquake of January 17, 1994: reconnaissance report, volume 1—highway bridges and traffic management. Earthq. Spectra **11**, 287–372.

Murakami, S., 1998. Overview of turbulence models applied in CWE–1997. J. Wind Eng. Ind. Aerodyn. **74–76**, 1–24. https://doi.org/10.1016/S0167-6105(98)00004-X

Muthukumar, S., DesRoches, R., 2006. A Hertz contact model with non-linear damping for pounding simulation. Earthq. Eng. Struct. Dyn. **35**, 811–828. https://doi.org/10.1002/eqe.557

Naderpour, H., Khatami, S.M., Barros, R.C., 2017. Prediction of critical distance between two MDOF systems subjected to seismic excitation in terms of artificial neural networks. Period. Polytech. Civ. Eng. **61**, 516–529. https://doi.org/10.3311/PPci.9618

Naserkhaki, S., Abdul Aziz, F.N.A., Pourmohammad, H., 2012. Parametric study on earthquake induced pounding between adjacent buildings. Struct. Eng. Mech. **43**, 503–526.

https://doi.org/10.12989/sem.2012.43.4.503

Naserkhaki, S., El-Richa, M., Abdul Azizb, F.N.A., Pourmohammadc, H., 2013. Separation gap, a critical factor in earthquake induced pounding between adjacent buildings. Asian J. Civ. Eng. **14**, 881–898.

National Bureau of Standards Building Science, 1987. Engineering Aspects of the September 19, 1985 Mexico Earthquake. Washington.

Neuss, C.F., Maison, B.F., Bouwkamp, J.G., 1983. Study of computer modeling formulation and special analytical procedures for earthquake response of multistory buildings, National Science Foundation.

NK, A., Nair, N., 2016. Evaluation of Seismic Pounding between Adjacent Buildings. Int. J. Innov. Sci. Technol. **3**, 138–147. https://doi.org/10.15224/978-1-63248-105-4-24

Pall, A.S., Marsh, C., 1981. Friction-damped concrete shearwalls. J. Proc. **78**, 187–193.

Pant, D.R., Wijeyewickrema, A.C., Ohmachi, T., 2010. Seismic pounding between reinforced concrete buildings : A study using two recently proposed contact element models. 14th Eur. Conf. Earthq. Eng. Proceesings 624.

Pantelides, C.P., Ma, X., 1998. Linear and nonlinear pounding of structural systems. Comput. Struct. **66**, 79–92. https://doi.org/10.1016/S0045-7949(97)00045-X

Papadrakakis, M., Apostolopoulou, C., Zacharopoulos, A., Bitzarakis, S., 1996a. Three-dimensional simulation of structural pounding during earthquakes. J. Eng. Mech. **122**, 423–431.

Papadrakakis, M., Mouzakis, H.P., Alevridis, A.S., 1996b. Three dimensional non-linear analysis of building pounding during earthquakes **3**, 15.

Papadrakakis, M., Mouzakism, H.P., 1995. Earthquake simulator testing of pounding between

adjacent buildings. Earthq. Eng. Struct. Dyn. **24**, 811–834.

Park, J., Reed, D., 2001. Analysis of uniformly and linearly distributed mass dampers under harmonic and earthquake excitation. Eng. Struct. **23**, 802–814. https://doi.org/10.1016/S0141-0296(00)00095-X

Patel, C.C., Jangid, R.S., 2010. Seismic response of dynamically similar adjacent structures connected with viscous dampers. IES J. Part A Civ. Struct. Eng. **3**, 1–13. https://doi.org/10.1080/19373260903236833

Penzien, J., 1997. Evaluation of building separation distance required to prevent pounding during strong earthquakes. Earthq. Eng. Struct. Dyn. **26**, 849–858. https://doi.org/10.1002/(SICI)1096-9845(199708)26:8<849::AID-EQE680>3.0.CO;2-M

Petronijević, P., Zdravković, S., Mladenović, B., Zlatkov, D., Momčilović-petronijević, A., 2014. Analysis of a potential collision of buildings during earthquake based on computer simulation. Teh. Vjesn. **21**, 1125–1133.

Pham, D., Karaboga, D., 2012. Intelligent Optimisation Techniques: Genetic Algorithms, Tabu Search, Simulated Annealing and Neural Networks. Springer Science & Business Media.

Polycarpou, P.C., Komodromos, P., 2011. Numerical investigation of potential mitigation measures for poundings of seismically isolated buildings. Earthq. Struct. **2**, 1–24. https://doi.org/10.12989/eas.2011.2.1.001

Polycarpou, P.C., Komodromos, P., Polycarpou, A.C., 2013. A nonlinear impact model for simulating the use of rubber shock absorbers for mitigating the effects of structural pounding during earthquakes. Earthq. Eng. Struct. Dyn. **42**, 81–100. https://doi.org/10.1002/eqe.2194

Pourzeynali, S., Salimi, S., Kalesar, H.E., 2013. Robust multi-objective optimization design of TMD control device to reduce tall building responses against earthquake excitations using

genetic algorithms. Sci. Iran. **20**, 207–221. https://doi.org/10.1016/j.scient.2012.11.015

Pourzeynali, S., Zarif, M., 2008. Multi-objective optimization of seismically isolated high-rise building structures using genetic algorithms. J. Sound Vib. **311**, 1141–1160. https://doi.org/10.1016/j.jsv.2007.10.008

Pratesi, F., Sorace, S., Terenzi, G., 2014. Analysis and mitigation of seismic pounding of a slender R/C bell tower. Eng. Struct. **71**, 23–34. https://doi.org/10.1016/j.engstruct.2014.04.006

Pratesi, F., Sorace, S., Terenzi, G., 2013. Seismic pounding mitigation of a modern heritage R/C bell tower. WIT Trans. Built Environ. **131**, 303–314. https://doi.org/10.2495/STR130261

Priestly, M.N., Seible, F., Calvi, G.M., 1996. Seismic design and retrofit of bridges. John Wiley Sons 704.

Qiang, H., Xiuli, D., Jingbo, L., Zhongxian, L., Liyun, L., Jianfeng, Z., 2009. Seismic damage of highway bridges during the 2008 Wenchuan earthquake. Earthq. Eng. Eng. Vib. **8**, 263–273. https://doi.org/10.1007/s11803-009-8162-0

Qin, W., Shi, J., Yang, X., Xie, J., Zuo, S., 2022. Characteristics of wind loads on Twin-Tower structure in comparison with single tower. Eng. Struct. **251**, 112780. https://doi.org/10.1016/j.engstruct.2021.112780

Rahman, A., Fancy, S.F., Bobby, S.A., 2012. Analysis of drift due to wind loads and earthquake loads on tall structures by programming language c. Int. J. Sci. Eng. Res. **3**, 6–9.

Rajaram, C., Ramancharla, P.K., 2012. Three Dimensional Modeling of Breaking. Fourth Int. Conf. Struct. Stab. Dyn. (ICSSD 2012) 4–6.

Rea, D., Bouwkamp, J.G., Clough, R.W., 1968. The dynamic behavior of steel frame and truss buildings. Cent. Cold-Formed Steel Struct. Libr. **16**.

Rezavandi, A., Moghadam, A.S., 2007. Experimental and numerical study on pounding effects

and mitigation techniques for adjacent structures. Adv. Struct. Eng. **10**, 121–134. https://doi.org/10.1260/136943307780429752

Rezavandi, A., Moghadam, A.S., 2004. Using shaking table to study different methods of reducing effects of building pounding during earthquake, in: 13th World Conference on Earthquake Engineering. Vancouver.

Richardson, Andy, Walsh, K.K., Abdullah, M.M., 2013. Closed-form equations for coupling linear structures using stiffness and damping elements. Struct. Control Heal. Monit. **20**, 259–281. https://doi.org/10.1002/stc.490

Richardson, A., Walsh, K.K., Abdullah, M.M., 2013. Closed-form design equations for controlling vibrations in connected structures. J. Earthq. Eng. **17**, 699–719. https://doi.org/10.1080/13632469.2013.771590

Rosenblueth, E., Meli, R., 1986. The 1985 Mexico earthquake. Concr. Int. **8**, 23–34.

Rosmon, R., 1964. Approximate analysis of shear walls subject to lateral loads. Int. Concr. Abstr. Portal **61**, 717–734.

Sarebanha, A., Mosqueda, G., 2017. Effects of moat wall impact on the seismic response of base isolated nuclear power plants. Proc. 16th World Conf. Earthq. Eng. 1–13.

Sarebanha, A., Mosqueda, G., Kim, M.K., Kim, J.H., 2018. Seismic response of base isolated nuclear power plants considering impact to moat walls. Nucl. Eng. Des. **328**, 58–72. https://doi.org/10.1016/j.nucengdes.2017.12.021

Schiff, A.J., 1999. Hyogoken-Nanbu (Kobe) Earthquake of January 17, 1995: Lifeline Performance. Am. Soc. Civ. Eng. 335.

Schmidt, M., Lipson, H., 2009. Distilling free-form natural laws from experimental data. Science (80-.). **324**, 81–85. https://doi.org/10.1126/science.1165893

SharcNet [WWW Document], 2022. . SHARCNET is a Consort. Coll. Univ. Res. institutes Oper. a Netw. high-performance Comput. Clust. across south West. Cent. North. Ontario [Online]. Available <www.sharcnet. ca>; 2022.

Smagorinsky, J., 1963. GENERAL CIRCULATION EXPERIMENTS WITH THE PRIMITIVE EQUATIONS. Mon. Weather Rev. **91**, 99–164. https://doi.org/10.1175/1520-0493(1963)091<0099:GCEWTP>2.3.CO;2

Sołtysik, B., Falborski, T., Jankowski, R., 2020. Study on polymer elements for mitigation of earthquakeinduced pounding between buildings in complex arrangements. Seism. Behav. Des. Irregul. Complex Civ. Struct. III, Geotech. Geol. eathquake Eng. **48**, 391–401.

Sołtysik, B., Falborski, T., Jankowski, R., 2017. Preventing of earthquake-induced pounding between steel structures by using polymer elements-experimental study. Procedia Eng. **199**, 278–283. https://doi.org/10.1016/j.proeng.2017.09.029

Sołtysik, B., Jankowski, R., 2016. Problems of collisions between adjacent steel structures under earthquake excitation. Civ. Environ. Eng. Reports **20**, 147–158. https://doi.org/10.1515/ceer-2016-0012

Sorace, S., Terenzi, G., 2013. Damped Interconnection-Based Mitigation of Seismic Pounding between Adjacent R/C Buildings. Int. J. Eng. Technol. 406–412. https://doi.org/10.7763/ijet.2013.v5.585

Stafford Smith, B., Coull, A., 1991. Tall building structures: Analysis and design.

Stafford Smith, B., Crowe, E., 1986. Estimating periods of vibration of tall buildings. J. Struct. Eng. **112**, 1005–1019. https://doi.org/10.1061/(ASCE)0733-9445(1987)113:9(2098)

Stafford Smith, B., Hoenderkamp, J., Kuster, M., 1982. A graphical method of comparing the sway resistance of tall building structures. Proc. Inst. Civ. Eng. **73**, 713–729.

Stafford Smith, B., Kuster, M., Hoenderkamp, J., 1984. Generalized method for estimating drift in high-rise structures. J. Struct. Eng. **110**, 1549–1562.

Stavroulakis, G.E., Abdalla, K.M., 1991. Contact between adjacent structures. J. Struct. Eng. **117**, 2838–2850. https://doi.org/10.1061/(ASCE)0733-9445(1991)117:10(2838)

Stewart, J.P., Bray, J.D., Seed, R.B., Sitar, N., 1994. Preliminary report on the principal geotechnical aspects of the January 17, 1994 Northridge earthquake, EARTHQUAKE ENGINEERING RESEARCH CENTER.

Stone, W.C., Yokel, F.Y., Celebi, M., Hanks, T., Leyendecker, E. V., 1987. Engineering aspects of the September 19, 1985 Mexico earthquake, NBS Building Science Series 165.

Tagel-Din, H., Meguro, K., 2000. Applied Element Method for simulation of nonlinear materials: theory and application for RC structures. Struct. Eng./Earthquake Eng., Int. J. Japan Soc. Civ. Eng. **17**, 137–148.

Taiwan Building Code. Construction and planning administration Ministry of Interior, Seismic provisions, 1997.

Takabatake, H., Yasui, M., Nakagawa, Y., Kishida, A., 2014. Relaxation method for pounding action between adjacent buildings at expansion joint. Earthq. Eng. Struct. Dyn. **43**, 1381–1400. https://doi.org/10.1002/eqe.2402

Tinawi, R., Mitchell, D., Law, T., 1990. Les dommages dus au tremblement de terre du Saguenay du 25 novembre 1988. Can. J. Civ. Eng. **17**, 366–394. https://doi.org/10.1139/l90-042

Tominaga, Y., Mochida, A., Yoshie, R., Kataoka, H., Nozu, T., Yoshikawa, M., Shirasawa, T., 2008. AIJ guidelines for practical applications of CFD to pedestrian wind environment around buildings. J. Wind Eng. Ind. Aerodyn. **96**, 1749–1761. https://doi.org/10.1016/j.jweia.2008.02.058

Tse, K.T., Kwok, K.C.S., Hitchcock, P.A., Samali, B., Huang, M.F., 2007. Vibration control of a wind-excited benchmark tall building with complex lateral-torsional modes of vibration. Adv. Struct. Eng. **10**, 283–304. https://doi.org/10.1260/136943307781422208

Tse, K.T., Kwok, K.C.S., Tamura, Y., 2012. Performance and cost evaluation of a smart tuned mass damper for suppressing wind-induced lateral-torsional motion of tall structures. J. Struct. Eng. **138**, 514–525. https://doi.org/10.1061/(ASCE)ST.1943-541X.0000486

Tubaldi, E., Barbato, M., Ghazizadeh, S., 2012. A probabilistic performance-based risk assessment approach for seismic pounding with efficient application to linear systems. Struct. Saf. **36–37**, 14–22. https://doi.org/10.1016/j.strusafe.2012.01.002

Van, J., Kasai, K., Maison, B.F., 1992. A spectral difference method to estimate building separations to avoid pounding. Earthq. spectra **8**, 201–223.

Vasiliadia, L., Elenas, A., 2002. Performance of school buildings during the Athens earthquake of September 7 1999, in: 12th European Conference on Earthquake Engineering.

Vega, J., del Rey, I., Alarcon, E., 2009. Pounding force assessment in performance-based design of bridges. Earthq. Eng. Struct. Dyn. **38**, 1525–1544. https://doi.org/10.1002/eqe.916

Wada, A., Shinozaki, Y., Nakamura, N., 1984. Collapse of building with expansion joints through collision caused by earthquake motion. Proc. 8th World Conf. Earthq. Eng. **4**, 855–862.

Wang, D., Tse, T.K.T., Zhou, Y., Li, Q., 2015. Structural performance and cost analysis of wind-induced vibration control schemes for a real super-tall building. Struct. Infrastruct. Eng. https://doi.org/10.1080/15732479.2014.925941

Wang, W., Hua, X., Wang, X., Chen, Z., Song, G., 2017. Optimum design of a novel pounding tuned mass damper under harmonic excitation. Smart Mater. Struct. **26**, 055024. https://doi.org/10.1088/1361-665X/aa69a3

Westermo, B.D., 1989. The dynamics of interstructural connection to prevent pounding. Earthq. Eng. Struct. Dyn. **18**, 687–699. https://doi.org/10.1002/eqe.4290180508

Wolf, J.P., Skrikerud, P.E., 1980. Mutual pounding of adjacent structures during earthquakes. Nucl. Eng. anf Des. **57**, 253–275.

Wolfgang, S., 1977. High-rise building structures. High-rise Build. Struct.

Wu, Q., Yan, H., Zhu, H., Ding, L., 2020. Probabilistic Performance-Based Assessment for Critical Separation Distance of Adjacent Buildings: Theoretical Analysis. J. Perform. Constr. Facil. **34**, 04020047. https://doi.org/10.1061/(asce)cf.1943-5509.0001453

Xue, Q., Zhang, C., He, J., Zou, G., Zhang, J., 2016a. An Updated Analytical Structural Pounding Force Model Based on Viscoelasticity of Materials. Shock Vib. **2016**, 1–15. https://doi.org/10.1155/2016/2596923

Xue, Q., Zhang, J., He, J., Zhang, C., 2016b. Control performance and robustness of pounding tuned mass damper for vibration reduction in SDOF structure. Shock Vib. **2016**. https://doi.org/10.1155/2016/8021690

Xue, Q., Zhang, J., He, J., Zhang, C., Zou, G., 2017. Seismic control performance for Pounding Tuned Massed Damper based on viscoelastic pounding force analytical method. J. Sound Vib. **411**, 362–377. https://doi.org/10.1016/j.jsv.2017.08.035

Ye, K., Li, L., Zhu, H., 2009. A modified Kelvin impact model for pounding simulation of base-isolated building with adjacent structures. Earthq. Eng. Eng. Vib. **8**, 433–446. https://doi.org/10.1007/s11803-009-8045-4

Ye, L., Ma, Q., Miao, Z., Guan, H., Zhuge, Y., 2013. Numerical and comparative study of earthquake intensity indices in seismic analysis. Struct. Des. Tall Spec. Build. **22**, 362–381. https://doi.org/10.1002/tal

Zhang, P., Li, L., Patil, D., Singla, M., Li, H.N., Mo, Y.L., Song, G., 2015. Parametric study of pounding tuned mass damper for subsea jumpers. Smart Mater. Struct. **25**, 015028. https://doi.org/10.1088/0964-1726/25/1/015028

Zhou, L., Haghighat, F., 2009. Optimization of ventilation system design and operation in office environment, Part I: Methodology. Build. Environ. **44**, 651–656. https://doi.org/10.1016/j.buildenv.2008.05.009

Zhou, Y., Kijewski, T., Kareem, A., 2003. Aerodynamic loads on tall buildings: Interactive database. J. Struct. Eng. **129**, 394–404. https://doi.org/10.1061/(ASCE)0733-9445(2003)129:3(394)

Zhu, P., Abe, M., Fujino, Y., 2002. Modelling three-dimensional non-linear seismic peformance of elevated bridges with emphasis on pounding of girders. Earthq. Eng. Struct. Dyn. **31**, 1891–1913. https://doi.org/10.1002/eqe.194

Zhu, Z., Lei, W., Wang, Q., Tiwari, N., Hazra, B., 2020. Study on wind-induced vibration control of linked high-rise buildings by using TMDI. J. Wind Eng. Ind. Aerodyn. **205**, 104306. https://doi.org/10.1016/j.jweia.2020.104306

Zienkiewicz, O.C., Taylor, R.L., 2000. The Finite Element Method: Solid Mechanics.